

DUAL POLARIZED SLOTTED
WAVEGUIDE ARRAY ANTENNA

A THESIS SUBMITTED TO
THE GRADUATE SCHOOL OF NATURAL AND APPLIED SCIENCES
OF
MIDDLE EAST TECHNICAL UNIVERSITY

BY

DOĞANAY DOĞAN

IN PARTIAL FULFILLMENT OF THE REQUIREMENTS FOR THE DEGREE
OF
MASTER OF SCIENCE
IN
ELECTRICAL AND ELECTRONICS ENGINEERING

FEBRUARY 2011

Approval of the thesis:

DUAL POLARIZED SLOTTED WAVEGUIDE ARRAY ANTENNA

submitted by **DOĞANAY DOĞAN** in partial fulfillment of the requirements for the degree of **Master of Science in Electrical and Electronics Engineering Department, Middle East Technical University** by,

Prof. Dr. Canan Özgen
Dean, Graduate School of **Natural and Applied Sciences** _____

Prof. Dr. İsmet Erkmek
Head of Department, **Electrical and Electronics Eng. Dept.** _____

Prof. Dr. Özlem Aydın Çivi
Supervisor, **Electrical and Electronics Engineering Dept, METU** _____

Examining Committee Members:

Prof. Dr. Altunkan Hızal
Electrical and Electronics Engineering Dept., METU _____

Prof. Dr. Özlem Aydın Çivi
Electrical and Electronics Engineering Dept., METU _____

Prof. Dr. S. Sencer Koç
Electrical and Electronics Engineering Dept., METU _____

Assoc. Prof. Dr. Lale Alatan
Electrical and Electronics Engineering Dept., METU _____

Can Barış Top, M.Sc.
REHİS, ASELSAN _____

Date: 11.02.2011

I hereby declare that all information in this document has been obtained and presented in accordance with academic rules and ethical conduct. I also declare that, as required by these rules and conduct, I have fully cited and referenced all material and results that are not original to this work.

Name, Last Name: Doğanay Doğan

Signature :

ABSTRACT

DUAL POLARIZED SLOTTED WAVEGUIDE ARRAY ANTENNA

Doğan, Doğanay
M.Sc. Department of Electrical and Electronics Engineering
Supervisor: Prof. Dr. Özlem Aydın Çivi

February 2011, 88 pages

An X band dual polarized slotted waveguide antenna array is designed with very high polarization purity for both horizontal and vertical polarizations. Horizontally polarized radiators are designed using a novel non-inclined edge wall slots whereas the vertically polarized slots are implemented using broad wall slots opened on baffled single ridge rectangular waveguides. Electromagnetic model based on an infinite array unit cell approach is introduced to characterize the slots used in the array. 20 by 10 element planar array of these slots is manufactured and radiation fields are measured. The measurement results of this array are in very good accordance with the simulation results. The dual polarized antenna possesses a low sidelobe level of -35 dB and is able to scan a sector of ± 35 degrees in elevation. It also has a usable bandwidth of 600 MHz.

KEYWORDS: Dual polarization, Polarization Agility, Slotted Waveguide Arrays, Non-Inclined Edge Wall Slots, Broad Wall Slots, Travelling Wave Arrays.

ÖZ

ÇİFT POLARİZASYONLU YARIKLI DALGA KILAVUZU DİZİ ANTEN

Doğan, Doğanay
Yüksek Lisans, Elektrik ve Elektronik Mühendisliği Bölümü
Tez Yöneticisi: Prof. Dr. Özlem Aydın Çivi

Şubat 2011, 88 sayfa

X frekans bandında çalışan, hem yatay hem dikey polarize bileşenleri çok yüksek polarizasyon saflığına sahip olan çift polarizasyonlu bir yarıklı dalga kılavuzu dizi anten tasarlanmıştır. Yatay polarize anten elemanları yeni bir eğimsiz dar kenar yarık türüyle oluşturulmuşken, dikey polarize elemanlar ızgaralı ve tek sırtlı dalga kılavuzlarına açılmış geniş kenar yarıklarından oluşmaktadır. Dizi elemanlarını karakterize etmek için sonsuz dizi yaklaşımını kullanan “birim hücre” tabanlı bir yöntem geliştirilmiştir. Önerilen yeni eğimsiz dar kenar yarıkları 20 elemana 10 elemanlı bir dizi üretilerek doğrulanmıştır. Üretilen dizinin ölçüm sonuçları benzetim sonuçlarıyla örtüşmektedir. Tasarlanan çift polarizasyonlu antenin yan huzmeleri düşük olup 35 dB seviyesindedir ve antenin yükselişte 70 derecelik elektronik tarama kabileyeti bulunmaktadır. Anten aynı zamanda 600 MHz’lik bir kullanılabilir bant genişliğine sahiptir.

ANAHTAR KELİMELER: Çift polarization, Polarizasyon Çevikliği, Yarıklı Dalga Kılavuzu Diziler, Eğimsiz Dar Kenar Yarıkları, Geniş Kenar Yarıkları, İlerleyen Dalga Tipi Diziler

To My Family and Begim

ACKNOWLEDGEMENTS

The author wishes to express his sincere gratitude to his supervisor Prof. Dr. Özlem Aydın Çivi, for her guidance, support and technical suggestions throughout the study.

The author would like to thank Mr. Mehmet Erim İnal for proposing this topic to him and providing every support throughout the study.

The author is very glad to have Can Barış Top and Erdiñ Erçil as his friends at Aselsan. The motivation they provided and the experiences they shared are invaluable.

The mechanical design, making the production of the designed antenna possible, performed by the author's colleagues Rahmi Dündar, Görkem Akgül and Ozan Gerger is sincerely acknowledged.

The author is grateful to Aselsan for providing both financial and technical opportunities to complete this study.

The author also thanks TÜBİTAK for providing financial support during his studies.

The author specially thanks his family and Begüm Şen for providing every possible support and motivation, sometimes even by sacrificing their own comfort. This work would be impossible to complete without their encouragement and faith.

TABLE OF CONTENTS

ABSTRACT	iv
ÖZ.....	v
ACKNOWLEDGEMENTS	vii
TABLE OF CONTENTS	viii
LIST OF FIGURES.....	xi
CHAPTERS	
1. INTRODUCTION.....	1
1.1 Importance of Antenna Polarization	3
1.2 Polarization Agility and Dual Polarization	3
1.2.1 Shared Aperture Dual Polarization.....	4
1.3 Literature Survey on Dual Polarized SWGA Antennas.....	6
1.4 Organization of the Thesis	7
2. SLOTTED WAVEGUIDE ARRAYS	9
2.1 Slot Types.....	9
2.1.1 Offset Broad Wall Slots.....	10
2.1.2 Inclined Broad Wall Slots	12
2.1.3 Compound broad wall slots	13
2.1.4 Inclined Edge Wall Slots.....	14

2.2 Slotted Waveguide Array Types	15
2.2.1 Standing Wave Type Slotted Waveguide Arrays.....	15
2.2.2 Travelling Wave Type Slotted Waveguide Arrays	17
3. A NOVEL NON-INCLINED EDGE WALL SLOT	20
3.1 Introduction	20
3.2 Excitation of Non-Inlined Slots	21
3.3 Slot Modeling.....	23
3.3.1 Radiation Control	23
3.3.2 Characterization.....	24
3.3.3 Equivalent Circuit Model	35
3.4 Slots in Array Environment	42
3.4.1 Mutual Coupling Effects	42
3.4.2 Infinite Array Approach	43
3.5 Horizontally Polarized Array Design.....	48
3.6 Verification of the Slot by a Test Antenna.....	54
4. BROAD WALL SHUNT SLOT ARRAY WITH BAFFLE.....	58
4.1 Baffles	58
4.2 Requirement of Single Ridge Waveguide.....	59
4.3 Unit Cell Design for Characterization of Broad Wall Slots.....	60
4.4 Characterization Data.....	65
4.5 Vertically Polarized Array Design.....	68

5. DUAL POLARIZED SLOTTED WAVEGUIDE ARRAY SIMULATIONS ..	71
6. CONCLUSION	81
APPENDIX	83
REFERENCES	86

LIST OF FIGURES

FIGURES

Figure 1.1 The geometry of the designed dual polarized array	2
Figure 1.2 A close up view of the dual polarized SWGA.....	2
Figure 1.3 A dual polarized pyramidal horn	6
Figure 1.4 A polarization agile transmission system comprising a power divider phase shifter and power amplifiers	6
Figure 2.1 Current Distribution on a rectangular waveguide for TE ₁₀ excitation.. ..	10
Figure 2.2 Most popular slot geometries carved on a rectangular waveguide.....	11
Figure 2.3 Shunt equivalent for offset broad wall slots.....	12
Figure 2.4 Series equivalent for inclined broad wall slots.....	13
Figure 2.5 An eight element center fed standing wave type SWGA.....	15
Figure 2.6 Lumped equivalent circuit of the SWGA in Figure 2.5.....	16
Figure 2.7 A conceptual uniform distribution eight element travelling wave SWGA	18
Figure 3.1 Typical azimuth radiation pattern for an inclined edge wall slot array.. ..	21
Figure 3.2 Proposed slot geometry for non-inclined edge wall slots with its attributed parameter terminology.....	23
Figure 3.3 The simulation model for an isolated slot.....	25

Figure 3.4 The integration line on which the slot voltage is calculate.....	25
Figure 3.5 Normalized radiated power vs. wrap depth.....	26
Figure 3.6 Radiation phase vs. wrap depth.....	27
Figure 3.7 Normalized radiated power vs. inset height.....	28
Figure 3.8 Radiation phase vs. inset height.....	28
Figure 3.9 Normalized radiated power vs. inset depth.....	29
Figure 3.10 Radiation phase vs. inset depth.....	30
Figure 3.11 S parameter angle vs. inset depth.....	31
Figure 3.12 S parameter magnitude vs inset depth.....	31
Figure 3.13 Normalized radiated power vs slot-inset distance.....	32
Figure 3.14 Normalized radiated power vs. frequency for different slot widths.....	33
Figure 3.15 Normalized radiated power vs. slot width.....	35
Figure 3.16 Admittance parameters vs. frequency for inset height of 1.0mm.....	36
Figure 3.17 Admittance parameters vs. frequency for inset height of 2.0mm.....	37
Figure 3.18 Admittance parameters vs. frequency for inset height of 3.0mm.....	37
Figure 3.19 Admittance parameters vs. frequency for inset height of 4.0mm.....	38
Figure 3.20 Admittance parameters vs. frequency for inset height of 5.0mm.....	39
Figure 3.21 Admittance parameters vs. frequency for inset width of 0.5mm.....	39
Figure 3.22 Admittance parameters vs. frequency for inset width of 1.0mm.....	40
Figure 3.23 Admittance parameters vs. frequency for inset width of 1.5mm.....	40
Figure 3.24 Admittance parameters vs. frequency for inset width of 2.0mm.....	41

Figure 3.25 Admittance parameters vs. frequency for inset depth of 6.3mm and inset height of 4.0mm.....	41
Figure 3.26 Admittance parameters vs. frequency for inset depth of 7.0mm and inset height of 5.0mm.....	42
Figure 3.27 Unit cell structure with periodic boundary pairs.....	44
Figure 3.28 The phase reversal mechanism with mirroring of the consecutive slots	46
Figure 3.29 Normalized radiated power vs. frequency for a sample slot resonant at the center frequency.....	48
Figure 3.30 35dB SLL Taylor Amplitude Distribution with 31 elements for $\tilde{n}=6$	49
Figure 3.31 Array Factor of the distribution in Figure 3.29 with the correct phasing	49
Figure 3.32 Conductance values required for various efficiencies.....	51
Figure 3.33 Periodic model of the designed planar array.....	51
Figure 3.34 Azimuth radiation pattern of the designed horizontally polarized array without tuning.....	53
Figure 3.35 Azimuth radiation pattern of the designed horizontally polarized array after tuning.....	54
Figure 3.36 Desired excitation amplitudes for the 20 element array.....	55
Figure 3.37 Resulting array factor for the distribution in Figure 3.33.....	55
Figure 3.38 The manufactured small edge wall slot array.....	56
Figure 3.39 A close view of the manufactured slots.....	56

Figure 3.40 Measurement azimuth pattern of the manufactured array compared with simulation results.....	57
Figure 4.1 A side view of the single ridge waveguide array.....	60
Figure 4.2 Unit cell structure used to characterize broad wall slots.....	61
Figure 4.3 Ports defined in the unit cell structure.....	62
Figure 4.4 A sample frequency sweep data for a slot resonant at center frequency.....	66
Figure 4.5 Integration line used to calculate slot voltage.....	67
Figure 4.6 Simulation radiation pattern of the tuned array.....	67
Figure 4.7 Resonant lengths of broad wall slots for various offset values.....	68
Figure 4.8 Integration line used to calculate slot voltages.....	69
Figure 4.9 Simulation radiation pattern of the tuned array.....	69
Figure 5.1 The infinite array model used to simulate the dual polarized array.....	72
Figure 5.2 The side view of the simulated periodic model.....	73
Figure 5.3 Power transmitted to the terminating load.....	74
Figure 5.4 Reflection coefficients and the isolation of the two arrays.....	75
Figure 5.5 Azimuth radiation patterns of the designed array at f_0 -300MHz, obtained with simulation.....	76
Figure 5.6 Azimuth radiation patterns of the designed array at f_0 -200MHz, obtained with simulation.....	76
Figure 5.7 Azimuth radiation patterns of the designed array at f_0 -100MHz, obtained with simulation.....	77

Figure 5.8 Azimuth radiation patterns of the designed array at f_0 , obtained with simulation.....	77
Figure 5.9 Azimuth radiation patterns of the designed array at $f_0+100\text{MHz}$, obtained with simulation.....	78
Figure 5.10 Azimuth radiation patterns of the designed array at $f_0+200\text{MHz}$, obtained with simulation.....	78
Figure 5.11 Azimuth radiation patterns of the designed array at $f_0+300\text{MHz}$, obtained with simulation.....	79
Figure 5.12 Azimuth radiation patterns of the horizontally polarized part of the designed array at 7 different frequencies, obtained with simulation.....	79
Figure 5.12 Azimuth radiation patterns of the vertically polarized part of the designed array at 7 different frequencies, obtained with simulation.....	80
Figure A.1 Far field phase difference variations of the orthogonally polarized components for different source spacing.....	84
Figure A.2 Axial ratio variations of the polarization ellipse for different source spacing.....	85

CHAPTER 1

INTRODUCTION

Slotted waveguide arrays (SWGA) are used in many radar and satellite applications, especially when high power capability and low manufacturing costs are desired. It is also possible to implement electronic beam steering easily with SWGA antennas. Apart from electrical advantages, waveguide antennas are mechanically very durable and they can withstand space conditions. In this work, an X-band dual polarized travelling wave type SWGA with side lobe level (SLL) less than -35 dB having a usable frequency bandwidth of 600 MHz is designed with dimensions 31 elements by 22 elements. Dual polarization is achieved by interleaving two types of linear SWGA's having orthogonal polarizations, namely, vertical and horizontal. For vertical polarization, a broad wall shunt slot array is used. For horizontal polarization a novel, non-inclined slot is proposed and used to achieve high polarization purity. The usefulness of these novel slots is tested by manufacturing and measuring a relatively small sized planar array. Both types of slots are characterized using infinite array approach. Additionally, customized waveguide cross sections are used in order to achieve an electronic scan ability of ± 35 degrees in elevation. An illustration of the antenna is seen in Figure 1.1 and a close up view is available in Figure 1.2.

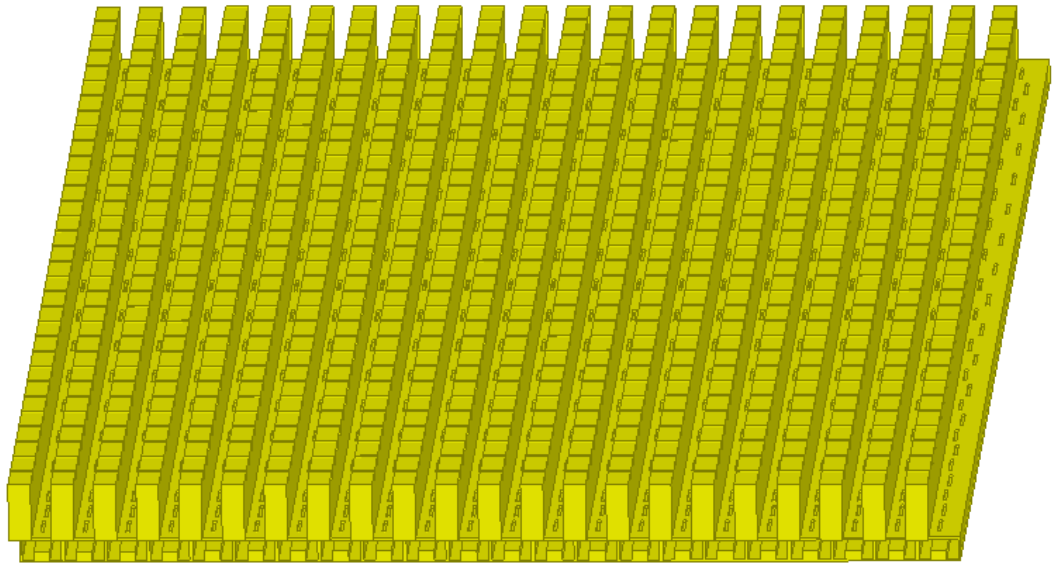


Figure 1.1 The geometry of the designed dual polarized array

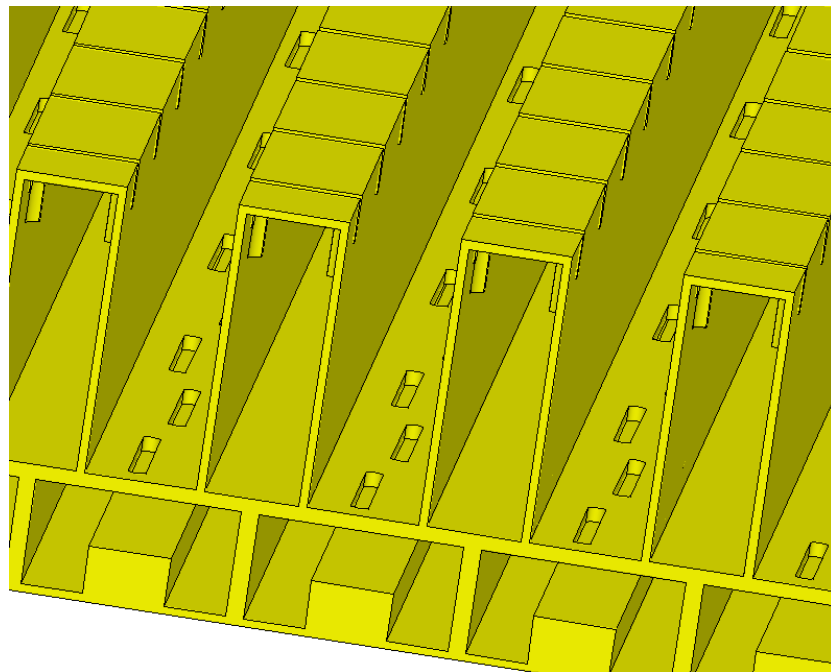


Figure 1.2 A close up view of the dual polarized SWGA

1.1 Importance of Antenna Polarization

Polarization of an antenna defines the polarization of electromagnetic waves which can be transmitted or received by an antenna. Most of the antennas are capable of receiving only a single polarization component. This fact restricts most of the communication and radar systems to transmit and receive a single polarization component. The obligation of working with a single polarization can create various real life problems. A few example cases where an overall degradation in the system performance is expected are as follows:

- A mobile line-of-sight (LOS) communication system where the orientation of the transmitter antenna is changing with respect to the receiver antenna.
- A radar system being jammed by a stand of jammer with a fixed polarization.
- A radar, tracking a target and suddenly starting to receive very low echoes from the target due to a reduction of radar cross section of the target for current aspect angle or due to the multi-path cancellation effects.
- A jammer whose polarization is orthogonal or nearly orthogonal to the polarization of the targeted radar.
- A radar, receiving strong clutter signal due to specific geographical properties or due to non-optimum weather conditions.

In addition to these problems, having a fixed polarization in synthetic aperture radar (SAR) systems, prevents the system from determining the polarizations of the reflected signals from the target surfaces. This obstructs the gathering of additional information about the reflecting surface which is carried by the knowledge of the reflected signal's polarization and prevents the full exploitation of the SAR system's potential, deteriorating the final image quality.

1.2 Polarization Agility and Dual Polarization

To overcome all of these problems caused by the fixed polarization of the antenna, a concept known as the "polarization agility" is implemented in many modern systems. Polarization agility for a system can be defined as the ability of altering

the polarization of electromagnetic waves transmitted and/or received by the system. Polarization agility can be achieved either by mechanical means or electrical means. Mechanically achieved polarization agility is granted by an antenna whose orientation can be changed between desired states intentionally. This technique is rather slow and very inadequate when extreme beam agility or pulse-to-pulse polarization agility is desired due to the inertia of the antenna. Electronically achieved polarization agility is implemented using a dual polarized antenna which can be defined as an antenna able to radiate or receive two differently polarized electromagnetic waves independently. This type of agility controls the polarization using electronic switches or electronic phase shifters, thus, it can achieve extreme agility by transitioning between different polarization states at durations in the order of nanoseconds or microseconds depending on the type of switching or phase shifting hardware used.

The most basic dual polarized antenna can be thought as an antenna comprising two sub antennas of different polarizations. However, although this configuration is very simple, it requires twice the aperture area required by a singly polarized antenna to achieve the same gain for both polarizations. Additionally, the large distance between the far zone phase centers of the two antennas makes it impossible to combine the two polarization components in space to achieve any desired polarizations. A detailed illustration of this phenomenon can be found in Appendix I.

1.2.1 Shared Aperture Dual Polarization

A cleverer implementation of dual polarization relies on the sharing of a single aperture by two orthogonally polarized antennas. This approach eliminates the need for a larger aperture and allows one to make the phase centers of the two orthogonally polarized antennas coincide. A very common example for shared aperture dual polarization is the dual polarized pyramidal horn. By independently exciting the two fundamental orthogonal modes of a square cross section waveguide, namely, TE_{10} and TE_{01} , and proceeding with the flare section, a shared aperture dual polarized antenna is obtained as seen in Figure 1.3. Using this

antenna, a simple polarization agile transmission setup can be obtained as seen in Figure 1.4.

The dual polarized antenna designed in this work is implemented by interleaving waveguide antenna rows of orthogonal polarizations. Due to the interleaved structure, a shared aperture type antenna is obtained sharing all of its advantages.

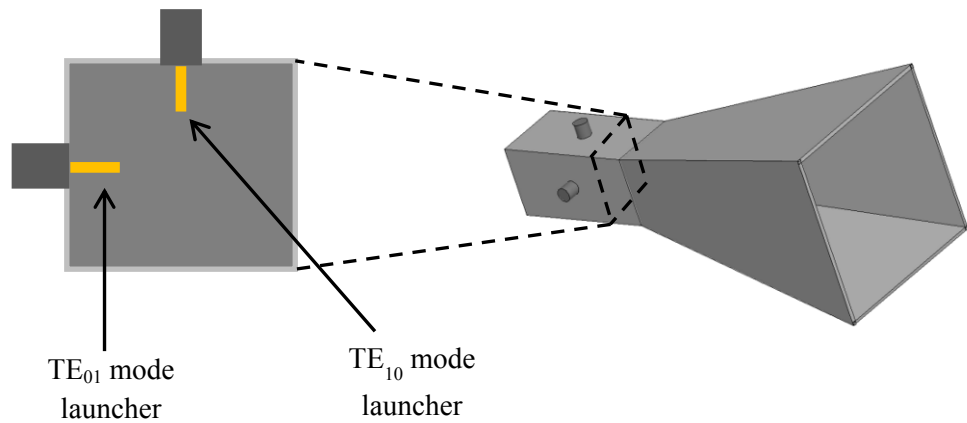


Figure 1.3 A dual polarized pyramidal horn

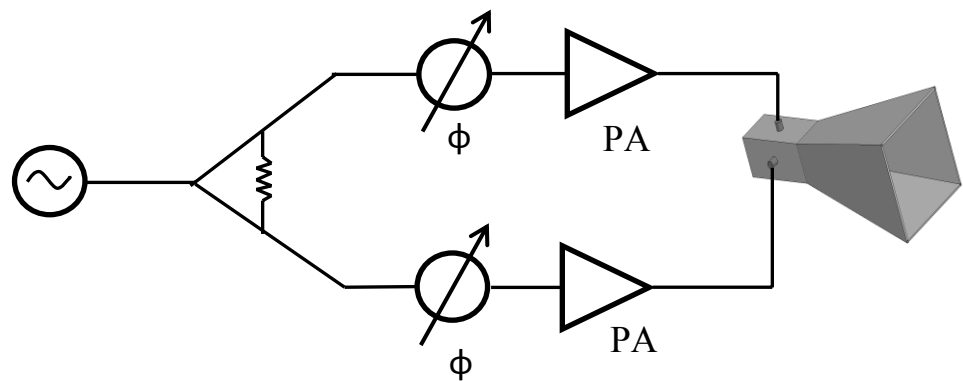


Figure 1.4 A polarization agile transmission system comprising a power divider phase shifter and power amplifiers

1.3 Literature Survey on Dual Polarized SWGA Antennas

Many radar systems are using travelling wave type slotted waveguide array antennas. The design methodology for this type of antennas is well defined in various sources [1,2]. Almost all of the commonly used slotted waveguide arrays are implemented using vertically or horizontally polarized elements because the developed design techniques are based on these slots [2]. In order to take advantage of the polarization agility without sacrificing the numerous advantages gained by using a slotted waveguide array, a dual polarized slotted waveguide array should be used.

The most basic dual polarized SWGA architecture can be seen in [3]. This incorporates broad wall shunt slots for vertical polarization and inclined edge wall slots for horizontal polarization. Although the architecture is simple and easy to design and manufacture, it has the major drawback of low polarization purity for the horizontally polarized array due to the inclined slots. To overcome this drawback, various antennas are developed to replace the inclined edge wall slots with non-inclined edge wall slots [4-6]. All of these examples propose almost the same array structure where horizontally and vertically polarized array elements are interleaved. In [4-6], non-inclined edge wall slots are used as the horizontally polarized radiators; however, the excitation of these slots is provided by placing wires or shaped irises inside the waveguides. The placement of these structures requires a very precise workmanship and a long time to obtain low sidelobes and this increases the costs. Since these antennas are specifically built for SAR missions, the slots are uniformly excited and the sidelobe level is not a very critical issue. In [7], only broad wall slots are used. However, the transverse broad wall slots providing the horizontal polarization have no means of radiation control and their impedances are fixed to a very high value as mentioned in the text. Therefore, they are not suitable for low sidelobe applications.

Another dual polarized SWGA is given in [8] which uses slots, opened on slot coupled cavities as radiators. The cavities of orthogonal polarizations are rotated by 90 degrees with respect to each other. Ridged waveguides are used for feeding the

cavities and the coupling slots feeding the cavities cannot have a wide variation range. Therefore, it is difficult, if not impossible to control the excitation of the cavities which makes this array topology not suitable for low sidelobe applications. It is far more suitable for uniformly excited standing wave type arrays. Additionally, excessive amount of layers involved requires a robust fixing technique relying on sophisticated brazing and bonding facilities

There are also antennas comprising bifurcated waveguide structures [9] and compound circularly polarized slots [10]. The former topology uses a large bifurcated waveguide structure which makes it impossible to implement a scanning planar array. On the other hand, the latter topology makes use of circularly polarized compound slots whose axial ratio bandwidth is very limited and the characterization and design phases are very cumbersome.

According to the author's knowledge, there is a lack for a dual polarized SWGA having high polarization purity for both polarizations and easy manufacturability at the same time. Additionally, having a relatively large bandwidth, high electronic scan ability and low sidelobes would be better. This work is aimed to fill this gap by completely designing the mentioned dual polarized array starting from slot characterization and ending with simulations and measurements of the complete arrays. The polarization purity of the horizontally polarized array is provided by the utilization of a novel non-inclined edge wall slot, which does not have the manufacturability problems found in the non-inclined edge wall slots in the literature. Additionally, the characterization of the slots used in the design is performed using an infinite array approximation based unit cell approach, which greatly reduces computational requirements for the characterization. The arrays designed using characterization data obtained with unit cell technique are tuned with an iterative method to perfect their radiation patterns.

1.4 Organization of the Thesis

A brief introduction to SWGA is presented in Chapter 2 focusing on radiation mechanism of waveguide slots, different slot types and different array topologies.

Chapter 3 focuses on the geometrical details of the proposed non-inclined edge-wall slots followed by the infinite array based characterization technique. A small planar array is designed and manufactured using the characterization data obtained to verify the usefulness of these slots. Finally, waveguide rows which are used in the dual polarized antenna for horizontal polarization are designed.

The characterization and design of single ridge broad wall shunt slot array with baffles are presented in Chapter 4. Infinite array approach used in Chapter 3 is extended to the baffled single ridge broad wall shunt slots by slightly modifying the unit cell geometry. Using the characterization data, vertically polarized waveguide rows used in the dual polarized array are designed.

Interleaving of the waveguide rows to achieve dual polarization is given in Chapter 5. Resource efficient infinite array based simulations of the interleaved dual polarized array are performed and the simulation results are discussed.

The overall achievements of this study are assessed in Chapter 6. Furthermore, future work is discussed.

CHAPTER 2

SLOTTED WAVEGUIDE ARRAYS

Slotted waveguide antenna arrays are used widely as radar antennas for many years starting from mid 1940s because:

- They are inexpensive and relatively easy to manufacture,
- Very low side lobe levels can be achieved with aperture distribution control,
- Very large arrays can be built easily,
- They can handle lots of power and are highly efficient,
- They are robust and durable.

The studies on waveguide slots begin with the pioneering works of Stevenson, Stegan and Oliner [11-13]. The notion of active admittance of slots proposed by Elliott for broad wall slotted arrays given in [14-16] is later partially extended to other slot types [2].

2.1 Slot Types

Many slot geometries are possible to open on waveguide walls. However, some of those slots dominate the area because they may be easier to manufacture, easier to analyze and design or may have superior performance.

The main principle behind all waveguide slots is creating an electric field at the slot aperture across the width of the slot. This is done by blocking waveguide surface currents using slots. A slot is said to block surface currents if there are surface current components at the slot's location before opening the slot, which are perpendicular to the slot's length. The current distribution on the waveguide walls

for a TE_{10} excitation can be seen in Figure 2.1. This current distribution gives an idea on the type of slots which can be opened on a rectangular waveguide as radiating elements.

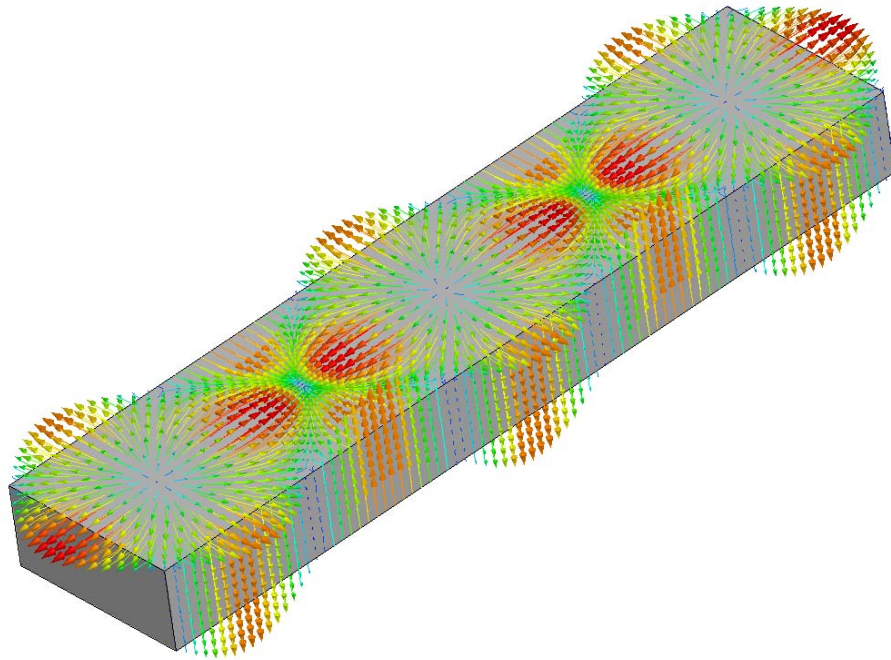


Figure 2.1 Current Distribution on a rectangular waveguide for TE_{10} excitation

In Figure 2.2, many slot types which may be opened on rectangular waveguides as radiating elements are shown. Basics of these slots are presented in the following sections.

2.1.1 Offset Broad Wall Slots

Offset broad wall slots are parallel to the waveguide centerline and they are blocking the transversal current components on the waveguide's broad wall. The slot with index "a" in Figure 2.2 is such a slot. The polarization of these slots is vertical when the waveguide is held parallel to the ground. As seen in Figure 2.1, the transversal current component is 0 on the centerline of the broad wall, however, if one moves closer to the narrow walls, the transversal current component

increases. Therefore, the radiation amplitude of these slots increase as they are farther away from the centerline and that is why they are called offset slots. This is the most widely used slot type on waveguides and the first one to have been analyzed. It has been shown that, those slots can be modeled as lumped shunt admittances [11] as seen in Figure 2.3. The admittance value is determined by the offset and length of the slot. The real part of the admittance (conductance) is mainly controlled by the offset of the slot whereas the imaginary part (susceptance) is mainly controlled by the length of the slot. The real part of the admittance is directly proportional to the excitation amplitude of the slot for a known excitation voltage created inside the waveguide at the slot's position. The angle of the admittance can be directly related to the phase of the field at the far zone of the slot. This far zone phase will be called the “radiation phase” throughout this work.

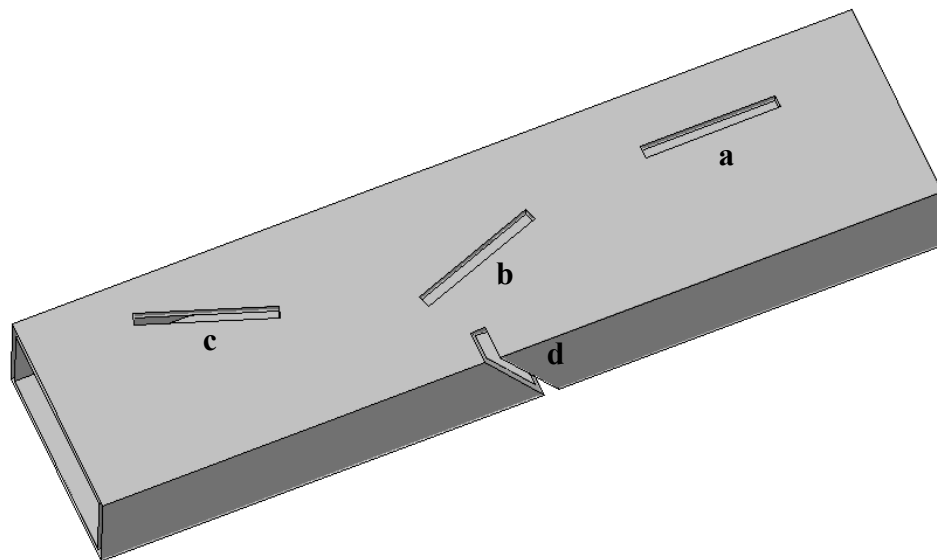


Figure 2.2 Most popular slot geometries carved on a rectangular waveguide

It is possible to obtain slots with purely real admittance. This condition is called resonance and a slot satisfying this condition is called resonant. A slot resonant at

the center frequency gives the best impedance bandwidth and therefore, most of the slotted waveguide arrays constitute resonant slots at the center frequency.

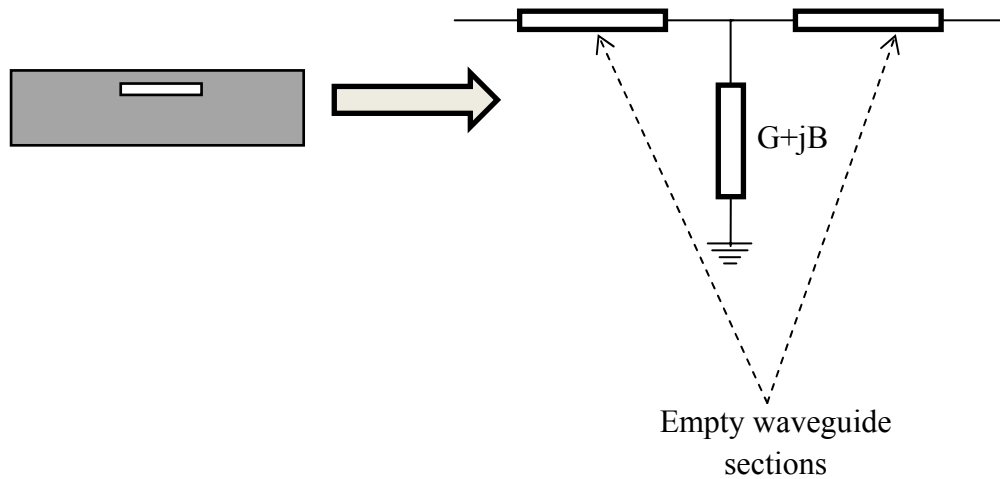


Figure 2.3 Shunt equivalent for offset broad wall slots

2.1.2 Inclined Broad Wall Slots

The slot with index “b” in Figure 2.2 is a typical inclined broad wall slot. These slots are able to block the longitudinal current components on the broad wall of the waveguide due to their inclined nature. Their polarization is mainly vertical; however, due to the inclination, a horizontal component exists as well whose amplitude depends on the inclination angle. As it can be inferred from Figure 2.1, the more inclined these slots are, the more they are excited. It has been shown in [11] that those slots have a series impedance equivalent circuit model as seen in Figure 2.4 as opposed to the shunt admittance model of the offset broad wall slots. The imaginary part (reactance) of the impedance is mainly controlled by the length of the slot and the real part (resistance) is mainly controlled by the inclination angle of the slot. It is again possible to obtain resonant slots by carefully choosing the slot parameters.

A major disadvantage of this slot against the broad wall slot is its low polarization purity. Since those slots are inclined, their aperture electric field vectors become inclined too and this create major cross polarization components at the far zone. Therefore, those slots are less likely to be chosen over their shunt counterparts.

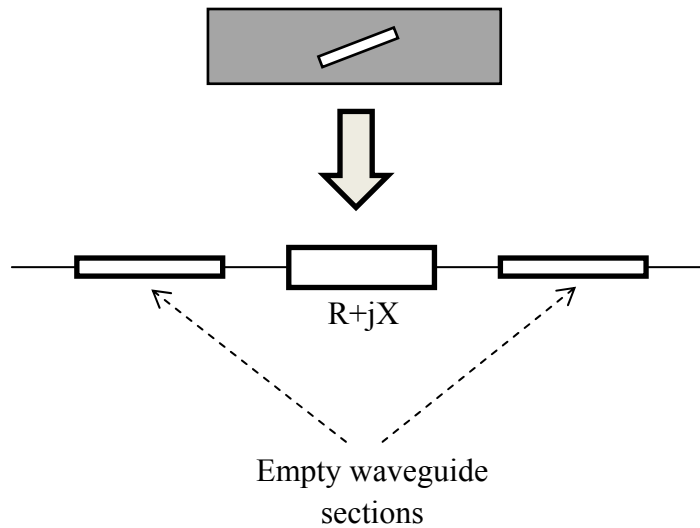


Figure 2.4 Series equivalent for inclined broad wall slots

2.1.3 Compound broad wall slots

The slot “c” on Figure 1.2 is a compound type of slot. These are a combination of offset broad wall and inclined broad wall slots. They have the advantage of controllable radiation phase while they are still resonant. That is, their radiation phase can be controlled without creating bandwidth problems. However, they have the same cross polarization problem as the inclined series slot. Additionally they lack a simple circuit model and can be represented by “pi” or “T” equivalent networks. These equivalent circuits do not provide a simple analysis procedure for a linear array and a scattering matrix based analysis is preferred. However, the design process becomes very complex using the scattering matrix of the slots instead of a simple lumped equivalent. Consequently, these slots are hardly used.

2.1.4 Inclined Edge Wall Slots

Inclined edge wall slots differ from the previous types in that they are carved on the narrow wall of the waveguide as seen in the slot with index “d” in Figure 2.2. These slots should interrupt the transversal current on the narrow wall because this is the only current component excited along the narrow wall as seen in Figure 2.1. Their polarization is mainly horizontal with a smaller vertical component depending on the slot’s inclination angle.

If an edge wall slot is non-inclined, it obviously becomes parallel to the narrow wall currents and is therefore not excited. By tilting the slot, the currents become interrupted and the slot radiates. The more tilted the slot is, the more intense the radiation. It has been shown that those slots have a shunt admittance equivalent circuit model as do the broad wall offset slots.

Most of the waveguides’ narrow walls are so narrow that slots opened on them cannot have purely real admittances without being wrapped around the waveguide corner as seen in Figure 2.2. The extra length due to the wrapping enables the slot to achieve its resonant length and a purely real admittance can be obtained.

These slots have the advantage of smaller inter-waveguide spacing when a planar array is formed because; planar arrays with these slots are formed at the E-plane of the waveguide. On the other hand, planar array with broad wall slots are formed at the H-plane, restricting the minimum inter-waveguide spacing to the width of the waveguide. This fact enables the edge wall slots to achieve greater electronic scan ability.

The major disadvantage of these slots is the same as the inclined type broad wall slots: severe cross polarization due to the inclined nature of the slots. Due to this, they are used instead of offset broad wall slots only when horizontal polarization is desired or extreme scanning capability is needed.

2.2 Slotted Waveguide Array Types

For creating uniform linear slotted waveguide arrays, there are two main topologies used, namely, standing wave type arrays and travelling wave type arrays.

2.2.1 Standing Wave Type Slotted Waveguide Arrays

A standing wave slotted waveguide array supports a standing voltage/field wave along the waveguide. At the center frequency, voltage maximum occurs at the location of each slot and the slots become excited in-phase if they have the same impedance or admittance angle. This behavior deteriorates with changing frequency and thus, a resonant behavior is observed.

An eight element center fed standing wave SWGA with uniform amplitude and in phase element excitation is seen in Figure 2.5. This array is terminated by waveguide shorts $\lambda_g/4$ away from the last and the first slots at the center frequency. Also, the slot spacing is $\lambda_g/2$ at the center frequency. This results in the equivalent network of Figure 2.6. Since the quarter wave lines transform shorts to opens and since the half wavelength lines does not affect the impedances; if the slot admittances normalized to the waveguide characteristic admittance are chosen as 0.25, the input admittance seen from left hand side of the feed and right hand side of the feed are both equal to 1. This occurrence of purely real input impedance at a definite frequency is called resonance.

If we solve for the voltages across the admittances in Figure 2.6, it is seen that they are all equal. Therefore, a uniform and in-phase excitation is achieved.

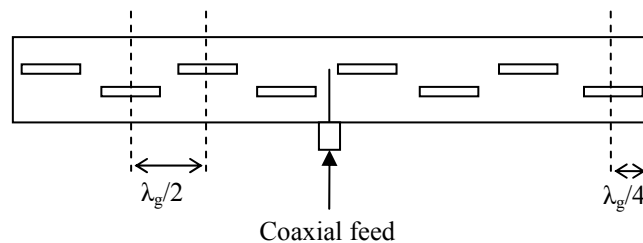


Figure 2.5 An eight element center fed standing wave type SWGA

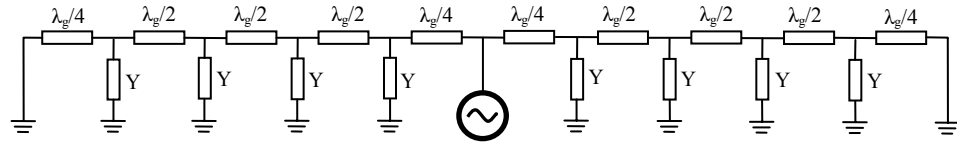


Figure 2.6 Lumped equivalent circuit of the SWGA in Figure 2.5

When the frequency deviates from the center frequency, the electrical lengths between spacings change and they are no longer $\lambda_g/2$. This causes the input impedance to be complex. Additionally, the desired in-phase and uniform distribution is no longer available because, for a spacing different than $\lambda_g/2$, the voltages across the admittances vary from slot to slot in terms of both the magnitude and phase.

The speed of variations on the slot voltages and input impedance with respect to the amount of deviation from the center frequency is a function of the array's size. The smaller the array is, the smaller the variations are and thus the greater the usable bandwidth is. This effect can be directly seen by analyzing the voltages of the circuit in Figure 2.6 for fixed frequency with different array sizes. Therefore this type of arraying is not suitable for creating large, low sidelobe planar arrays without using sub-arraying techniques at each waveguide row.

In Figure 2.5, it is seen that the slot offset direction is alternating between consecutive slots. This is required to create an in-phase excitation because, there exists a 180 degrees phase difference between consecutive voltage maxima. The alternation of slot offset creates another 180 degrees phase difference completely nullifying any phase difference at the center frequency. The phase reversal with opposite offset is best understood by referring to Figure 1.1. It is seen in Figure 1.1 that, transversal currents on the upper half of the broad wall are exactly pointing to the opposite direction compared to the transversal currents at their mirror locations with respect to the broad wall center line. Therefore, electric fields created on a slot's aperture by these currents are 180 out of phase. This phase reversal mechanism is used in almost all of the slotted waveguide arrays.

2.2.2 Travelling Wave Type Slotted Waveguide Arrays

Travelling wave arrays principles are the same as the travelling wave continuous line sources' principles given in [17]. It is a series fed array topology where energy enters to the array from one side, radiated by each of the array's elements and the remaining energy is dissipated at the matched load connected to the end of the array. The only difference with the travelling wave continuous line source radiators is that the radiation locations are discretized to the element locations.

For travelling wave arrays to work properly, it is required that the reflection coefficient of each element is small (-10dB may be used as an upper limit for the reflection coefficient) and that the reflected wave from the elements do not add up in the backward direction. For SWGA case the adding up of the reflected fields from each element is prevented by choosing a slot spacing not very close to $\lambda_g/2$ [1]. The small reflection coefficient criterion is also satisfied by using shunt elements. The following assumptions can be made for a large, travelling wave array if certain conditions are satisfied:

- Each slot radiates a fraction of the incident power on them determined by the conductance of the slot and the rest of the power is totally transmitted to the next slot.
- The normalized input impedance after each slot towards the load is always equal to 1.

These assumptions are mostly satisfied if the following criterion is met by the array [2] and if the array is large:

$$g_{\max} < 0.447 \sin(\beta_g d) \quad (2.1)$$

The inequality (2.1) relates the maximum usable slot conductivity " g_{\max} " to slot spacing " d " and waveguide propagation constant " β_g " for the satisfaction of the two previously mentioned assumptions. The satisfaction of the two assumptions leads to a basic design equation for travelling wave type SWGA:

$$g_n = \frac{P_n}{P_L + \sum_{k=n+1}^N P_k} \quad (2.2)$$

Where g_n is the n^{th} slot's conductance, P_n is the normalized radiated power by the n^{th} slot, P_L is the power dissipated at the terminating load and N is the total number of slots in a single row. If (2.1) is not satisfied, the excitation coefficients differ from the desired values. The deviation from the desired values is directly related to g_{max} value; the more severely it violates (2.1), the greater the deviation is.

It is seen from (2.2) that for designing a travelling wave SWGA with uniform amplitude distribution, the conductance of the slots should increase from the feed end towards the load end. This is due the decrease in the magnitude of the incident power on the slots when the load side is approached. Incident power is decreasing but the radiated power is always constant; therefore, conductance of the slots should increase towards the load. An eight element uniform amplitude design should look like the array in Figure 2.7. It is seen that the offsets of the slots increase towards the load to keep the conductance increasing.

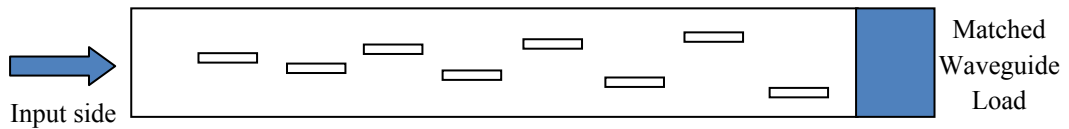


Figure 2.7 A conceptual uniform distribution eight element travelling wave SWGA

It is also worth noting that the phase reversal mechanism employed in standing wave arrays is used again in this case. Normally, the phase difference between the excitation voltages of the two consecutive slots is determined by:

$$\phi = \beta_g d \quad (2.3)$$

However, since this progressive phase difference is generally between 130 and 230 degrees, an extreme squint angle occurs for the main beam of the array which changes very rapidly with the frequency and which greatly reduces the directivity

of the array. In order to reduce this squint and make it more slowly varying with respect to the frequency, the phase reversal mechanism is used and the progressive phase difference is generally restricted to the interval of -50 to 50 degrees. The final progressive phase difference expression is therefore:

$$\phi = \beta_g d - \pi \quad (2.4)$$

Travelling wave type SWGA has the advantage of broadband impedance match when compared to its standing wave counterpart. Additionally, the amplitude distribution across the array is degraded more slowly with respect to the frequency because, the feeding mechanism of the slots does not affect the amplitude distribution. The only degradation in the amplitude distribution occurs due to the variations in the admittances of the slots with changing frequency.

The most severe disadvantage of the travelling wave SWGA is the squint of the beam due to a progressive phase difference given by (2.4). Since the rectangular waveguide is a dispersive medium, this phase difference does not change linearly with respect to the frequency, the squint angle of the main beam changes with the frequency and prevents the antenna from being used in applications where a large instantaneous bandwidth is required like SAR applications.

CHAPTER 3

A NOVEL NON-INCLINED EDGE WALL SLOT

This chapter focuses on the characterization of novel non-inclined edge wall slot geometry for the isolated case and for the case of an infinite array where the mutual coupling effects are considered. Using the characterization data, the horizontally polarized part of the dual polarized array is designed using non-standard waveguide geometry. Additionally, to verify the proposed geometry, a smaller planar array is designed, simulated and manufactured. The measurement results are compared with the simulation results.

3.1 Introduction

The requirement of very low cross polarization for both polarization components of the antenna prevents us from using the inclined edge wall slots as the horizontally polarized radiator part of the antenna. As analyzed in [18] a linear or planar inclined edge wall slot array has an azimuth radiation pattern like the one given in Figure 3.1 where the second order cross polarized lobes are easily observed. Therefore it is decided to use a non-tilted edge wall slot which is again wrapped around the corners of the waveguide. This choice makes the aperture electric field vectors of the slots parallel to the horizontal axis minimizing the cross polarized components at the far zone.

The following requirements are imposed for the design of the radiation element for horizontal polarization:

- Slot should have very low cross polarization levels.

- The manufacturing process should be simple, reliable and accurate and precise.
- Slot's radiation amplitude and phase should be controllable.
- Slot's scattering characteristics should allow its use in travelling wave type arrays.
- The waveguide on which the slots are carved should allow its use in a dual polarized array with phase scanning abilities.

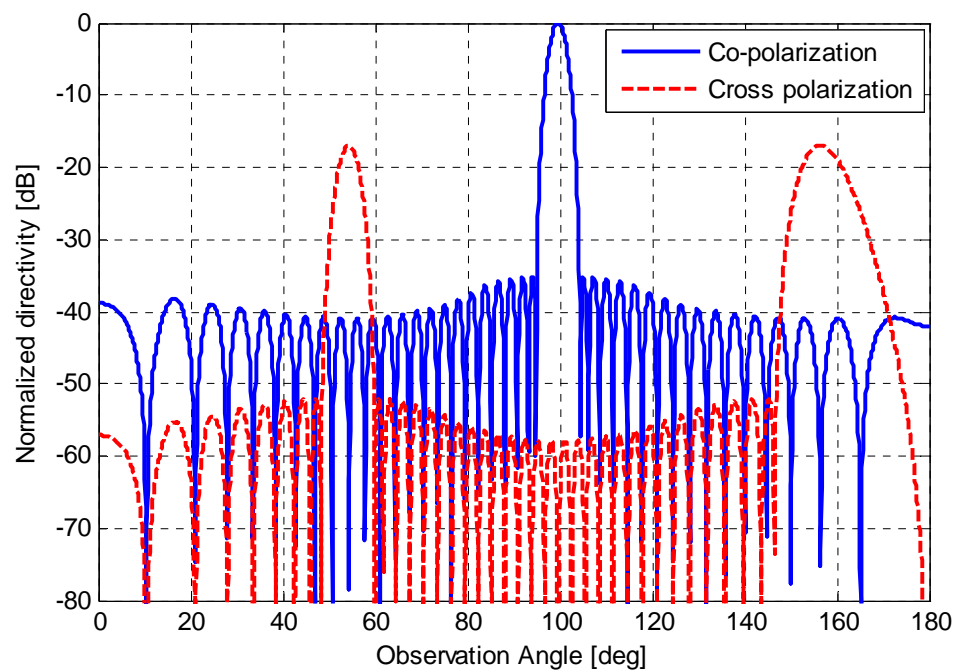


Figure 3.1 Typical azimuth radiation pattern for an inclined edge wall slot array.

3.2 Excitation of Non-Inclined Slots

Many non-tilted slot configurations can be found in the literature [4-6,19-21]. However, since the non-tilted slot is unexcited by nature, all of the non-tilted slots in the literature requires placement of excitation structures near the slot. This is performed by first carving the slots on an empty waveguide and then, carefully inserting the excitation structures and fixing them to the waveguide walls. The

excitation structures are generally inclined metallic wires as in [5,6,19], iris structures as in [4,20] and dielectric structures with metal parts [21]. To obtain the desired amplitude distribution across the waveguide, each excitation structure should have a different geometry than the others. These differences may include different iris sizes, shapes, iris to slot distances, different wire placement angles etc. The disadvantages of this fact are: need for precise post-production placement of these structures, lack of reliable fixing methods and increased labor costs.

To eliminate the aforementioned disadvantages, it is desirable to design a slot with excitation structures integrated to the waveguide walls. This provides the ability to manufacture the whole antenna structure from a single aluminum block. Therefore, the excitation structures should be different from wire or thin iris type structures. Additionally, to further facilitate the manufacturing and to make it more robust, it is better to have only right angled corners on the excitation structure as opposed to non-right angled vertices created by tapered edges as seen in [4]. Consequently a novel inset structure suitable to production with a 3-axis CNC milling machine is proposed as the excitation mechanism.

The proposed slot comprises a standard non-tilted slot with two excitation insets at each side of the slot sitting on opposite broad walls as seen in Figure 3.2. These insets are like iris structures seen in [4,20] and they alter the edge wall currents so that they become interrupted by the non-tilted slot. However, they are free of tapered edges, they are not necessarily thin and they have the advantage of being manufactured together with the rest of the antenna from a single aluminum block. The integrated manufacturing causes finite radii at the edges of the insets where connection with the broad wall is established. These radii do not cause problems when they are modeled in the electrical analysis. These insets alter the edge wall currents so that they become interrupted by the non-tilted slot. Thus, the slot radiates.

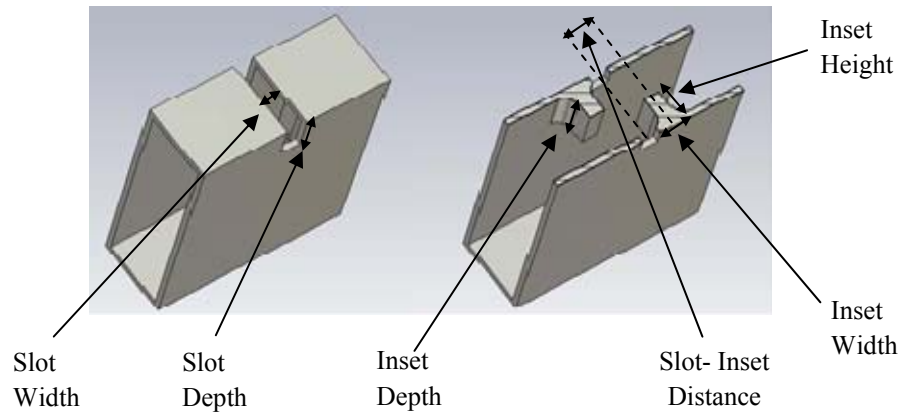


Figure 3.2 Proposed slot geometry for non-inclined edge wall slots with its attributed parameter terminology.

3.3 Slot Modeling

3.3.1 Radiation Control

In order to design an array out of these slots, it is essential that the radiation property of each slot on the array be controllable. That is, there should be a control mechanism for the radiation amplitudes and phases of the slots. In these slots' case, there are many parameters controlling the radiation properties namely, slot depth, inset height, inset depth and slot-inset distance. Slot width and inset width also have effects on radiation properties related to the frequency bandwidth and equivalent circuit models and they are mentioned in the Section 3.3.3.

Since the array to be designed will be a travelling wave type, it is expected that the return loss of the structure seen in Figure 3.2 be low. It is desired that the reflected power from a slot should be 20dB smaller than the power radiated by the neighboring slots. Otherwise, the reflected power may alter the radiation amplitude and phase of the neighboring slots. That is, almost all of the power which is not radiated by a slot should be incident to the next slot. If this is not the case, the design formula (2.2) cannot be used and full scattering properties of the slots should be taken into account to determine the slot parameters required to create the desired distribution. In the following section, it will be shown that these slots have

reflection coefficients similar to the shunt slots and further, they can be modeled as shunt slot if certain conditions are met.

3.3.2 Characterization

The proposed slot's radiation properties should be characterized with respect to the geometrical parameters of the slot as previously mentioned. For this purpose, a waveguide section with a single slot, as seen in Figure 3.3 is used for simulation in Ansoft HFSS, an FEM based electromagnetic simulator. All of the simulations are performed using this software. Waveports are defined at each end of the waveguide so that scattering parameters of the slot are obtained for the TE₁₀ mode excitation.

Waveports in HFSS are excitation surfaces defined by the user over a cross section of an arbitrarily shaped waveguide. They are used by the simulator to find the field distribution and parameters of the different modes to be excited. After the excitation modes are found, the problem is solved for unity excitation from each mode of each waveport defined such that all the other modes have zero excitation. This way, couplings of all of the modes defined in the model are calculated which give the S-parameters of the model.

The boundaries of the air box surrounding the waveguide are defined as radiation boundaries except the bottom boundary which is defined as PEC. Various parameter sweeps are performed with the created model and the results are plotted. In fact there are a total of two parameters to plot in terms of geometrical parameters. The first parameter is the normalized radiation power calculated using the S-parameters as follows:

$$P_r = \frac{1 - |S_{11}|^2 - |S_{21}|^2}{|S_{21}|^2} \quad (3.1)$$

The numerator of (3.1) is the radiated power by the slot when 1W is incident from port 1. The denominator is the power transferred to the rest of the waveguide. Therefore, the radiated power by the slot is normalized by the power transferred to the rest of the waveguide.

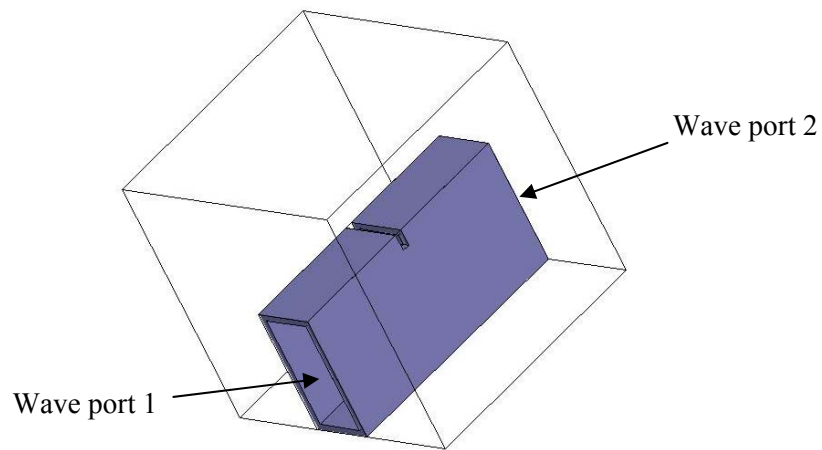


Figure 3.3 The simulation model for an isolated slot

The second parameter which is the phase of the radiated fields by the slot can be determined by any of the following two methods: calculating the voltage across the aperture of the slot by integrating the E-field along a line across the slot width as seen in Figure 3.4 and taking its phase or by directly looking to the far zone phase. Both of these methods are used in this work and they give the same results.

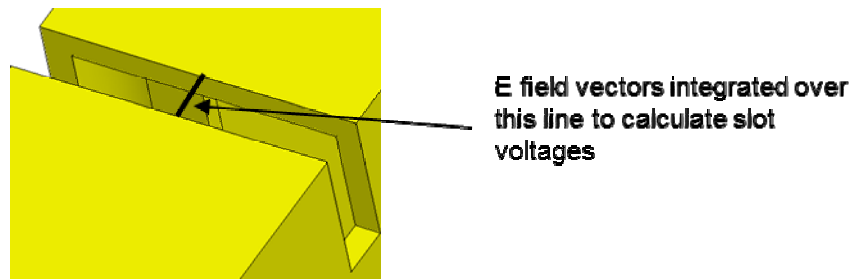


Figure 3.4 The integration line on which the slot voltage is calculated

In the first sweep, a slot with the following parameters is created on a standard WR90 waveguide section with width 22.86mm, height 10.16mm and wall thickness 1.27mm:

- Slot width 1.5 mm
- Inset width 1 mm
- Inset-slot distance 1.5 mm
- Inset height 2 mm
- Inset depth 6mm

The slot's wrap depth is swept from 2 mm to 5 mm with a step size of 0.2 mm. The radiation amplitude and phase are plotted with respect to wrap depth in Figure 3.5 and 3.6, respectively. As seen in those figures, changing the wrap depth greatly changes the radiation phase of the slot. The radiation amplitude also changes too; however, the maximum amplitude achieved is very low. Therefore, changing wrap depth is a tool to control the radiation phase but is not enough to control the radiation amplitude.

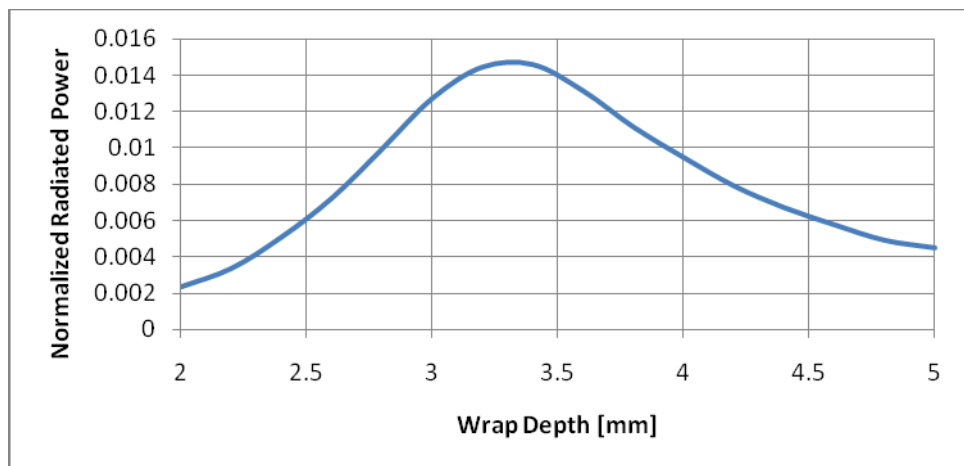


Figure 3.5 Normalized radiated power vs. wrap depth

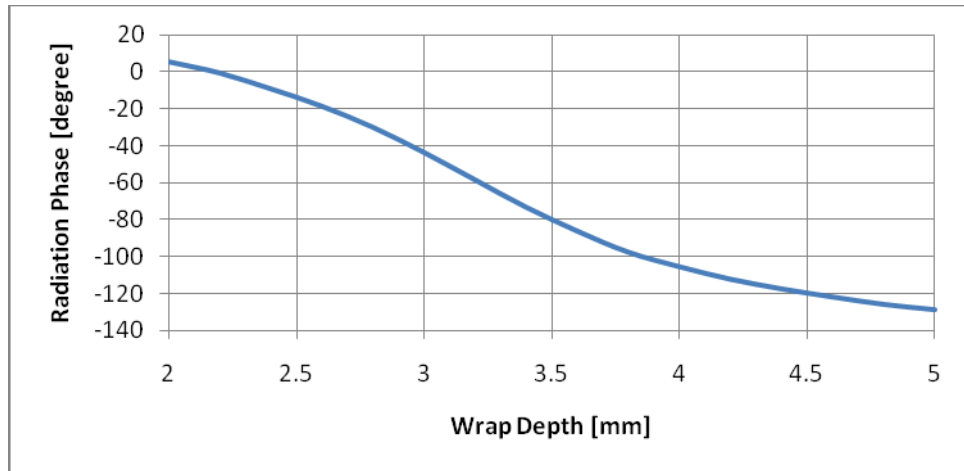


Figure 3.6 Radiation phase vs. wrap depth

The next sweep is on the height of the slot. The slot parameters are same as before except the wrap depth is fixed to 3.3 mm. The inset height is swept from 0.5 mm to 4.5 mm. The radiation amplitude and phase are plotted with respect to inset height in Figure 3.7 and 3.8, respectively. It is seen that, the inset height can modify the slot's radiation amplitude in a great range. Both very low and very high amplitudes can be achieved. On the other hand, the inset height has a minor effect on the radiation phase.

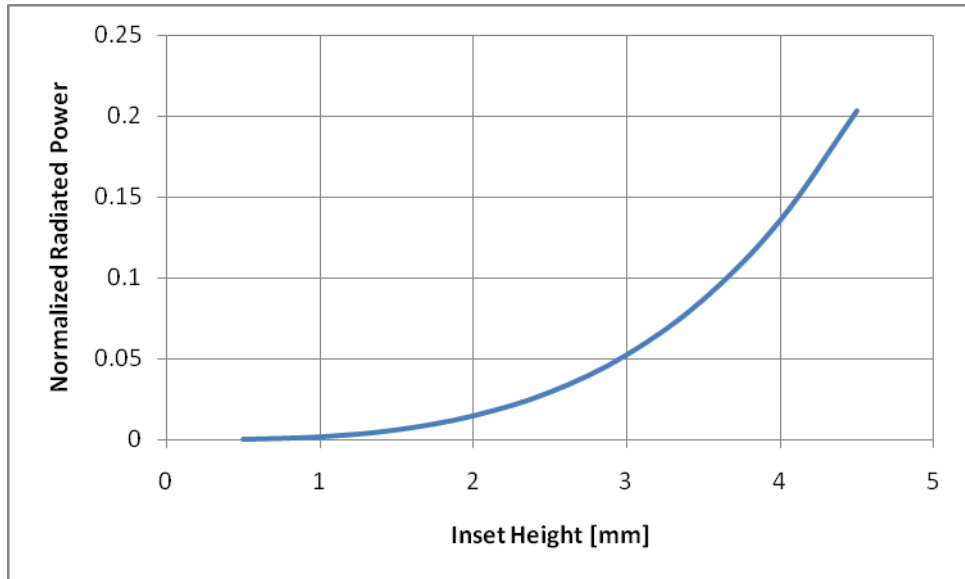


Figure 3.7 Normalized radiated power vs. inset height

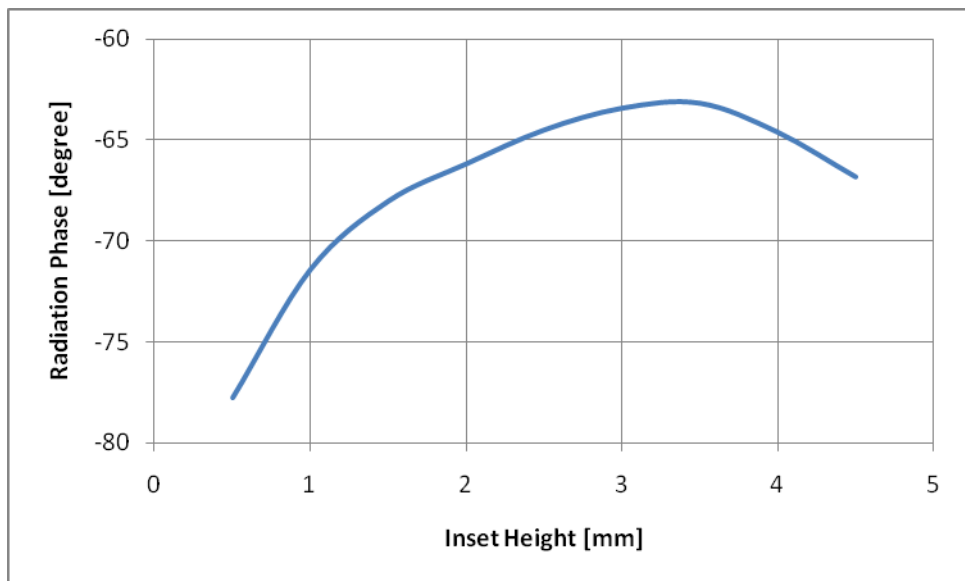


Figure 3.8 Radiation phase vs. inset height

The next sweep is on the depth of the insets. The slot parameters are kept the same as before. The inset depth is swept from 3 mm to 10 mm. The variation of the normalized radiated power and radiation phases are plotted in Figure 3.9 and 3.10, respectively. It is observed that the radiation amplitude is affected by the inset depth but it almost becomes constant after the inset depth reaches 8 mm. When the radiation phase is considered, it is seen that it is almost independent of the inset depth.

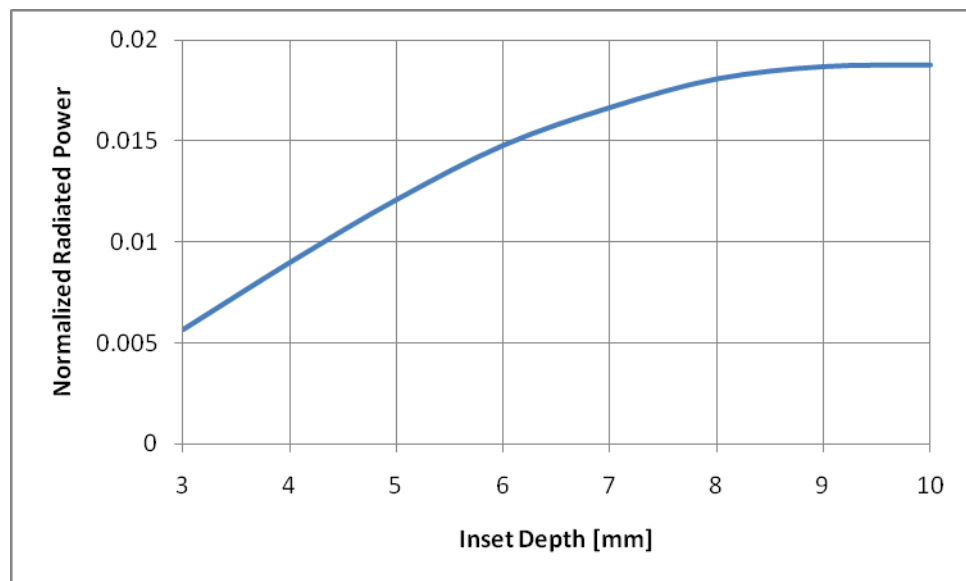


Figure 3.9 Normalized radiated power vs. inset depth

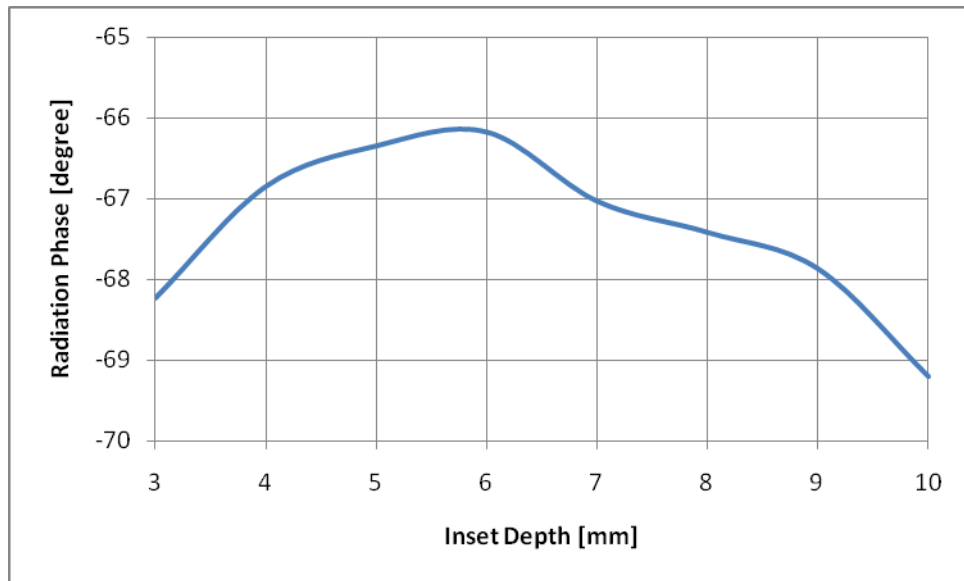


Figure 3.10 Radiation phase vs. inset depth

Apart from the radiation properties of the slot, the inset depth has other effects related to the scattering parameters of the slot. As seen in the Figure 3.11, the inset depth greatly affects the reflection phase from the slot while keeping the transmission phase constant. Also, as observed from Figure 3.12, the inset depth affects the reflection magnitude from the slot too. For traveling wave type of arrays, it would be better to choose a reflection coefficient as low as possible. Additionally, the variation of the scattering parameters with respect to the inset depth will have a key role in the determination of the equivalent circuit model which is presented in Section 2.2.3 in detail.

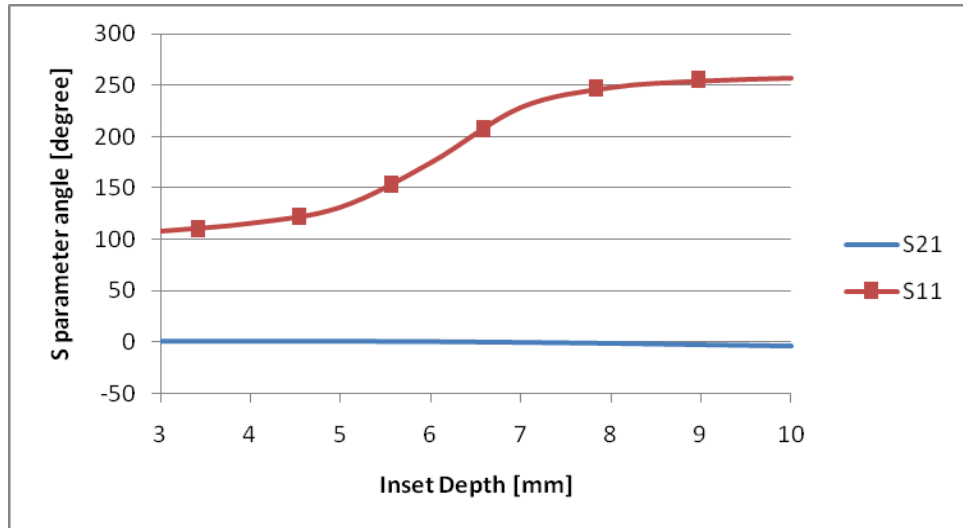


Figure 3.11 S parameter angle vs. inset depth

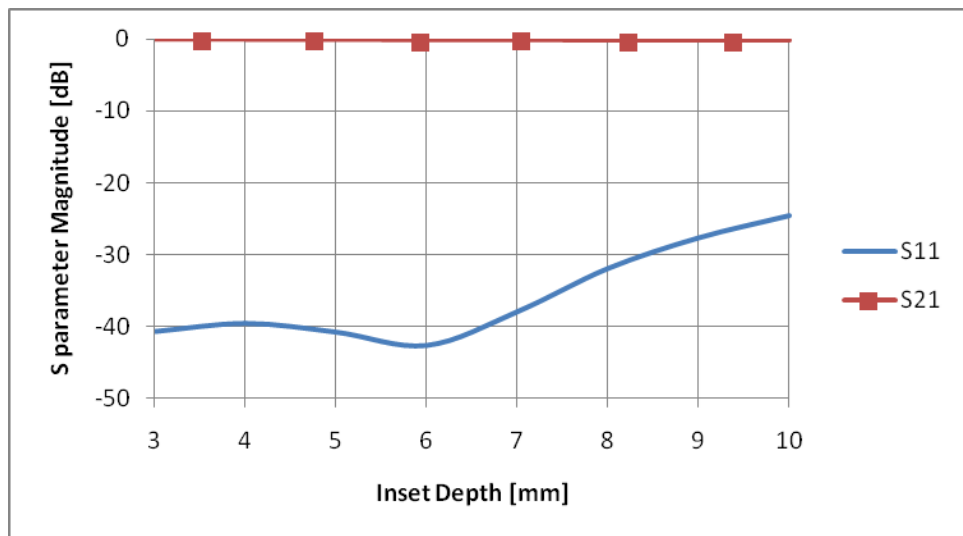


Figure 3.12 S parameter magnitude vs. inset depth

The distance between the slot and the insets is another slot parameter to be swept. Simulations are performed for this distance varying between 0.5mm and 2mm. Other parameters of the slot are constant with inset height being 4mm to obtain a high excitation. As expected, it is seen in Figure 3.13 that, the excitation gets weaker with increasing slot-inset distance. This is because of the slot getting farther away from the source of the surface current disruption. The surface currents resemble to their unperturbed counterparts when one looks at a distant point from the inset.

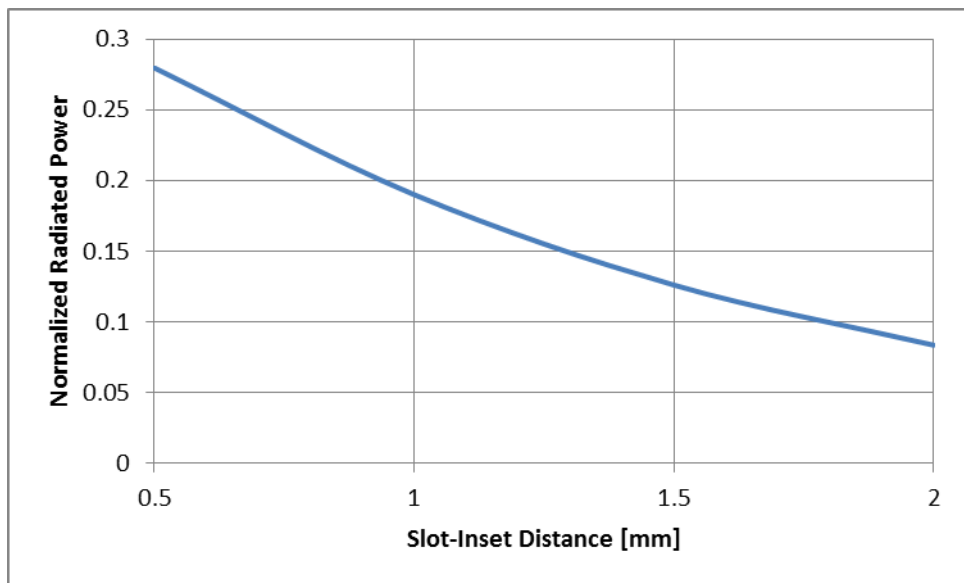


Figure 3.13 Normalized radiated power vs slot-inset distance

A careful choice should be made when determining the slot inset distance to be used in the array. A too large value can limit the maximum available radiated power from the slot, whereas, a too small value can make the slot excitation very sensitive to mechanical tolerances. For example, assume that the maximum normalized radiated power used in an array is 0.2. It can be achieved with an inset height of 3mm for an inset distance of 0.5mm and with an inset height of 4.5mm for an inset distance of 1mm. In the former case, a mechanical range of 3mm is required to obtain a normalized power range of 0.2. However, in the latter case, the

same normalized power range is obtained with a mechanical range of 4.5mm. It can be shown by a simple analysis that the same mechanical deviation in both cases causes more normalized power deviation in the former case. Therefore, the former case's slots are said to be more sensitive to mechanical tolerances.

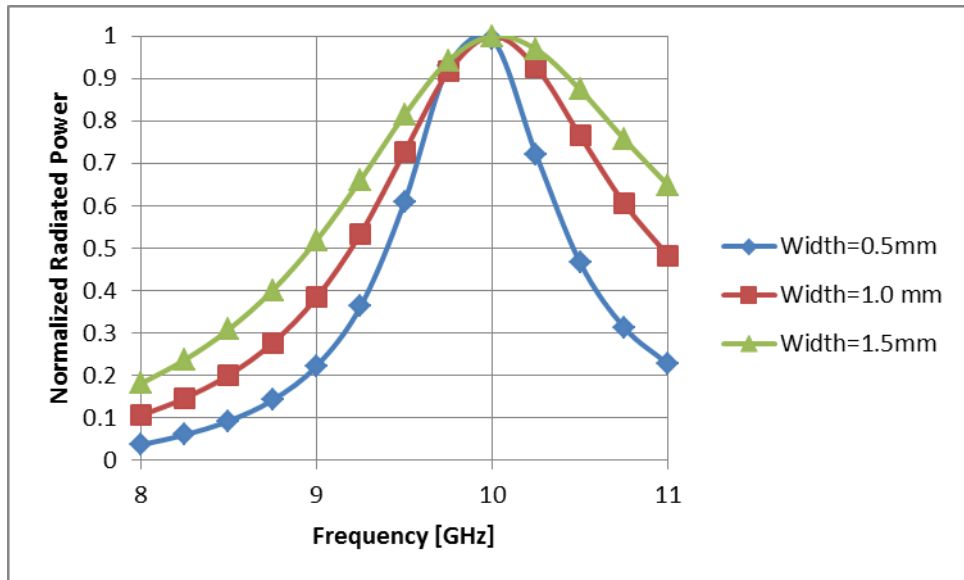


Figure 3.14 Normalized radiated power vs. frequency for different slot widths

A final sweep is performed on the width of the radiating slot. It is observed that width of the slot has a major effect on the bandwidth of the slots and therefore, frequency sweeps are performed in the X-band region for three different slot widths which are 0.5mm, 1.0mm and 1.5 mm. The radiated powers which are normalized to their respective maximum values for all slots width are plotted against the frequency in Figure 3.14. For the ideal case, it is desirable to have a constant normalized radiated power with respect to the frequency. However, this is not the case and the normalized radiated power is varying with frequency reaching a peak for a definite frequency which depends on the other parameters of the slot. As seen in Figure 3.14, the variation rate of the radiated powers with respect to frequency tends to increase with slot width getting smaller. Therefore, it is desirable to use a wider slot if more usable bandwidth for the final array is desired.

Nevertheless, it is seen in the Section 3.2.3 that mutual coupling effects greatly impact the bandwidth of the slots and the excellent bandwidth enhancement observed in Figure 3.14 by widening the slots does not provide the expected usable bandwidth in the final array.

Another effect of the slot broadening is a decrease in the radiated power from the slot. As the slot gets wider, the distance between the excitation insets gets larger and the excitation effect of the insets on the slot gets smaller. The maximum radiated power normalized to the corresponding transmitted powers provided by each slot in the previous frequency sweeps are plotted in Figure 3.15. The decrease in the radiated power from the slot with increasing width has two major effects for the array design:

- It restricts the maximum power which can be radiated by a slot in the array to a lower value. This is a disadvantage especially for smaller arrays because; it desirable to radiate as much of the available power as possible before it reaches the terminating load. Therefore, having a smaller maximum radiated power may decrease the efficiency of the array by letting more power going to the load.
- It maps the range of excitations to be used by the slots to a wider mechanical range as in the case of increased inset distance. This provides the same mechanical tolerance advantage gained in the increased inset distance case.

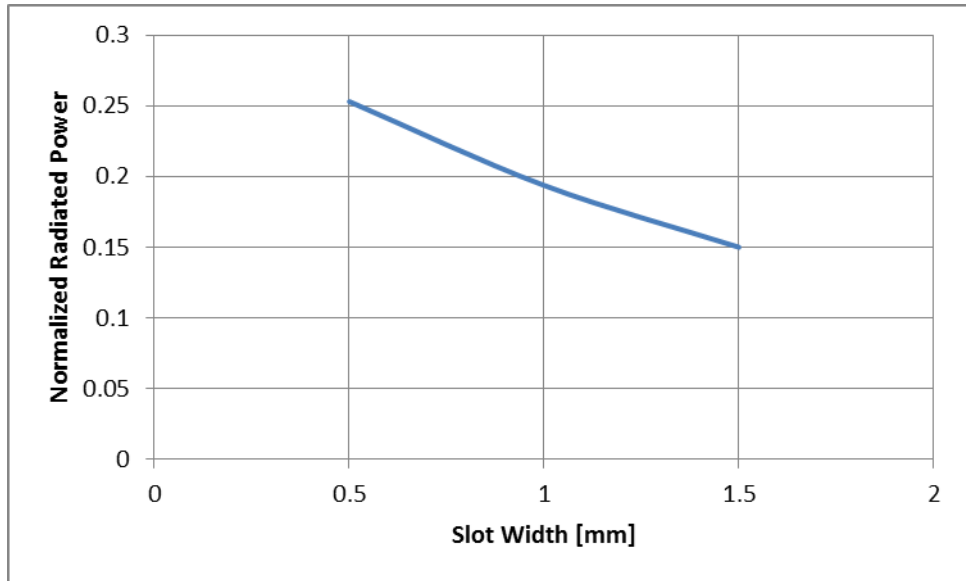


Figure 3.15 Normalized radiated power vs. slot width

To see more sophisticated effects of the slot parameters on the radiation and scattering characteristics of the slots, a possible existence of an equivalent circuit model is investigated.

3.3.3 Equivalent Circuit Model

It is already mentioned that the inclined edge wall slots can be modeled with a shunt admittance circuit equivalent for scattering analysis. In this section, it is investigated whether these slots have a shunt model equivalent.

For a two port network to have a shunt equivalent as seen in Figure 2.3, it is obvious that the following criterion on S parameters should be satisfied:

$$S_{21} = 1 + S_{11} \quad (3.2)$$

If (3.2) is satisfied, the admittance of the two-port can be expressed either in terms of the transmission parameter or the reflection parameter as follows:

$$Y = \frac{2(1 - S_{21})}{S_{21}} \quad (3.3)$$

$$Y = \frac{-2S_{11}}{1 + S_{11}} \quad (3.4)$$

To test the validity of the shunt admittance model for the proposed slots, various full wave EM simulations are performed for different excitation settings and possible admittance values are calculated using both (3.3) and (3.4).

First of all, a sweep is performed by HFSS for the slot structure in Fig 3.2 with inset height taking values between 1mm and 5mm. For each case, a frequency sweep is performed and the presumptive admittance values are calculated using both (3.3) and (3.4). The validity of the shunt slot model is checked by comparing the two admittance values obtained with two different scattering parameters. The variations of the two different types of -equivalent admittance values with respect to the frequency for each inset height are plotted in Figures 3.16 - 3.20. In all of these graphs, blue curves are for parameters calculated using reflection coefficient, equation (3.4) and red curves are for parameters calculated using the transmission coefficient, equation (3.3). Also, continuous lines are for conductance values, whereas, dashed lines are for admittance angle values.

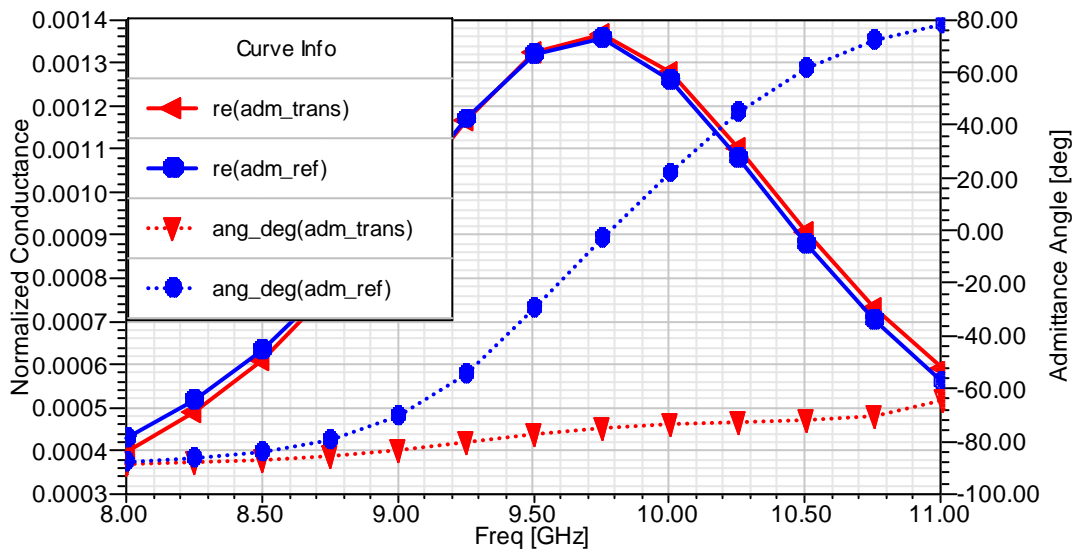


Figure 3.16 Admittance parameters vs. frequency for inset height of 1.0mm

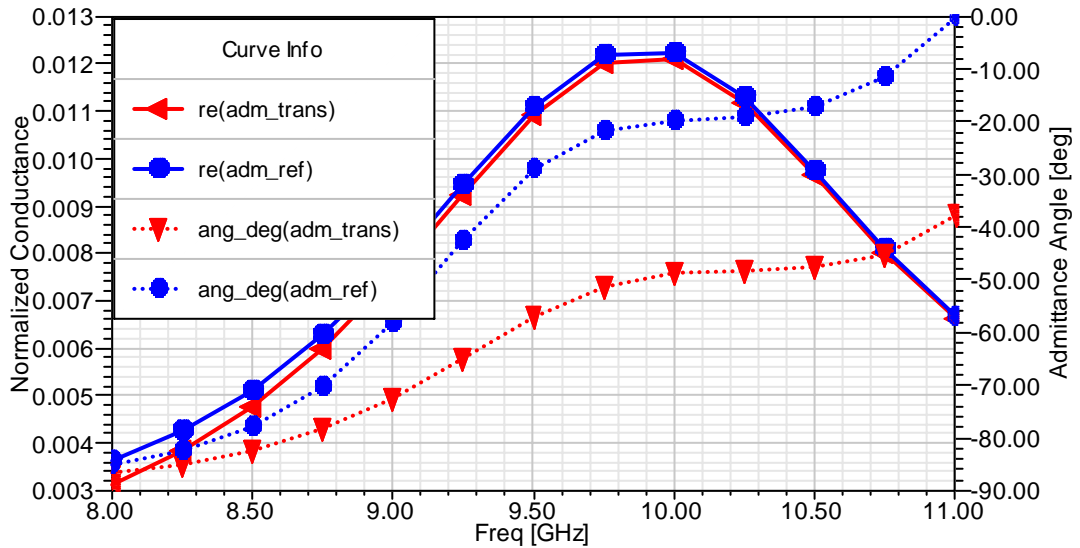


Figure 3.17 Admittance parameters vs. frequency for inset height of 2.0mm

It is seen from the Figures 3.16 – 3.20 that conductance values calculated using both (3.3) and (3.4) are almost the same regardless of the inset height. However, when the inset height is decreased, the angles of the calculated admittances start to differ from each other. It can be deduced that, these slots can be modeled as shunt admittances for moderate to high excitation values; however, the accuracy of the model is weakened as the excitation decreases.

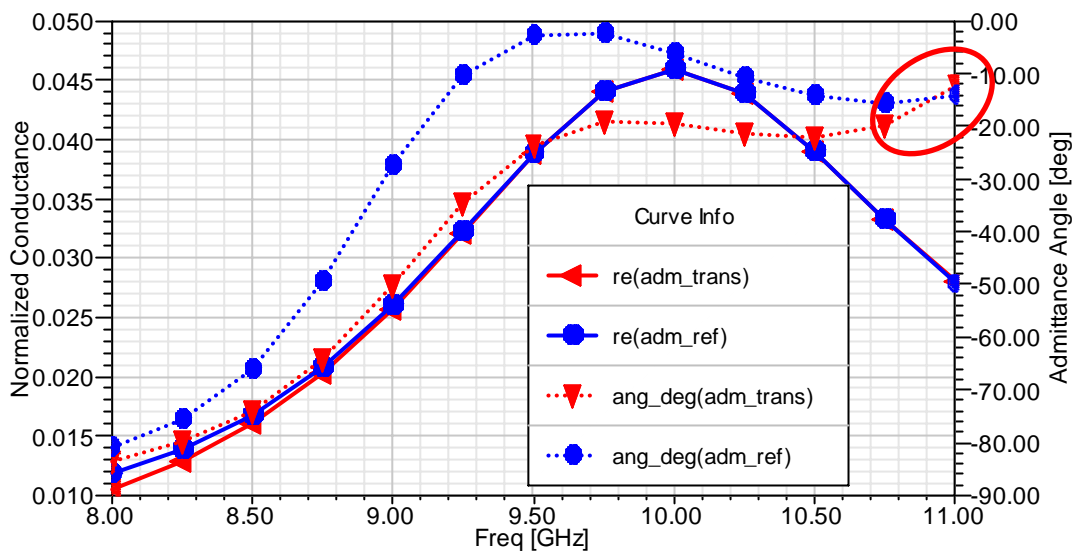


Figure 3.18 Admittance parameters vs. frequency for inset height of 3.0mm

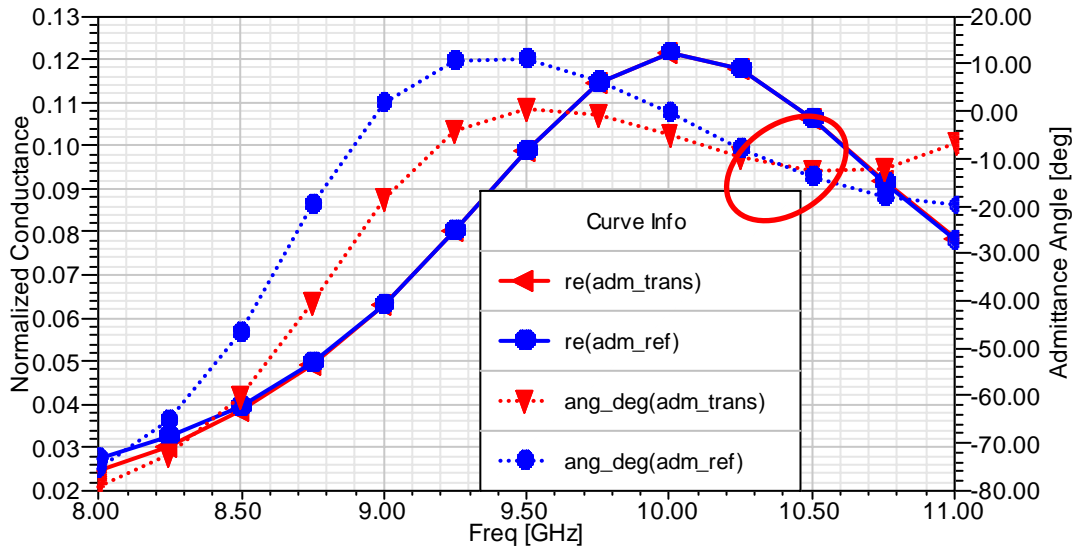


Figure 3.19 Admittance parameters vs. frequency for inset height of 4.0mm

There is also a slot parameter controlling the accuracy of the shunt admittance model used: the width of the inset. To see the effects of this parameter, the width is changed from 0.5mm to 2mm with 0.5mm steps. Frequency sweeps are performed and - equivalent admittances are calculated as it is done for other parameters. The results are seen in Figure 3.21 – 3.24. It is clear that, decreasing inset width have a positive effect on the accuracy of the shunt admittance model. This is because the admittance angles calculated using (3.3) and (3.4) become closer to each other with decreasing inset width, around the frequency point where the normalized conductance value reaches its highest value. Therefore, it would be wise to make the insets thinner in applications critically depending on the accuracy of the shunt slot model. A standing wave type array is an example to this kind of application.

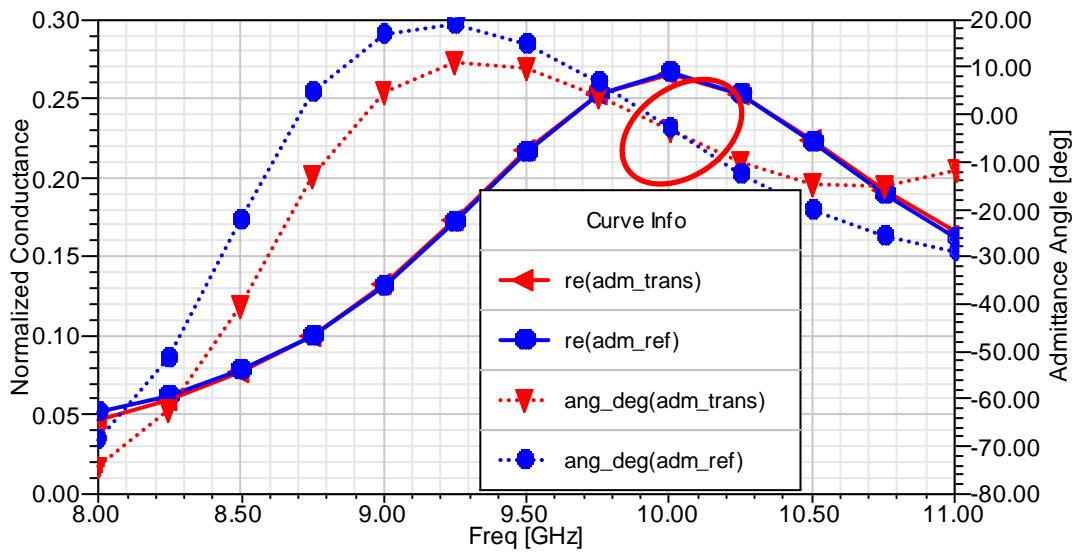


Figure 3.20 Admittance parameters vs. frequency for inset height of 5.0mm

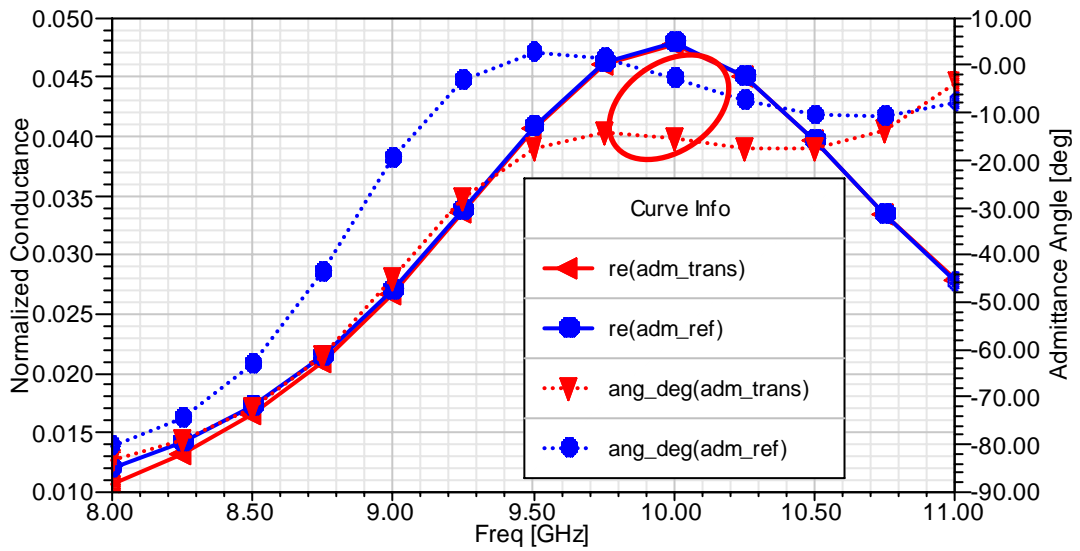


Figure 3.21 Admittance parameters vs. frequency for inset width of 0.5mm

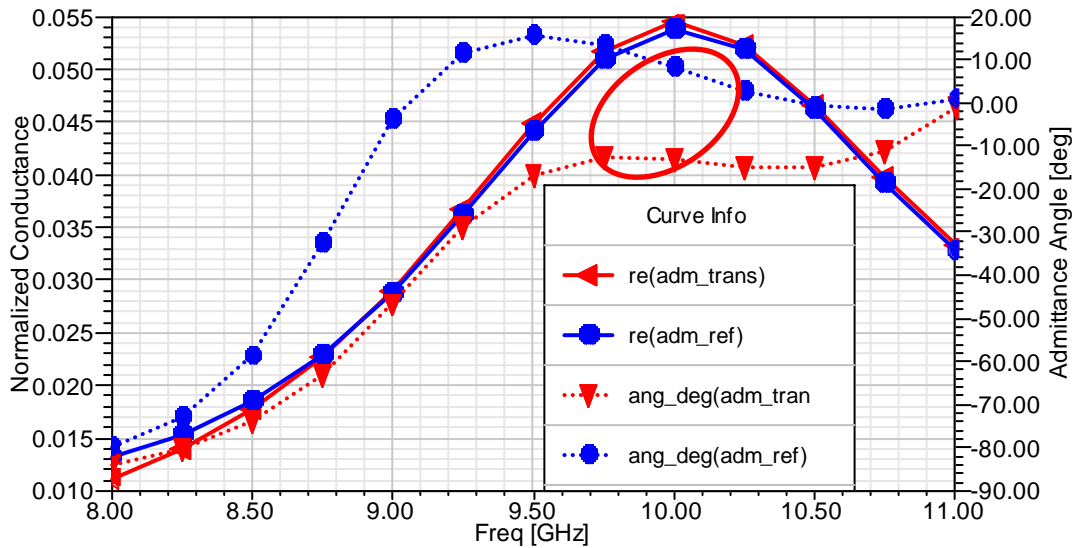


Figure 3.22 Admittance parameters vs. frequency for inset width of 1.0mm

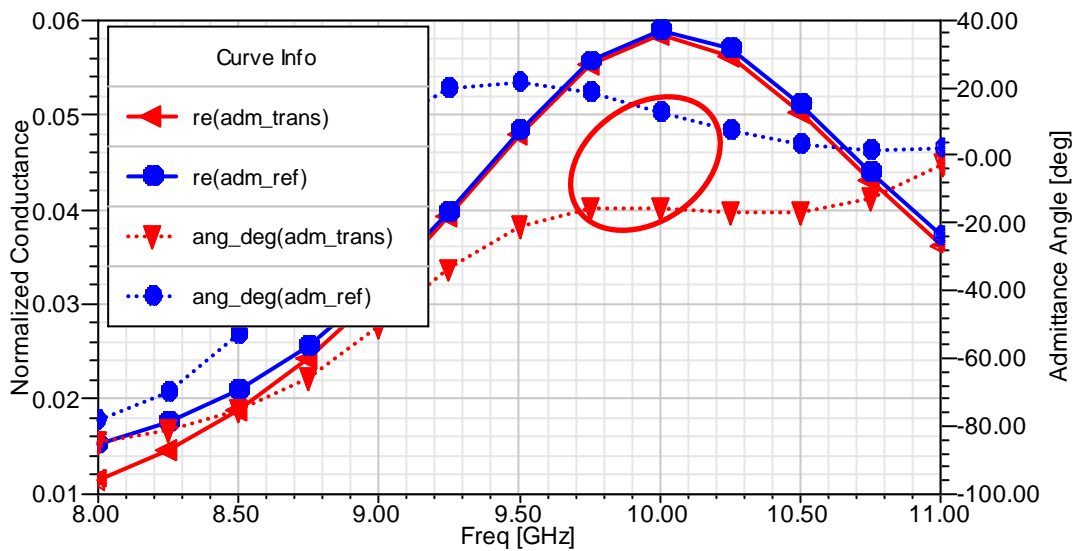


Figure 3.23 Admittance parameters vs. frequency for inset width of 1.5mm

Another interesting feature of these slots is that, the angle of their admittance values can be changed without affecting the radiation phase severely. This also changes the frequency at which the shunt slot model is satisfied exactly. To show this property, the simulations performed with inset height 4mm and 5mm repeated with inset depth values of 6.3mm and 7mm, respectively, instead of the previous value of 6mm for both cases. The new admittance values are plotted in Figure 3.25

and 3.26. For both of the cases, the frequency at which the shunt model is exactly valid, has changed and so do the admittance phases at the frequency where maximum conductance is achieved, when compared to Figures 3.19 and 3.20.

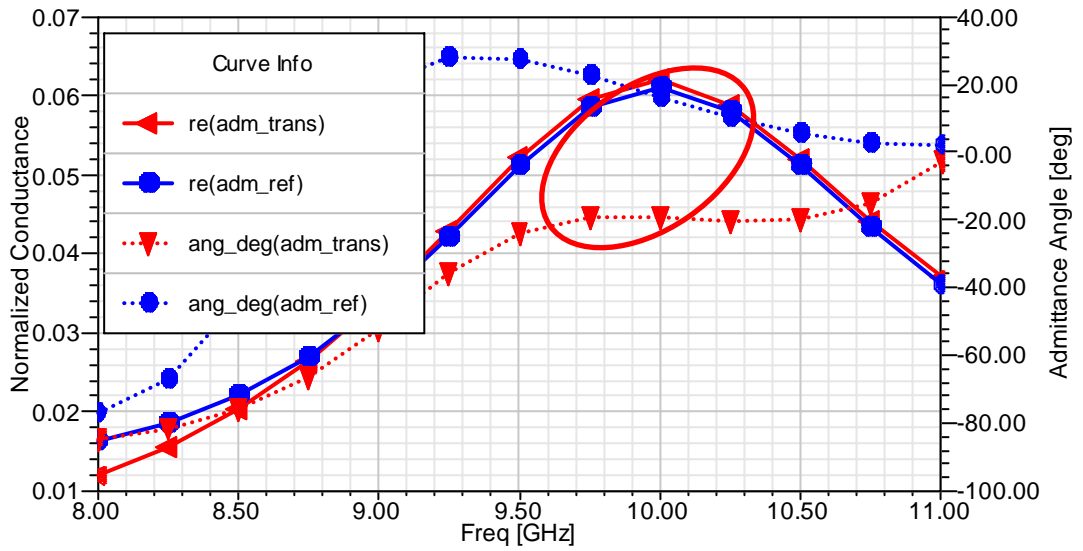


Figure 3.24 Admittance parameters vs. frequency for inset width of 2.0mm

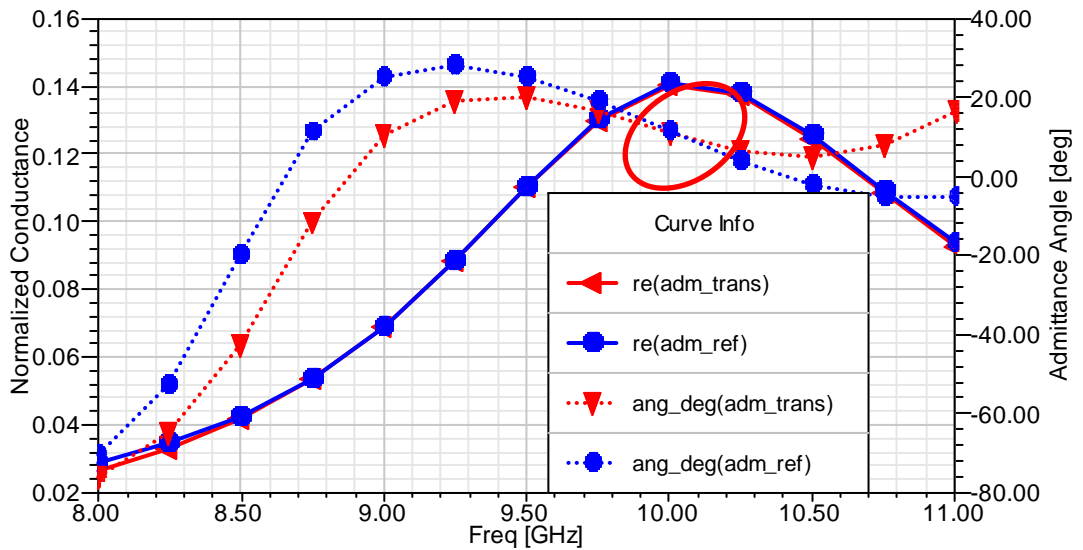


Figure 3.25 Admittance parameters vs. frequency for inset depth of 6.3mm and inset height of 4.0mm

A three parameter characterization, which includes the characterization of the slot admittance and radiation phase with variations in three different parameters of the slot is very cumbersome and time consuming when compared to a two parameter characterization. Since the important property of these slots for a travelling wave array design is their low reflection coefficient comparable to shunt slots, the inset depth is kept constant in the designed arrays and this allows us to proceed with a two parameter characterization with the parameters being inset height and slot depth.

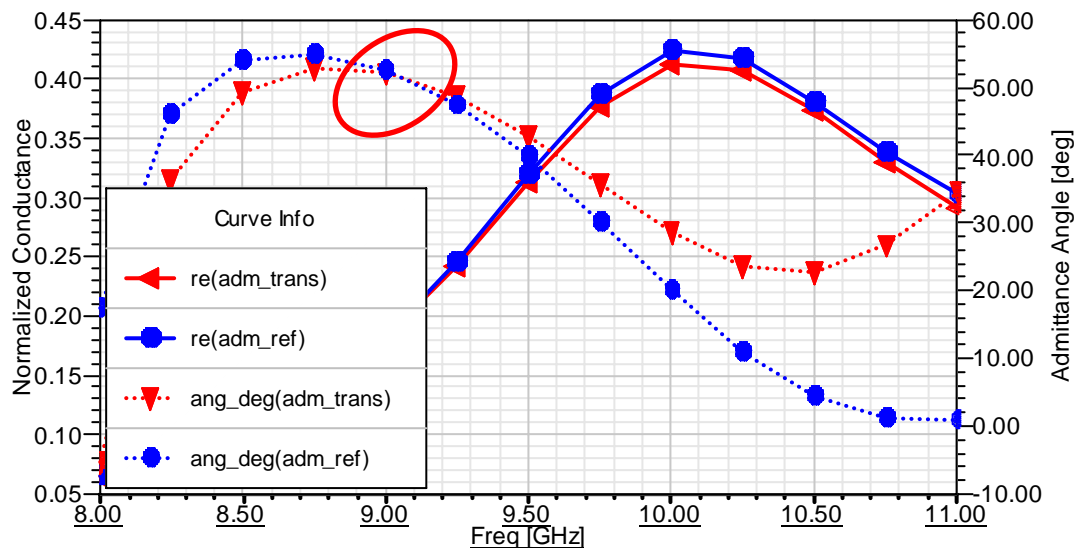


Figure 3.26 Admittance parameters vs. frequency for inset depth of 7.0mm and inset height of 5.0mm

3.4 Slots in Array Environment

3.4.1 Mutual Coupling Effects

It is evident that there is mutual coupling between different slots inside the array. There are two main approaches to exactly or approximately model this mutual coupling. The first one involves modeling of each slot separately by isolating it from the rest of the array and then calculating the mutual coupling impedances separately and modifying the isolated parameters using the mutual coupling terms.

This method proposed by Elliott given in [14-16] is widely used for broad wall waveguide slots radiating into free space. However, a computationally simple mutual coupling analysis technique between two edge wall slots wrapped around the waveguide corners is yet to be found making the design process for edge wall arrays a very tedious and long task if not impossible by using this first approach. The second method is based on the modeling of the slot as if the slot is inside the array. This method finds the scattering and radiation parameters of the slot including the mutual coupling. That is, the active scattering parameters and active radiated fields are found directly. It is seen that a technique which is of the second proposed type, namely, the incremental conductance technique [2,22], has been widely used for designing large arrays of edge wall slots. However, the incremental conductance technique involves simulation or manufacturing and measurement of many long waveguide sections with edge wall slots opened on them. For a planar array, the simulation time will be very long due to many waveguide rows modeled in a single simulation. For the manufacturing and measurement case, the amount of waveguides will be huge and the measurement process will be very cumbersome. At the end, the data obtained is not exact because the array environment that the slot is modeled (all of the slots are same) is different from the actual array environment (each slot is different).

3.4.2 Infinite Array Approach

In this study, an infinite array approach is introduced to characterize the slots. In this approach, it is assumed that the slot to be modeled is in an infinite array medium with identical elements. For planar array design, the array is infinite in both directions. Each element occupies a cuboid volume with dimensions dx , dy and dz with dx and dy being the inter-element spacings of the planar array in two dimensions. This volume is called a “unit cell” or simply a “cell”. It is also assumed that each element of the array has the same excitation coefficient or only the amplitudes are same and there exist a progressive phase shift across one or two dimension. This way, the current distribution inside each cell is the same to within a phase difference.

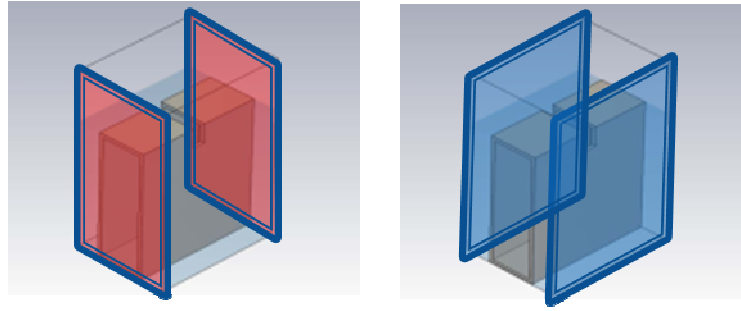


Figure 3.27 Unit cell structure with periodic boundary pairs

Infinite array environment can be created using a single slot model by applying the proper boundary conditions and excitations. An example cell for the slots is presented in Figure 3.27. The free space boundaries facing each other (boundaries with the same color) are expected to have exactly the same field distributions over them in the infinite array environment. Therefore, periodic boundary conditions are applied to the boundaries with the same color. In HFSS, if two boundaries are periodic, one of them is chosen as the “Master Boundary” and the other is chosen as the “Slave Boundary”. For any adaptive pass performed by the simulator, the mesh on the slave boundary exactly matches the mesh on the master boundary. Using this meshing, the fields on the slave boundary can be exactly matched to the fields on the master boundary by imposing an equality condition on the coefficients of the basis functions of the matched mesh pairs. That is, since the meshes are matched, the basis functions are matched too and the coefficients of the matching basis functions are made the same to within a phase difference. The phase difference between the master and slave boundaries is determined by the scan angle of the array or more precisely, by the progressive phase difference between the elements.

The top boundary covering the unit cell can be assigned as a radiation boundary or can be terminated by a perfectly matched layer (PML) object. However, in recent years, a more accurate termination for unit cell problems is developed, namely, the Floquet Port. Floquet Port is like waveport in HFSS which requires a rhomboid cross section (rectangular cross section being a special case) with opposite walls

being periodic. It is a multimode excitation port for a rectangular waveguide comprising only periodic boundary walls. It is based on the fact that the fields inside a unit cell possess a modal decomposition. The modes are plane waves propagating in different directions determined by the size of the unit cell and the phase difference applied between the boundaries. If enough modes are taken into account, Floquet Port is the best termination for unit cell problems, even better than PML.

In order to determine the dimensions of the unit cell to be used, the array geometry should be decided. To satisfy the scan requirements, an inter-waveguide spacing of 0.6λ is desired. Therefore, dy is chosen as 0.6λ for the unit cell. To determine the element spacing and the waveguide dimensions, the criterion given in (2.1) is considered. This relates the maximum usable slot conductance to the waveguide wavelength and element spacing. Using (2.1) the optimum width for the waveguide is found to be 0.76λ . Larger waveguide widths make the wavelength smaller and it becomes easier to satisfy (2.1). However, choosing a larger waveguide makes the antenna bulkier and thicker. This is why 0.76λ is determined as an optimum compromise. The height of the waveguide is chosen as 0.3λ including the wall thickness. The choice of the height is restricted by the vertically polarized elements. It is chosen such that; it is not too small to create bandwidth problems for slot excitations and it is not too large to restrict the area in which the vertically polarized slots radiate. The choice of 0.3λ for waveguide height including the wall thickness, creates a parallel plate region of 0.3λ width for the vertically polarized slots to radiate into, as seen in Figure 1.1 and 1.2.

Since the designed array is a part of the dual polarized array, it would be better to create the geometry of the dual polarized array while designing the unit cell. The other slots radiating the orthogonal polarization component are present in the unit cell. However, due to the orthogonality of the polarizations, the coupling to this slot is expected to be very close to zero and consequently, for the modeling of the horizontally polarized slots, vertically polarized slots are neglected and replaced by PEC. Therefore, the bottom boundary is completely defined as PEC. It is seen in Chapter 5 that this assumption is very accurate.

To determine the phase differences between periodic boundaries, one needs to know the delay caused by the waveguide section between two consecutive slots and the elevation scan angle for which the array to be designed is optimized. The phase difference applied between the red boundaries (left hand side) seen in Figure 3.27 is the phase difference between the excitation coefficients of any two consecutive slots along the horizontal axis is given by (2.4) and it is repeated here:

$$\phi_{az} = \beta_g d - \pi \quad (3.5)$$

The subtraction of π in (3.5) is caused by the need for a phase reversal as already mentioned in Chapter 2 and it is performed by mirroring of the consecutive slots' insets as seen in Figure 3.28 to limit the azimuth squint angle of the array to acceptable values. This is the phase difference between the excitation coefficients of any two consecutive slots along the horizontal axis. The phase difference between the blue boundaries (right hand side) of the unit cell given in Figure 3.27 is, for most of designs, taken as zero degree, since, most of the planar arrays are expected to be working optimally for zero scan angle in elevation which is the center of the scanned sector for a symmetrical scanning.

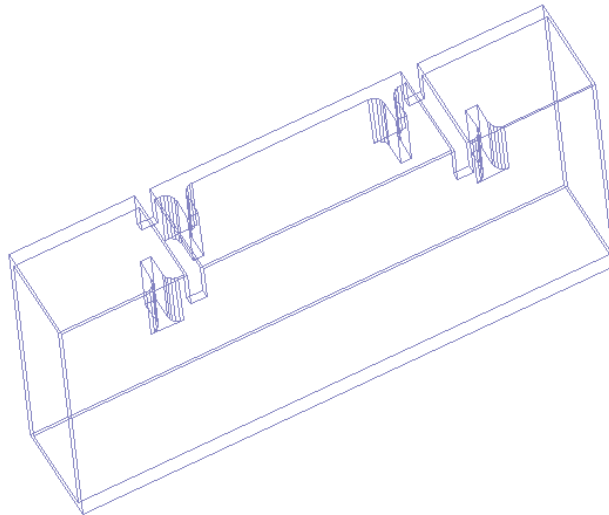


Figure 3.28 The phase reversal mechanism with mirroring of the consecutive slots

Using the given waveguide dimensions and unit cell parameter, the unit cell is formed in HFSS and various simulations are performed by changing the slot depth and inset height. It is desired that, any slot to be used in the array has its maximum power radiation at the center frequency of the array. To accomplish this, for various inset heights and slot depths, the slot's radiated power is observed with changing frequency. For each inset height, the slot depth maximizing the radiation is noted along with the value of the maximum normalized radiated power. This is in fact the procedure to determine the resonant slot parameters for various excitation amplitudes. After the simulations are finished, two polynomials are formed:

1. A polynomial relating the normalized radiated powers for the resonant cases to the inset heights.
2. A polynomial relating the resonant slot depths to the inset heights.

These two polynomials are the only characterization data required in order to design a travelling wave SWGA array.

A sample output for the unit cell simulation of a slot is seen in Figure 3.29. It is seen that, when compared to the data obtained without the periodic boundary conditions, the bandwidth of the slot is much narrower. This is interpreted as the bandwidth reduction due to the mutual coupling effects between slots of the array. This interpretation is also verified in the following section by analyzing the simulation results of the designed array.

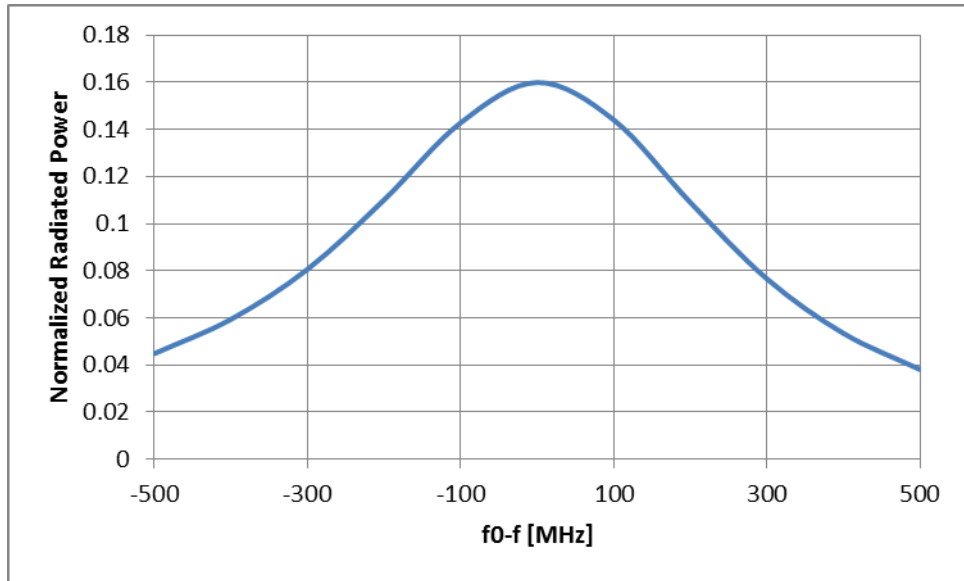


Figure 3.29 Normalized radiated power vs. frequency for a sample slot resonant at the center frequency

3.5 Horizontally Polarized Array Design

In order to design a linear array using the characterization data obtained, a decision should be made about the desired amplitude distribution, the maximum slot conductance to use and power allowed to the terminating load at the center frequency. The desired amplitude distribution is a Two Parameter Taylor Distribution with 31 elements, $\tilde{n}=6$ and side lobe level of -35 dB. The definition of the parameter \tilde{n} and the details of the Taylor Distribution can be found in [17]. The amplitude distribution is given in Figure 3.30. This distribution provides the array factor seen in Figure 3.31. The main beam's squint is due to the progressive phase shift given by the expression (3.5) and is common to travelling wave type antennas.

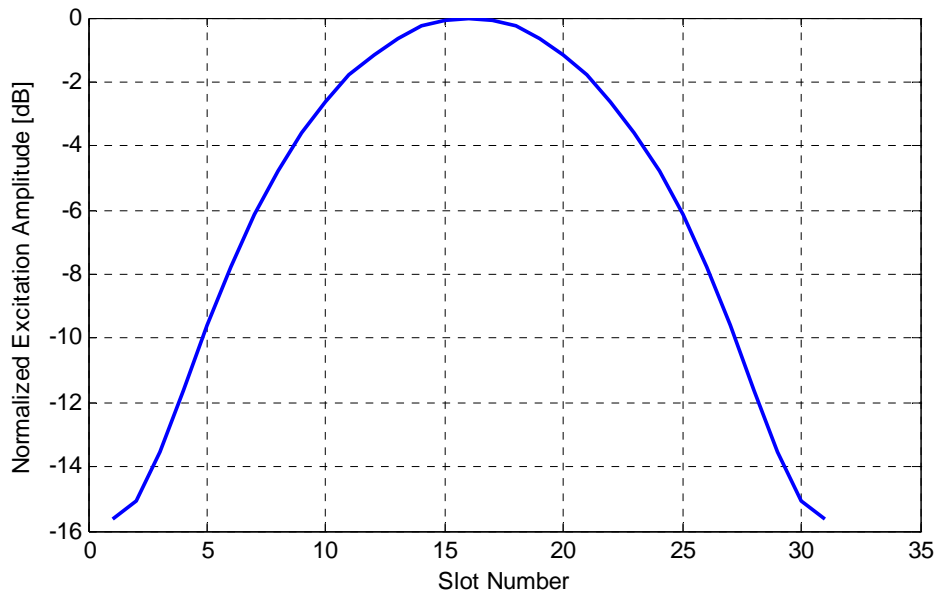


Figure 3.30 35dB SLL Taylor Amplitude Distribution with 31 elements for $\tilde{n}=6$

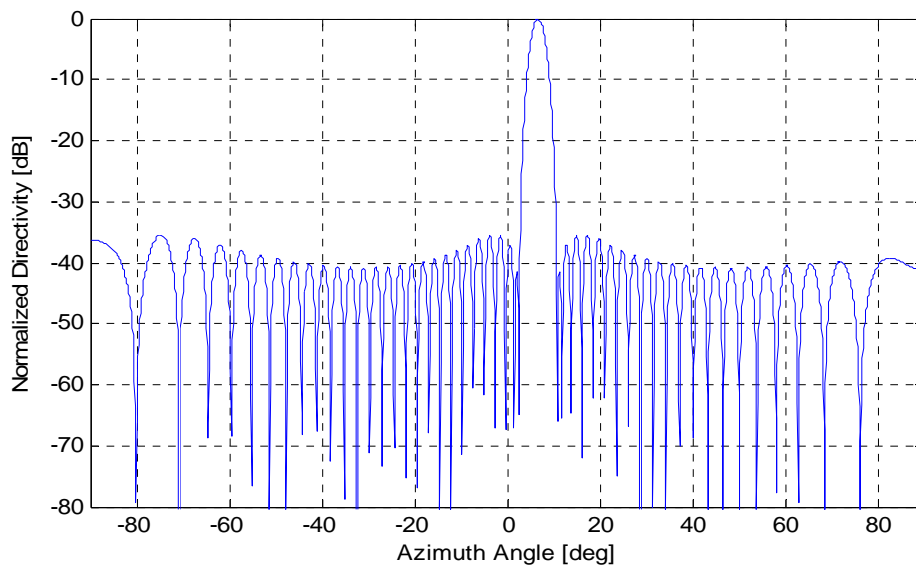


Figure 3.31 Array Factor of the distribution in Figure 3.30 with the correct phasing

The maximum allowed conductance value and the power allowed to the load should be determined together because they are heavily dependent on each other. If the power allowed to the load and the desired amplitude distribution are known, all of the required slot admittances can be found using the relation (2.2) which is the travelling wave type SWGA design equation. In Figure 3.32, conductance

distributions among the slots are seen for various power values allowed to the load (PL).

When the inequality (2.1) is used with the determined waveguide dimensions, the maximum allowed conductance value becomes 0.255. Therefore, PL values smaller than 0.04 seem to be inappropriate for the array to be designed. However, since the admittances of the slots tend to decrease with deviations from the center frequency, the efficiency of the array would be very low if a PL value larger than 0.04 is chosen. To keep the array efficiency above 0.90 in the whole frequency band of 600 MHz, PL value of 0.01 is chosen resulting in the maximum conductance value of 0.41 which is well above the maximum allowed value. It is shown in the next section that, the inaccurate slot excitations which are obtained after the first design due to high conductivities used and any other effects related to infinite array modeling which is only an approximate characterization technique, are compensated by an iterative tuning technique and finally, an array pattern satisfying the requirements is obtained.

Using the characterization polynomials and the desired slot conductances, slot depths and inset heights for 31 slots are calculated for obtaining resonant slots at the center frequency. All other parameters of the slots are same and they are chosen to enhance the bandwidth of the array as explained in Section 3.3. Using the calculated slot parameters, a linear array is formed and simulated by HFSS.

Since the main aim is to design a planar array and since the slots are characterized in a planar infinite array medium, it is best to simulate the constructed linear array in an infinite array medium as is done for single slots. For this purpose, the model in Figure 3.33 is prepared. The width “W” is chosen as the waveguide spacing used for the planar array. PEC is assigned for the bottom boundary, and the shaded boundaries are assigned as radiation boundaries. The remaining large longitudinal boundaries facing each other are assigned as periodic boundaries with 0 degree phase difference. This modeling creates the same geometry in the designed dual polarized array by keeping its waveguide spacing except that vertically polarized

slots are absent and the periodic boundaries extends the array to infinity in the elevation plane.

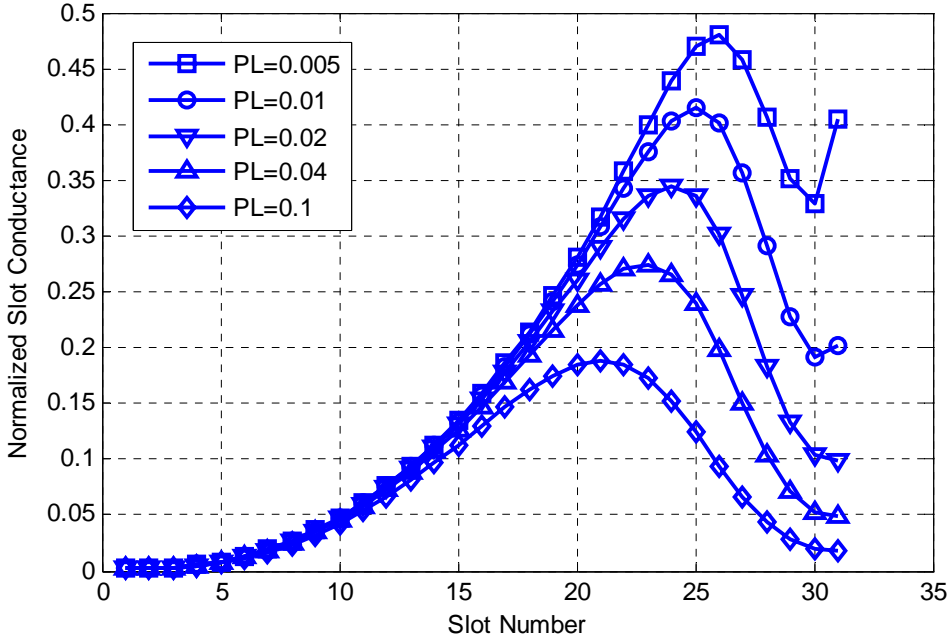


Figure 3.32 Conductance values required for various efficiencies

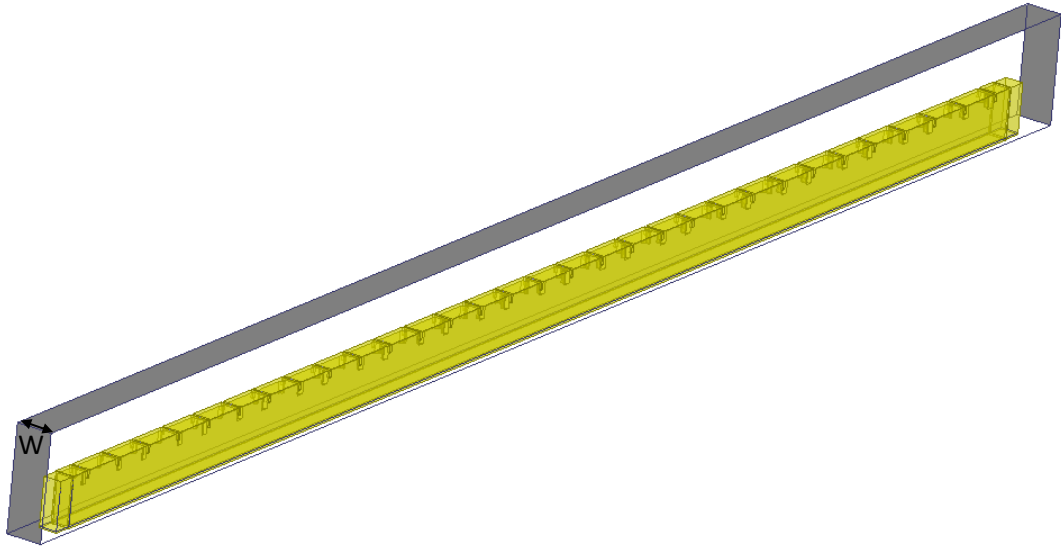


Figure 3.33 Periodic model of the designed planar array

Since the whole array is not simulated, the elevation pattern is not available. However, it is shown in the next section that a planar array of 10 waveguides designed using the infinite array approximation provides the expected elevation pattern when fed with the correct excitation amplitudes. The azimuth pattern obtained for the center frequency with simulation of the initial design is given in Figure 3.34. It is seen that the sidelobe level of the simulated antenna is higher than the desired one. This is due to the cumulative effects caused by the violation of the rule given by (2.1) and the errors caused by the infinite array assumption used in slot characterization. In Figure 3.34, it is also seen that the cross polarization level is very low, especially under the main beam. The cross polarized beam around -30° is due to the small cross polarized components at the slot apertures. Since this is a secondary beam position, it is concluded that the phase reversal effect caused by mirroring of the slots does not work for cross polarization as in the case of inclined edge wall slot array which also have secondary cross polarized beams.

As given by [2], if one knows the field values around the slots of the antenna either by simulation or with a back transformation of the near field measurements of the antenna, the source of the far field pattern problems can be tracked down to the element excitation errors. If the amount of an excitation error is known, some modifications to the slot which will hopefully remove or decrease the excitation errors could be made. In order to determine the realized slot excitations, a technique similar to the one presented in Section 3.3.2, which is used to determine radiation phases, is used. Integration lines looking like the one found in Figure 3.4 are drawn at each slot's aperture and slot voltages are calculated by integrating the E-field along the line. These slot voltages are equal to the realized element excitation values both in amplitude and in phase under a uni-modal assumption for the slots' fields. It is verified by experiment that this assumption is fairly valid and the proposed tuning method is working.

After the slot voltages are determined, the amount of excitation error for each slot is calculated and small modifications are performed on the slots to compensate for the calculated errors. For example, if the amplitude is higher than expected, the inset height is lowered. The simulation is then repeated with the new array. If the

desired pattern is not still satisfied, the procedure is repeated. The desired pattern is generally obtained in a maximum of five or six iterations. With the designed array, the pattern obtained after the fifth iteration is shown in Figure 3.35. This pattern complies with the performance requirements of the dual polarized array and the designed antenna is used in the final array. Radiation patterns for other frequencies are given in Chapter 5 where the array is simulated as a part of the dual polarized array.

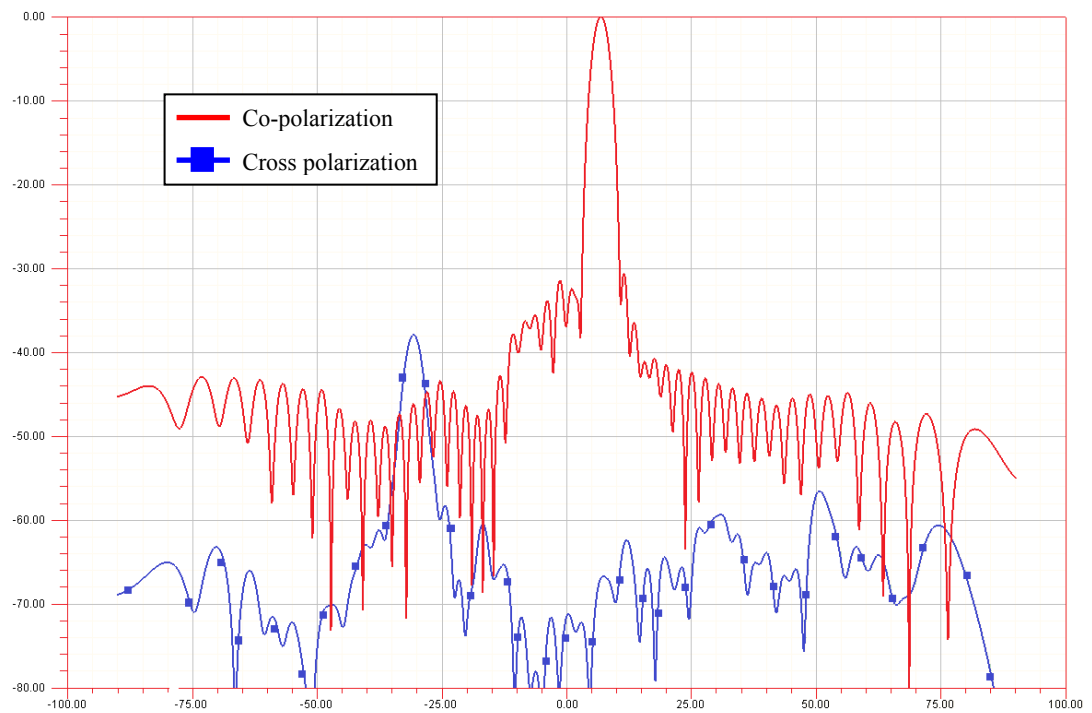


Figure 3.34 Azimuth radiation pattern of the designed horizontally polarized array without tuning

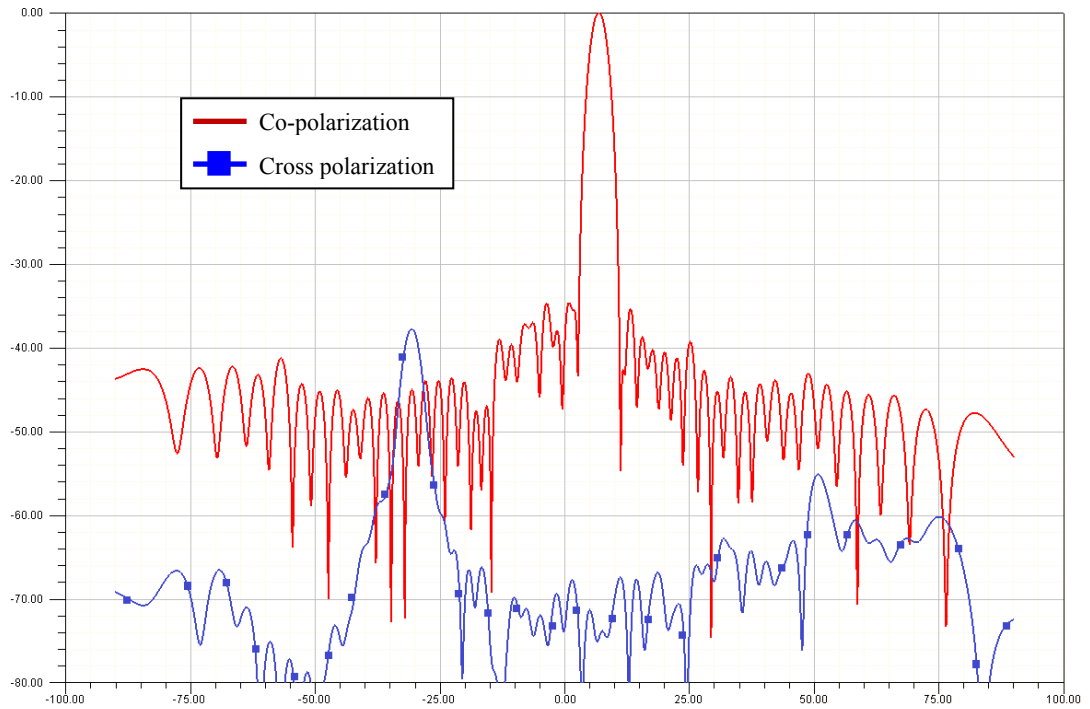


Figure 3.35 Azimuth radiation pattern of the designed horizontally polarized array after tuning

3.6 Verification of the Slot by a Test Antenna

Before manufacturing the dual polarized array which includes the designed non-inclined edge wall slot array, it is wiser to first manufacture a small array of these novel slots. Since their manufacturability and sensitivity to the mechanical tolerances are unknown, it is not certain that the manufactured array's performance would be the same as the simulated array's performance. For this purpose, a small planar array comprising 10 waveguides with 20 slots along each waveguide is designed. Due to the decreased size, a side lobe level of -30 dB is aimed. Other parameters of the array are exactly the same as the main array's parameters.

The same design procedure is used with the same characterization data. An infinite array simulation of a single waveguide row is performed. Since the array is relatively small, a complete simulation of the whole array is also performance. The array is manufactured without any tuning performed. The desired excitation amplitudes are seen in Figure 3.36. Also, the resulting array factor with the

progressive phase difference of the elements taken into account is seen in Figure 3.37.

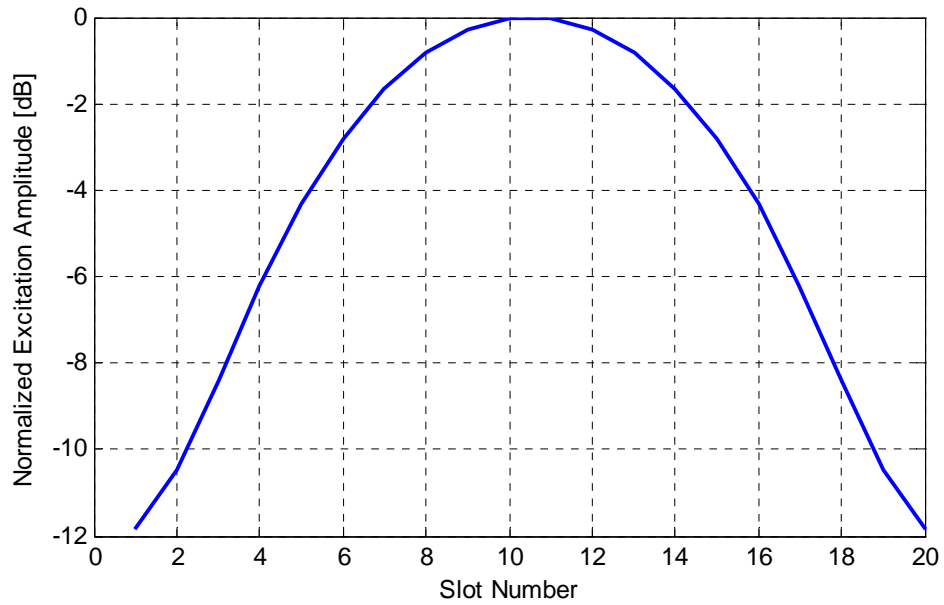


Figure 3.36 Desired excitation amplitudes for the 20 element array

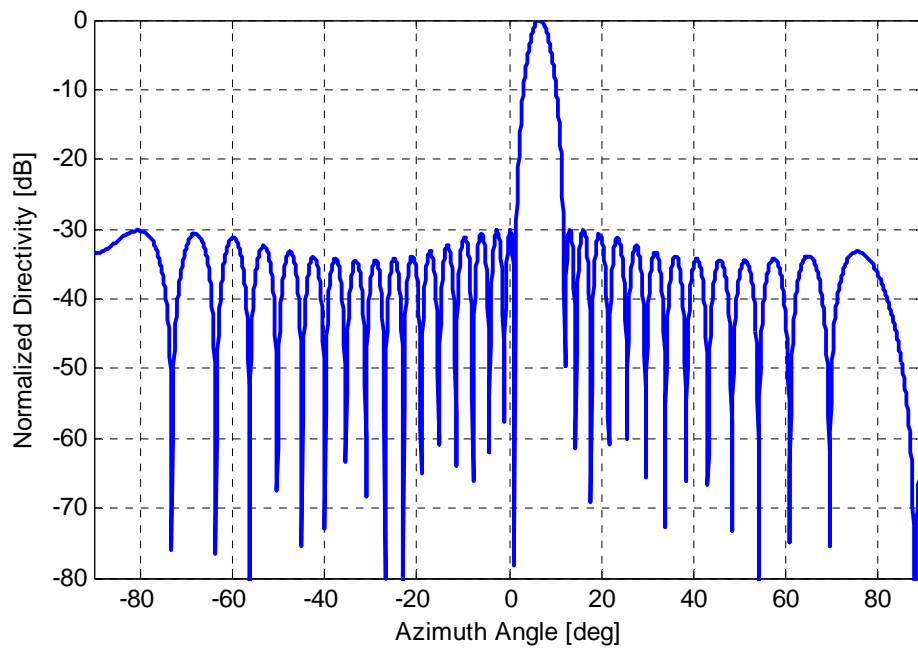


Figure 3.37 Resulting array factor for the distribution in Figure 3.36

The manufactured array's pictures are seen in Figure 3.38 and 3.39. The manufactured array is measured at the planar near field antenna test chamber of Aselsan. In Figure 3.40, it is seen that the measured pattern and the pattern obtained with simulation are in excellent accordance. Therefore, it is concluded that there is no problem related to manufacturability of the slots with 3-axis CNC machines.



Figure 3.38 The manufactured small edge wall slot array

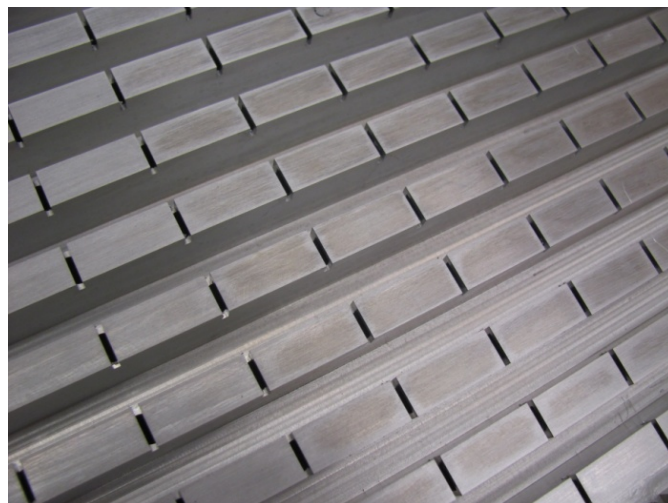


Figure 3.39 A close view of the manufactured slots

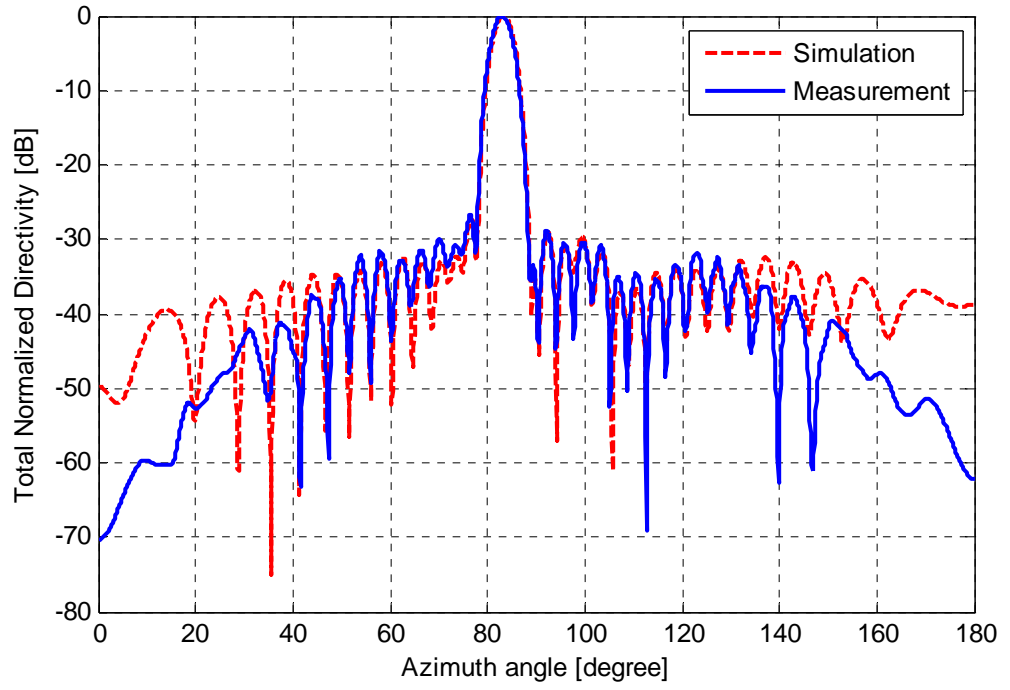


Figure 3.40 Measurement azimuth pattern of the manufactured array compared with simulation results

CHAPTER 4

BROAD WALL SHUNT SLOT ARRAY WITH BAFFLE

This chapter is about the design of the vertically polarized part of the dual polarized array. In order to fit side by side the waveguides having the same propagation constant as the waveguides of the horizontally polarized array, with a spacing of 0.6λ , single ridge waveguide geometry is required. The characterization of the slots opened on the single ridge waveguide is performed with a modified unit cell structure while the horizontally polarized array's waveguides act as baffles. The array is designed with the characterization data and then tuned to comply with the requirements.

4.1 Baffles

Due to the proposed topology of the dual polarized array, vertically polarized elements, namely, the broad wall slots, are forced to radiate into a parallel plate waveguide region. Although this fact makes the design of those slots harder, this geometry has the advantage of suppressed secondary lobes with respect to the case with no baffles. For the case without baffles, the secondary lobes are caused by the fact that any two consecutive slots are placed with alternating offset directions. This phenomenon is analyzed in [18,23]. The alternation of the offset direction disturbs the linear array topology and modifies the resulting array factor accordingly. A detailed analysis of this modification can be found in [18].

By placing baffles between waveguide rows, the field radiated by the antenna is forced to include only the parallel plate waveguide modes, all of which are symmetric with respect to the waveguide centerline if the width of the parallel plate

region is smaller than half a wavelength. This is due to the fact that the modes having asymmetrical field variations across the width of the region, are at cut off. This creates an eventually uniform field distribution across the width and the effect of the slot offsets is compensated. It is as if all of the slots radiate from the centerline of the waveguide. The effect of baffles on secondary lobes is found in [23,24].

Mutual coupling between broad wall slots with no baffle structures can be performed analytically as proposed by Elliott [14-16]. This gives an opportunity to iteratively design linear or planar arrays with the desired excitation coefficients for each element. In his work, Elliott uses coupling formulas for two slots opened on an infinite ground plane. The workload for this is equivalent to calculate the coupling between two dipoles in free space and hence, it is relatively easy. However, if the slot radiates into a parallel plate region before radiating into free space, Elliott's formulations become invalid and other coupling formulations should be used. Rengarajan provides us a technique to use in this case [25]. However, the formulation requires a very complex computer code which is hard to render error free when compared to Elliott's formulation and the convergence of the iterative algorithm for array design would be much slower than Elliott's. Since a large array is designed, it is decided that it would be wiser to use unit cell approach as in the case of edge wall slots.

4.2 Requirement of Single Ridge Waveguide

The inter-waveguide spacing for the dual polarized array was determined as 0.6λ in the previous chapter. This forces the same inter-waveguide spacing of 0.6λ for the vertically polarized elements. Additionally, in order to have the same beam squint of 6.8 degrees and the same slot spacing of 0.79λ as the horizontally polarized slots, the guided wavelength of the waveguides used in both polarizations should be the same. Therefore, if a rectangular waveguide would be used for vertically polarized slots, a waveguide with the same width, as the horizontally polarized slots' waveguide would be used which has a width of 0.76λ . Since the inter-waveguide spacing is 0.6λ , a ridge loading should be used to achieve the required

guided wavelength without exceeding the width limit of 0.6λ . Double ridged waveguide is not an option because broad wall slots are opened on the upper wall. Therefore a single ridged waveguide is designed and used. The designed single ridge waveguide has the same guided wavelength at the center frequency and in the design frequency band of the array; the wavelength is very similar to its non-ridged counterpart. A side view of the array with single ridge waveguides is seen in Figure 4.1 clearly showing the single ridge geometry.

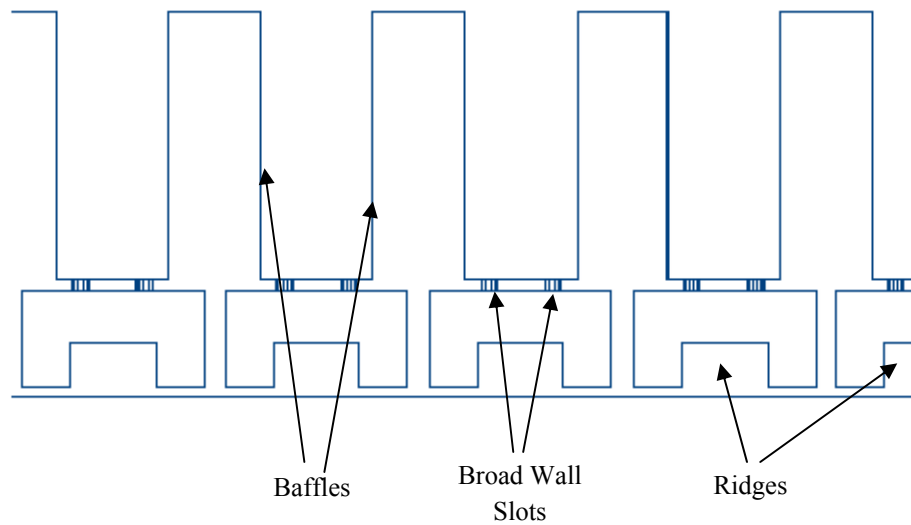


Figure 4.1 A side view of the single ridge waveguide array

4.3 Unit Cell Design for Characterization of Broad Wall Slots

The broad wall slots differ from the non-inclined edge wall slots in that the alternation of offset between two consecutive slots prevents the use of a single slot inside the unit cell. This is due to the doubling of the period of the array along the waveguide. The non-inclined edge wall slots can be said to be quasi-periodic with a period “d” because there are virtually no difference between the external region of the two consecutive slots. However, consecutive broad wall slots differ in their direction of offset which makes the exterior of the slots different. Therefore, a unit cell including two slots with equal amount of offsets but having opposite offset

directions are used. This approach would give enough accuracy if the offsets in the designed array are varying slowly with respect to each other and this implies a relatively large array. Also, in order to have the slots excited with equal amplitude and a desired phase difference and additionally, in order to obtain the S parameters of a single slot, the two slots should be excited with different waveports. These requirements result in the unit cell shown in Figure 4.2 with a total of 4 waveports and a Floquet port. The waveport locations can be seen in Figure 4.3.

The PBCs used for the side boundaries are the same as the PBC used in Chapter 3 as seen in Figure 4.2. However, the phase difference applied between boundaries labeled as “PBC I” are twice the progressive phase shift between two consecutive slots. This fact originates from the doubling of the unit cell size by including two slots.

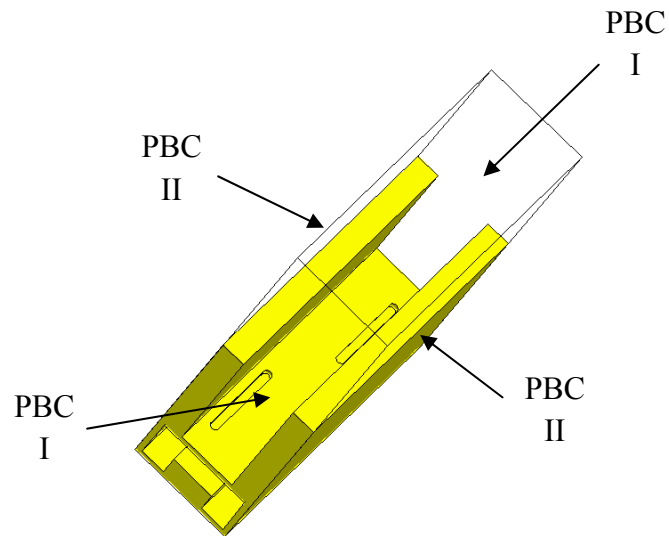


Figure 4.2 Unit cell structure used to characterize broad wall slots

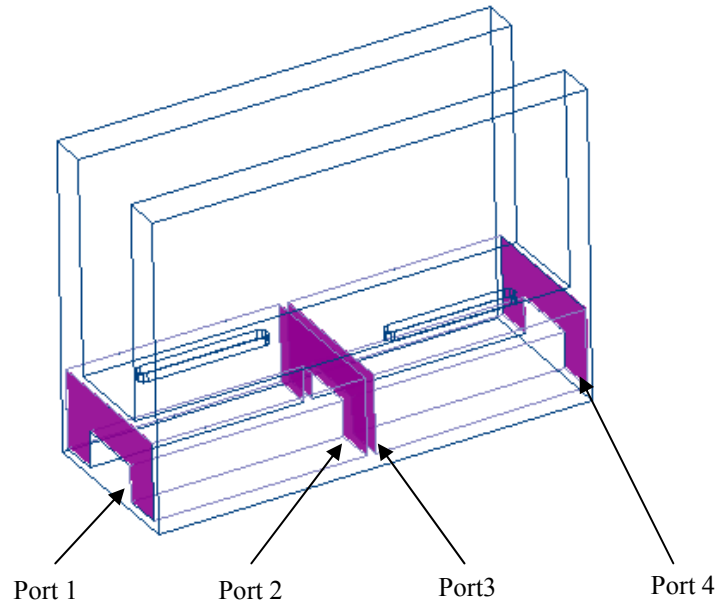


Figure 4.3 Ports defined in the unit cell structure

To obtain the active S-parameters of the slots when all of the slots are excited, some manipulations to the S parameters are required. First of all, the following assumptions are made on the unit cell model:

- The slot at the left in Figure 4.2 and 4.3 represents the slots with positive offsets (odd numbered slots), whereas the slot at the right represents the slots with negative offsets (even numbered slots).
- The left slot has its waveport numbers as: Left port: Port 1, Right Port: Port 2
- The right slot has its waveport numbers as: Left port: Port 3, Right Port: Port 4

Three different excitation conditions are defined for the unit cell solution:

1. Only the odd numbered slots are excited in phase and in an equi-amplitude form.
2. Only the even numbered slots are excited.
3. All of the slots are excited with an arbitrary progressive phase and in an equi-amplitude form.

S-parameters of the unit cell are obtained for different excitations.

The following facts are observed:

- The parameter S_{21} is the active transmission coefficient of the odd numbered slots when Excitation 1 is applied.
- The parameter S_{43} , being equal to S_{21} is the active transmission coefficient of the even numbered slots when Excitation 2 is applied.
- The parameter S_{11} is the active reflection coefficient of the odd numbered slots when Excitation 1 is applied.
- The parameter S_{33} , being equal to S_{11} is the active reflection coefficient of the even numbered slots when Excitation 2 is applied.
- The parameter S_{31} is the coupling coefficient to the input port of even numbered slots when Excitation 1 is applied.
- The parameter S_{13} , being equal to S_{31} is the coupling coefficient to the input port of odd numbered slots when Excitation 2 is applied.
- The parameter S_{23} is the coupling coefficient to the transmission port of odd numbered slots when Excitation 1 is applied.
- The parameter S_{41} being equal to S_{23} is the coupling coefficient to the transmission port of even numbered slots when Excitation 2 is applied.

Active S_{11} is the ratio of the received power wave from port 1 to the input power wave to port 1 when an excitation is applied to the array and active S_{21} is the ratio of the received power wave from port 2 to the input power wave to port 1. We can assume that all of the characteristic impedances are 1 ohm and replace the power waves by voltage waves. Let us define the following convention:

- A voltage wave $V1_{p,q}^{m,n}$, is the voltage received at the input port of the slot (p, q) (with horizontal position index p and vertical position index q) when the port with index (m, n) is excited with 1V.
- A voltage wave $V2_{p,q}^{m,n}$, is the voltage received at the transmission port of the slot (p, q) when the port with index (m, n) is excited with 1V.

Therefore, for any slot in an infinite array, the active reflection and transmission coefficients are expressed as:

$$\Gamma_a = \sum_{m=-\infty}^{m=\infty} \sum_{n=-\infty}^{n=\infty} \frac{a_{m,n}}{a_{p,q}} V1_{p,q}^{m,n} \quad (3.1)$$

$$T_a = \sum_{m=-\infty}^{m=\infty} \sum_{n=-\infty}^{n=\infty} \frac{a_{m,n}}{a_{p,q}} V2_{p,q}^{m,n} \quad (3.2)$$

$a_{m,n}$ is the excitation coefficient of slot with index (m,n).

In the infinite array simulation, it is assumed that a progressive phase shift of ϕ is desired along horizontal axis and a phase difference of 0 is desired along vertical axis. According to their previous explanations, the S parameters become:

$$S_{11} = \sum_{m=-\infty}^{m=\infty} \sum_{n=-\infty}^{n=\infty} e^{j2m\phi} V1_{1,1}^{(2m-1),(2n-1)} \quad (3.3)$$

$$S_{13} = \sum_{m=-\infty}^{m=\infty} \sum_{n=-\infty}^{n=\infty} e^{j(2m+2)\phi} V1_{1,1}^{2m,2n} \quad (3.4)$$

$$S_{21} = \sum_{m=-\infty}^{m=\infty} \sum_{n=-\infty}^{n=\infty} e^{j2m\phi} V2_{1,1}^{(2m-1),(2n-1)} \quad (3.5)$$

$$S_{23} = \sum_{m=-\infty}^{m=\infty} \sum_{n=-\infty}^{n=\infty} e^{j(2m\phi+2)} V2_{1,1}^{2m,2n} \quad (3.6)$$

For Excitation 3, the active reflection and transmission coefficients are expressed as:

$$\Gamma_a = \sum_{m=-\infty}^{m=\infty} \sum_{n=-\infty}^{n=\infty} e^{j(m+1)\phi} V1_{1,1}^{m,n} \quad (3.7)$$

$$T_a = \sum_{m=-\infty}^{m=\infty} \sum_{n=-\infty}^{n=\infty} e^{j(m+1)\phi} V2_{1,1}^{m,n} \quad (3.8)$$

It is clear that those two coefficients can be expressed in terms of the S parameters of the simulation as follows:

$$\Gamma_a = S_{11} + e^{j\phi} S_{13} \quad (3.9)$$

$$T_a = S_{21} + e^{j\phi} S_{23} \quad (3.10)$$

The given active reflection and transmission coefficients for the Excitation 3 will be henceforth called as the active S parameters of a slot and they will be simply denoted as S_{11} and S_{21} .

Using one of the active S parameters, the shunt equivalent of a broad wall slot can be obtained as previously given by (3.3) and (3.4).

4.4 Characterization Data

The equivalent admittance of a slot is controlled by its offset from the centerline and its length as mentioned in Chapter 2. This is also valid in the presence of baffles. The conductance of a slot can be increased by increasing the offset and it can be made resonant for a desired conductance value. Typically, resonant slots having normalized conductance values between 0 and 0.50 are easily obtained. In order to find the parameters of a slot having a particular conductance and admittance phase values, two characterization polynomials are required as in the case of edge wall slots.

The first polynomial relates the resonant conductance values to slot offset. It is obtained by sweeping slot length parameter for different offset values. For each offset from a finite set of offset values, the length at which the slot resonates is found and this length value and the resonant conductance value are noted. Then, a polynomial fitting is performed using the obtained conductance values and offset values.

The second polynomial relates the resonant length values to offset values. It is obtained by using the resonant length values obtained in the performed sweeps and the offset values.

The frequency characteristics of these slots are similar to edge wall slots but the conductance values are asymmetrical around the resonant frequency. A sample frequency sweep data for a slot resonant at the center frequency is shown in Figure 4.4 with both conductance and phase variations. Similar but scaled curves are obtained for different resonant slots. In Figure 4.5, conductance variations with respect to the frequency change for various slots are shown. All of these slots are resonant near the center frequency.

The characterization data embedded in the two polynomials used in the array design are seen in Figure 4.6 and Figure 4.7. The polynomials forming these two curves are used to obtain the slot parameters satisfying the excitation requirements of the array as it is done for the horizontally polarized antenna in Chapter 3.

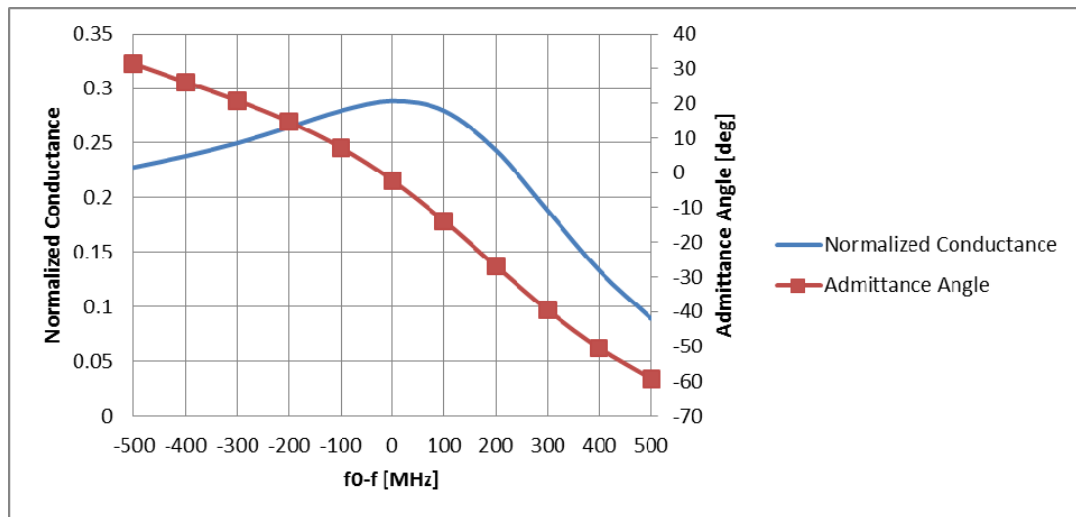


Figure 4.4 A sample frequency sweep data for a slot resonant at center frequency

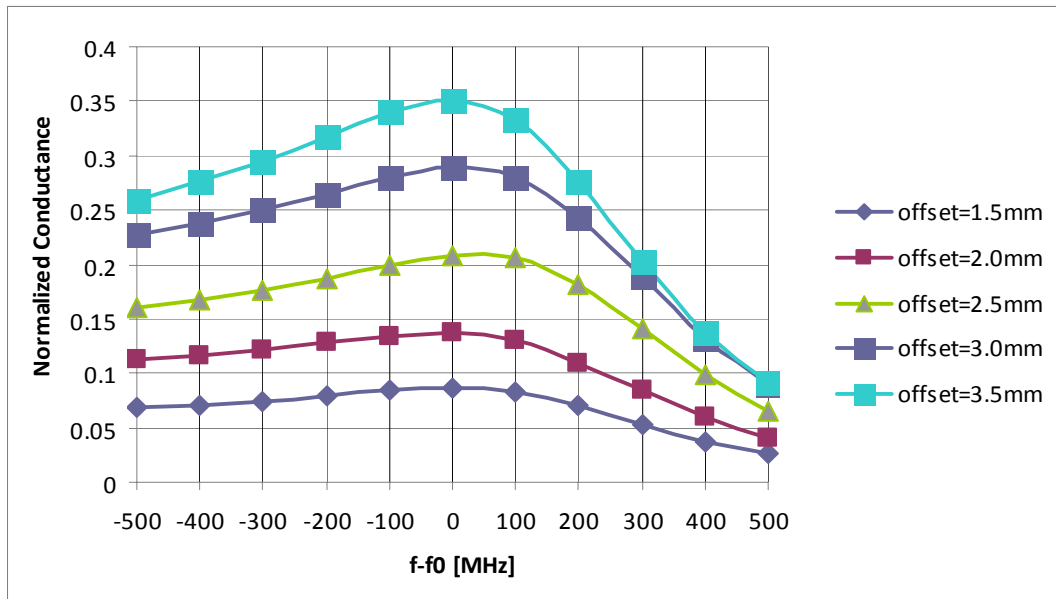


Figure 4.5 Conductance variations with changing frequency for several slot offset values.

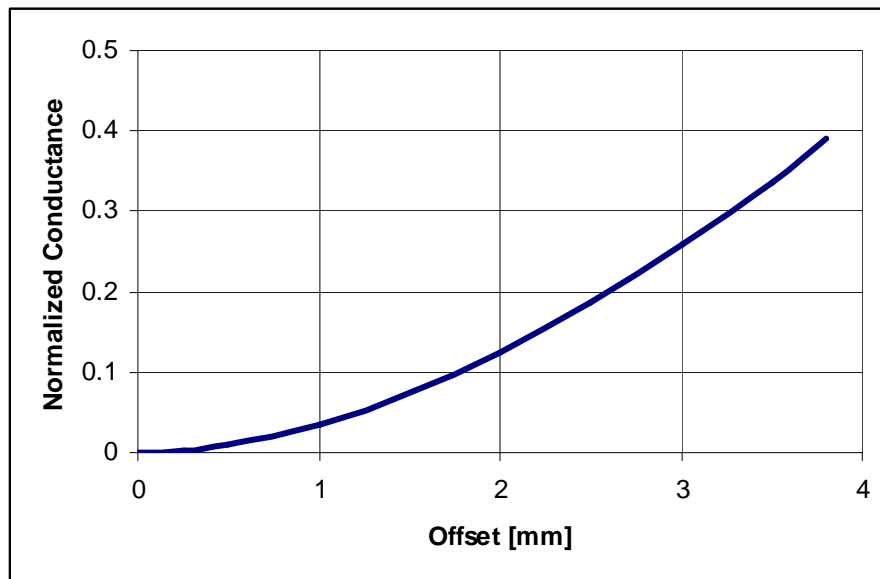


Figure 4.6 Normalized conductances of resonant broad wall slots

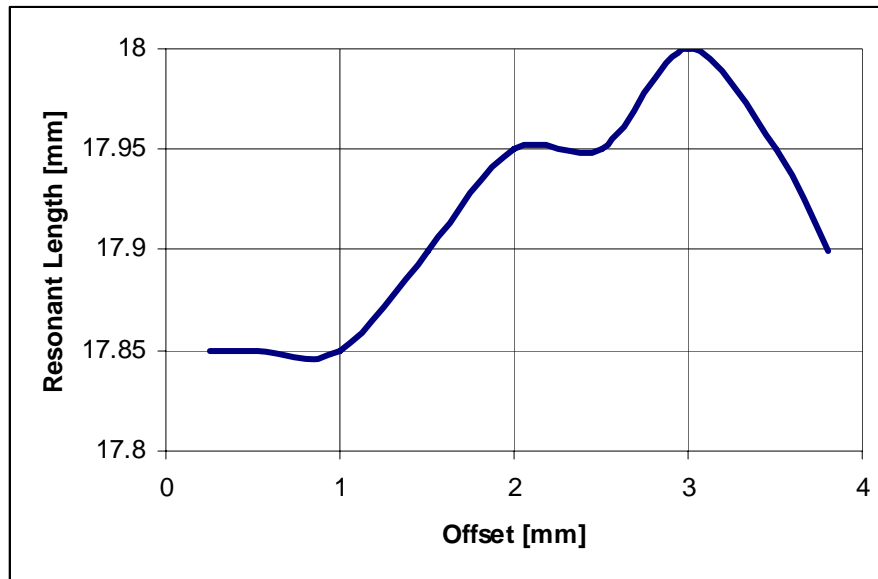


Figure 4.7 Resonant lengths of broad wall slots for various offset values

4.5 Vertically Polarized Array Design

The requirements of the designed vertically polarized array are obviously the same as the requirements for the dual polarized array. Using the characterization polynomials obtained and the procedure described in Section 3.5, the slot parameters for obtaining the excitation values given in Section 3.5 are found. It is seen in Chapter 3 that this excitation set is satisfying the design requirements. A total of four tuning iterations are performed to lower the initially obtained sidelobe level. The procedure to determine the slot voltages in case of broad wall slots is very similar to the case of edge wall slots. An integration line is created at the center of each slot in the array as seen in Figure 4.8 and the same iterations are performed as in Section 3.5 by calculating the slot voltages. The pattern obtained at the center frequency after the iterations are complete is given in Figure 4.9.

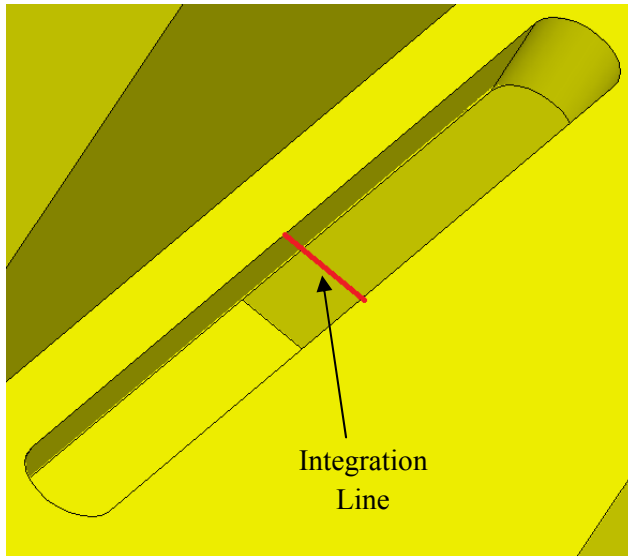


Figure 4.8 Integration line used to calculate slot voltages

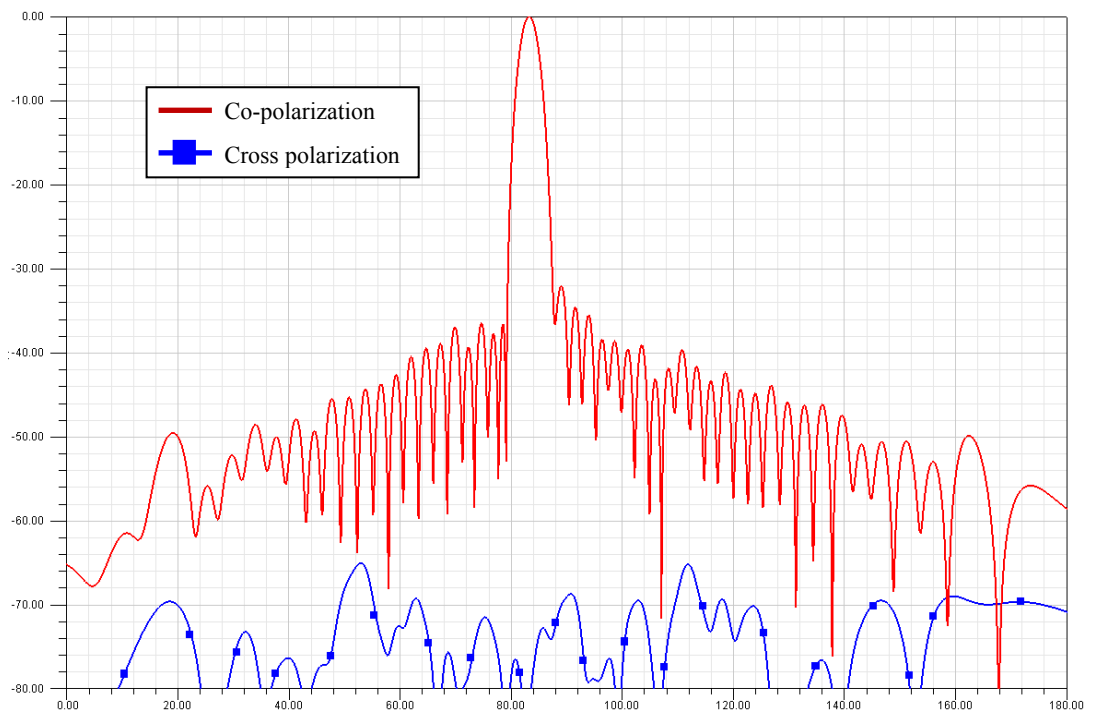


Figure 4.9 Simulation radiation pattern of the tuned array

The obtained pattern has the same beam squint as its horizontally polarized counterpart as expected and its cross polarization radiation level is very low as observed from Figure 4.9. Radiation patterns for other frequencies as well as the return loss and efficiency characteristics are given in Chapter 5 where the array is simulated as a part of the dual polarized array.

CHAPTER 5

DUAL POLARIZED SLOTTED WAVEGUIDE ARRAY SIMULATIONS

This chapter is about the merging of the two orthogonally polarized arrays designed in Chapter 3 and Chapter 4 in order to create the dual polarized array with:

- very high polarization purity
- -35dB sidelobe level at the center frequency,
- 600MHz usable bandwidth (in terms of input match, pattern, efficiency, etc.),
- better than 90% efficiency in the usable bandwidth
- ability to scan ± 35 degrees in elevation plane

To merge the two previously designed singly polarized arrays, a model having periodicity is created consisting of single row elements from both arrays in order to eliminate the need of complete simulation of the dual polarized array. Simulations are performed with this model and the results are given.

Since the two arrays constituting two polarizations have radiation elements which have orthogonal polarizations, it is expected and desired that the coupling between these two arrays will be very low. If this is the case, it is very likely that two arrays having orthogonal polarizations and having been designed separately can be put together without compromising the performance of the dual polarized array. In fact, it is shown in this Chapter that this is exactly the case.

The horizontally polarized array model designed in Chapter 3 has PEC boundary at the bottom face. Additionally, the vertically polarized array model designed in Chapter 4 has dummy baffle structures completely made of PEC. These two models are merged so that the dummy baffles are replaced by horizontally polarized array's waveguides and the bottom PEC is replaced by the slotted broad walls of the vertically polarized array's waveguides. The resulting periodic model is seen in Figure 5.1. It is obvious that by replicating this structure in the plane transversal to the waveguides, the structure seen in Figure 1.1 can be obtained. A side view of the periodic model is seen in Figure 5.2 where the defined periodic boundaries are clearly seen.

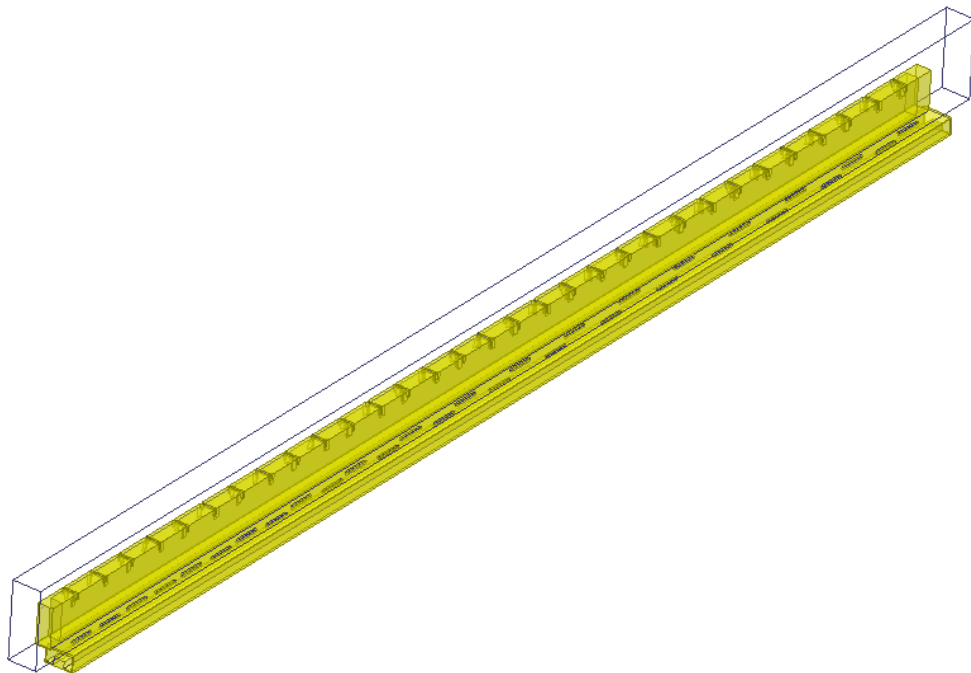


Figure 5.1 The infinite array model used to simulate the dual polarized array

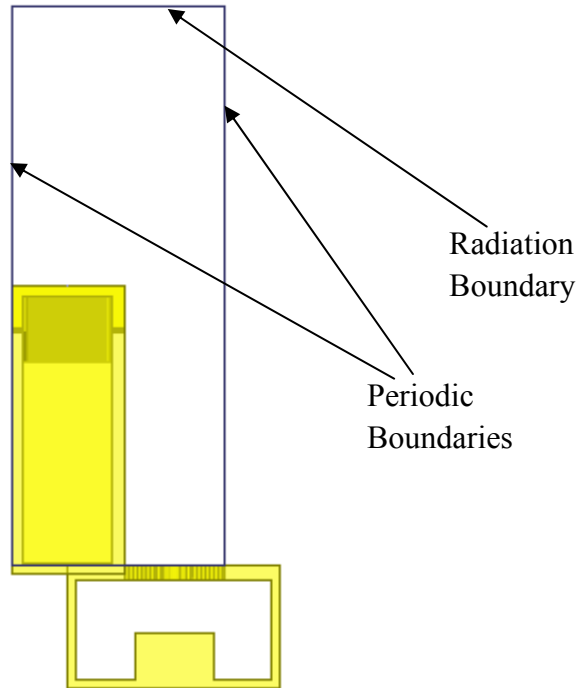


Figure 5.2 The side view of the simulated periodic model

Simulations are performed with the constructed geometry in the frequency range from $f_0 - 300\text{MHz}$ to $f_0 + 300\text{MHz}$ with 100MHz steps. The transmission coefficients of the two arrays interpreted as the amount of power transmitted to the load side are given in Figure 5.3. It is seen that the power allowed to the load at the center frequency is 1% of the total power which satisfies the design criterion for both arrays. However, as the frequency changes, the efficiency decreases with the decrease in the active conductances of the slots as mentioned in Chapter 3. Nevertheless, the efficiency is better than 90% for the entire frequency band.

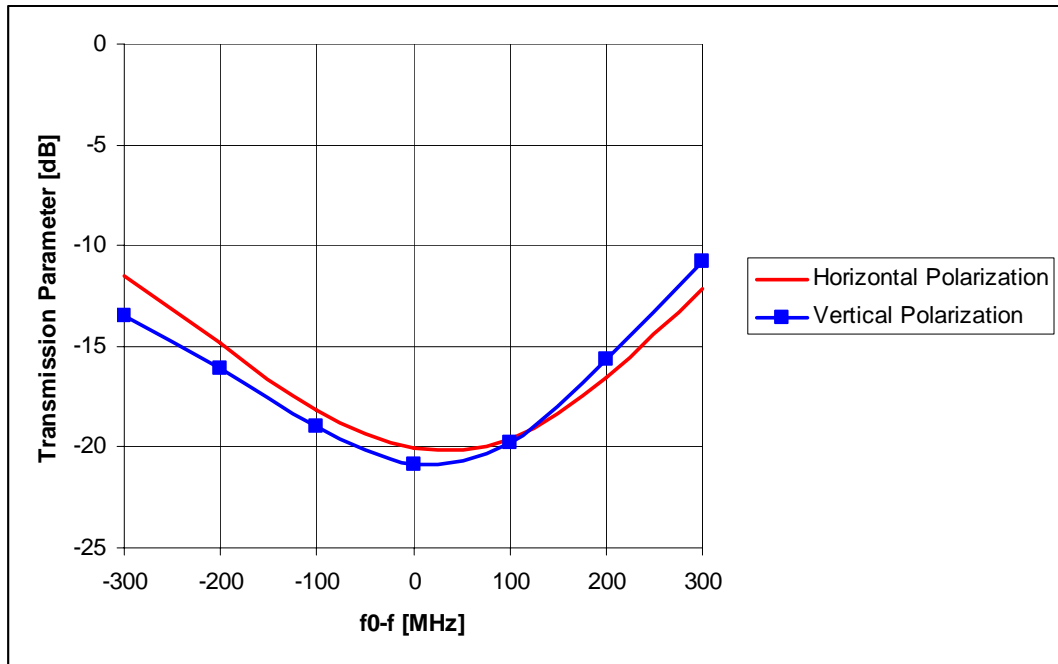


Figure 5.3 Power transmitted to the terminating load

The reflection coefficients of the antennas are below -40 dB in the entire frequency band as seen in Figure 5.4. Travelling wave nature of the antennas provides an excellent match in a very broad bandwidth. Additionally, due to the excellent polarization purity of both arrays, an exceptional isolation of maximum -75 dB is observed in the entire frequency band.

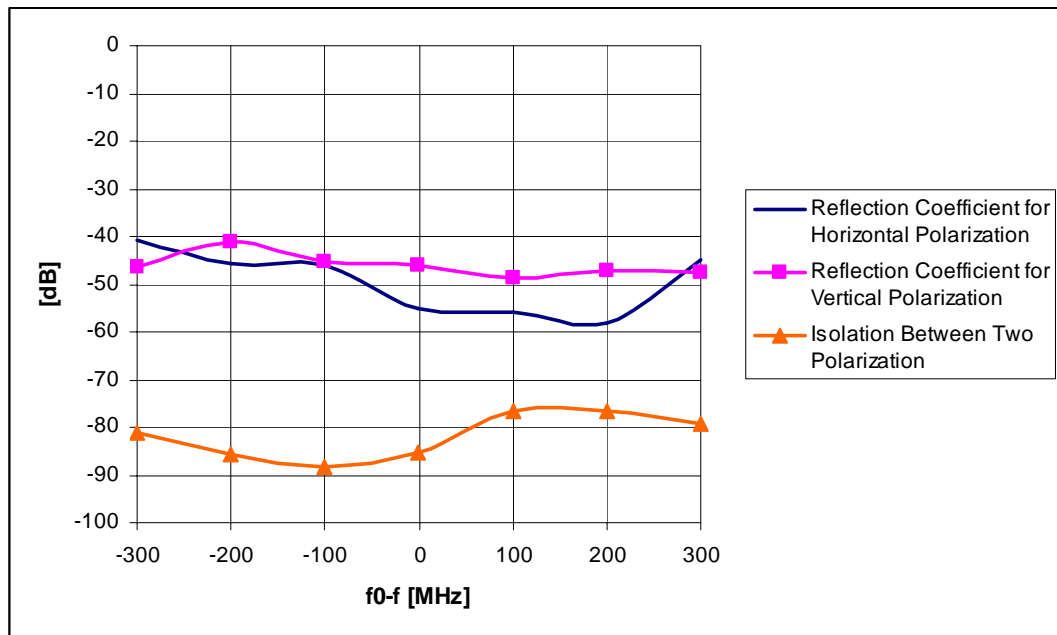


Figure 5.4 Reflection coefficients and the isolation of the two arrays

The azimuth radiation patterns of the array for 7 different frequencies are given for both polarizations in Figures 5.5 – 5.11. In these figures, cross polarized pattern of horizontally polarized array (Horizontal XP) means vertically polarized radiation by horizontally polarized array and vice versa.

It is seen the sidelobe level is below -30dB for all frequencies for almost all azimuth angles. Also, it can be said that a sidelobe level of -35dB is achieved around the center frequency. The beam pointing directions for two different polarizations are coinciding for all frequencies which is a very important property of dual polarized arrays. Finally, it is seen the cross polarization performance is unchanged when compared to the performance of the singly polarized arrays.

In Figure 5.12 and 5.13, radiation patterns for different frequencies are plotted together for each of the polarizations. They clearly show the change in the beam squint angle with changing frequency. Within a bandwidth of 600 MHz, direction of the beam changes 4.5°.

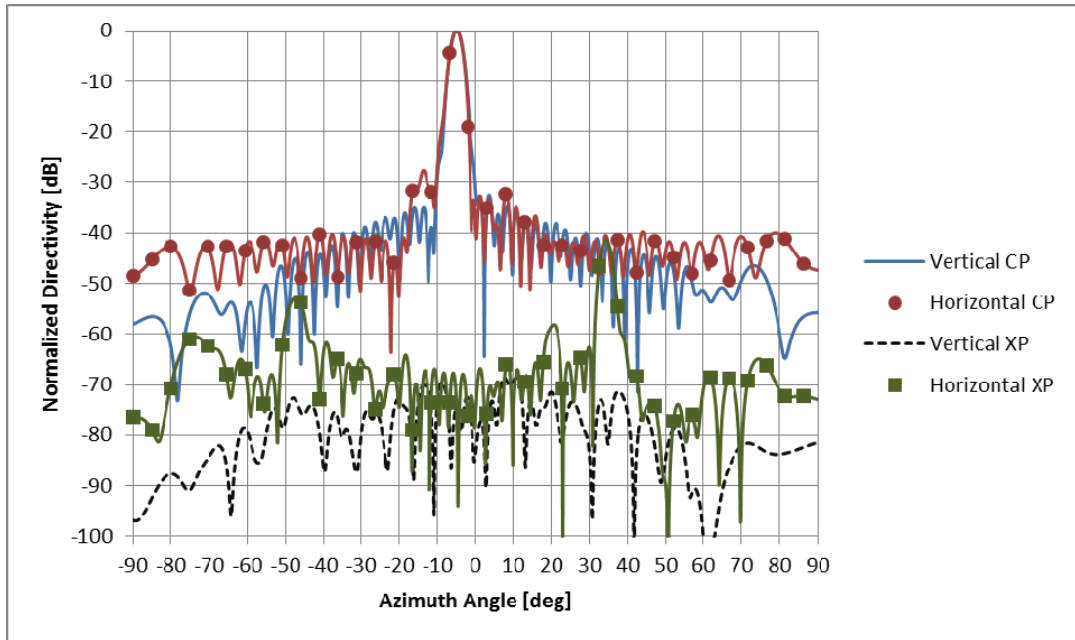


Figure 5.5 Azimuth radiation patterns of the designed array at f_0 -300MHz, obtained with simulation

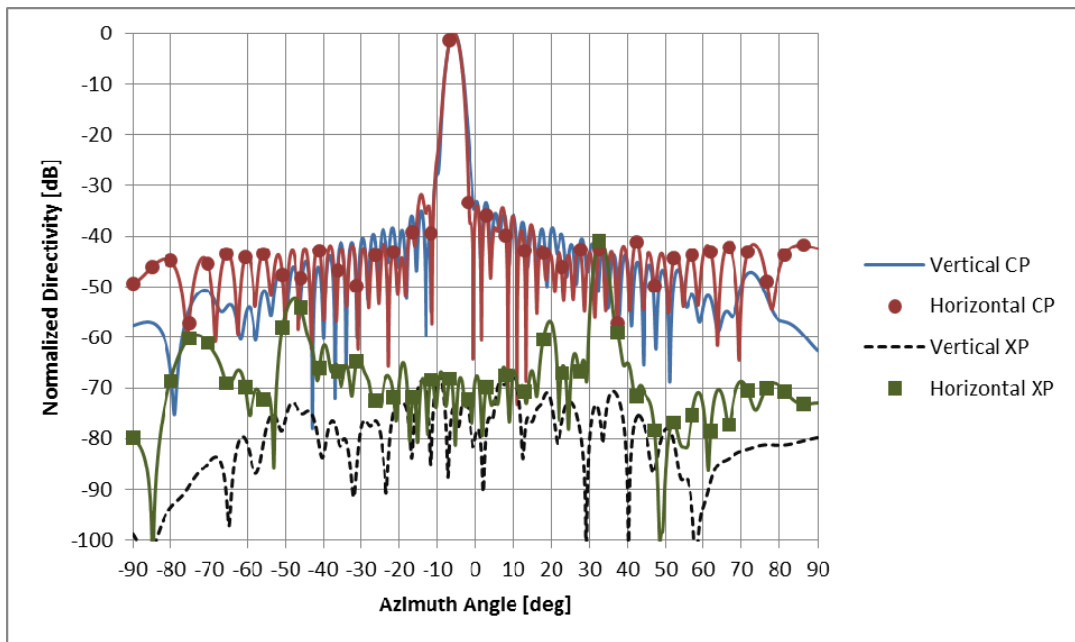


Figure 5.6 Azimuth radiation patterns of the designed array at f_0 -200MHz, obtained with simulation

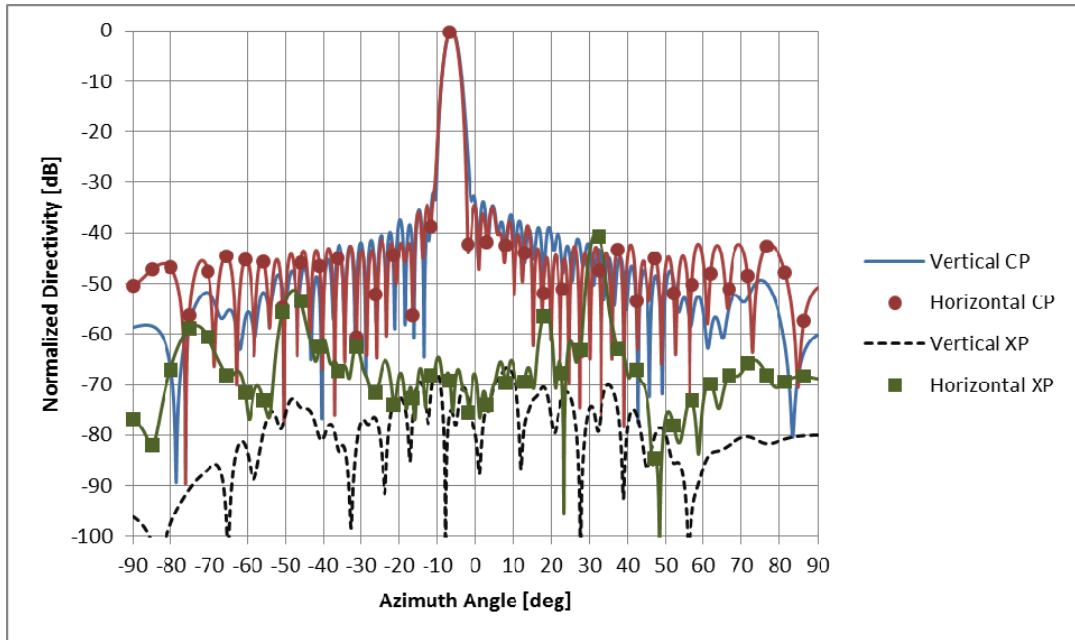


Figure 5.7 Azimuth radiation patterns of the designed array at $f_0=100\text{MHz}$, obtained with simulation

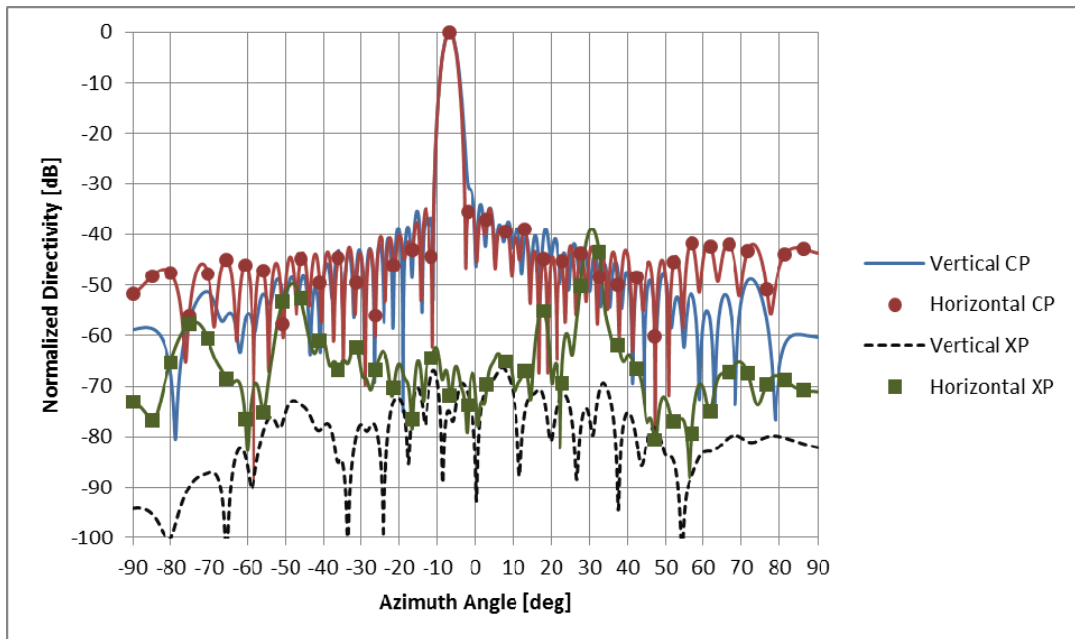


Figure 5.8 Azimuth radiation patterns of the designed array at f_0 , obtained with simulation

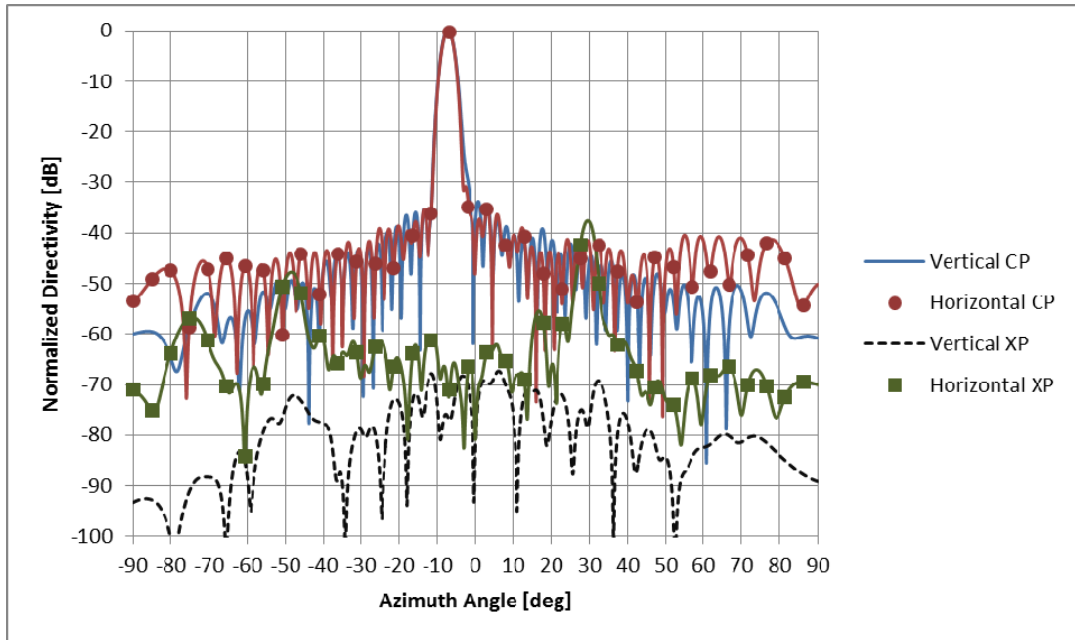


Figure 5.9 Azimuth radiation patterns of the designed array at f_0+100 , obtained with simulation

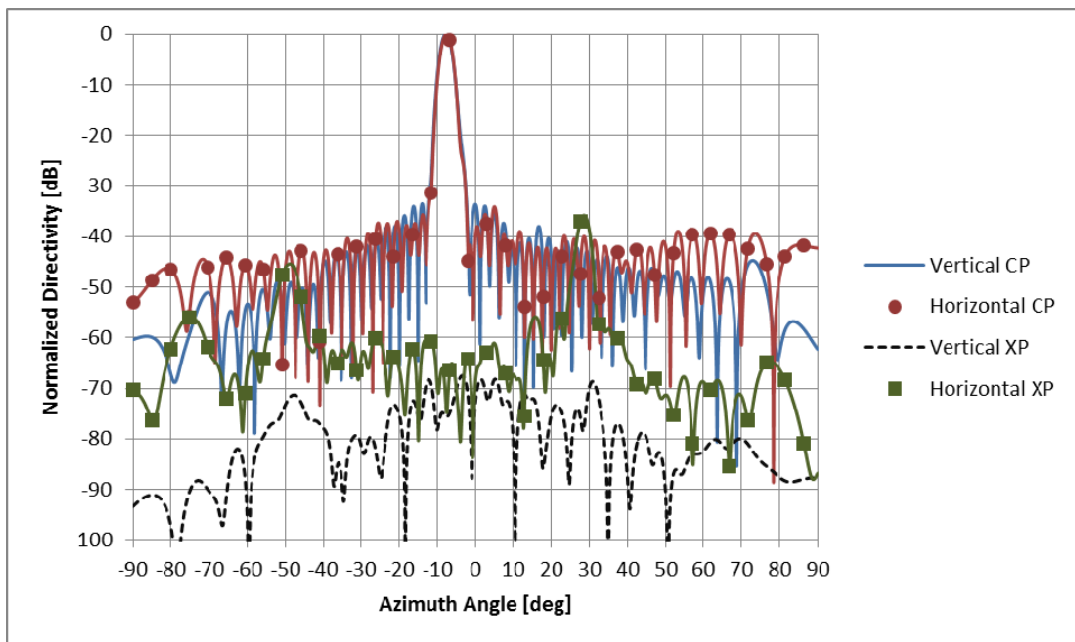


Figure 5.10 Azimuth radiation patterns of the designed array at $f_0+200\text{MHz}$, obtained with simulation

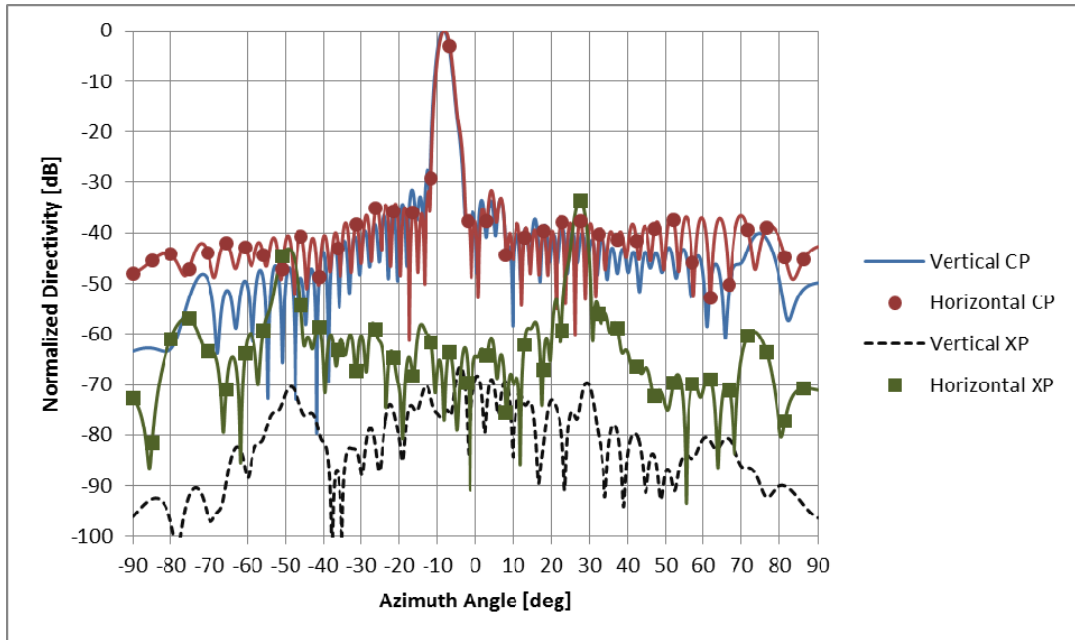


Figure 5.11 Azimuth radiation patterns of the designed array at $f_0+300\text{MHz}$, obtained with simulation

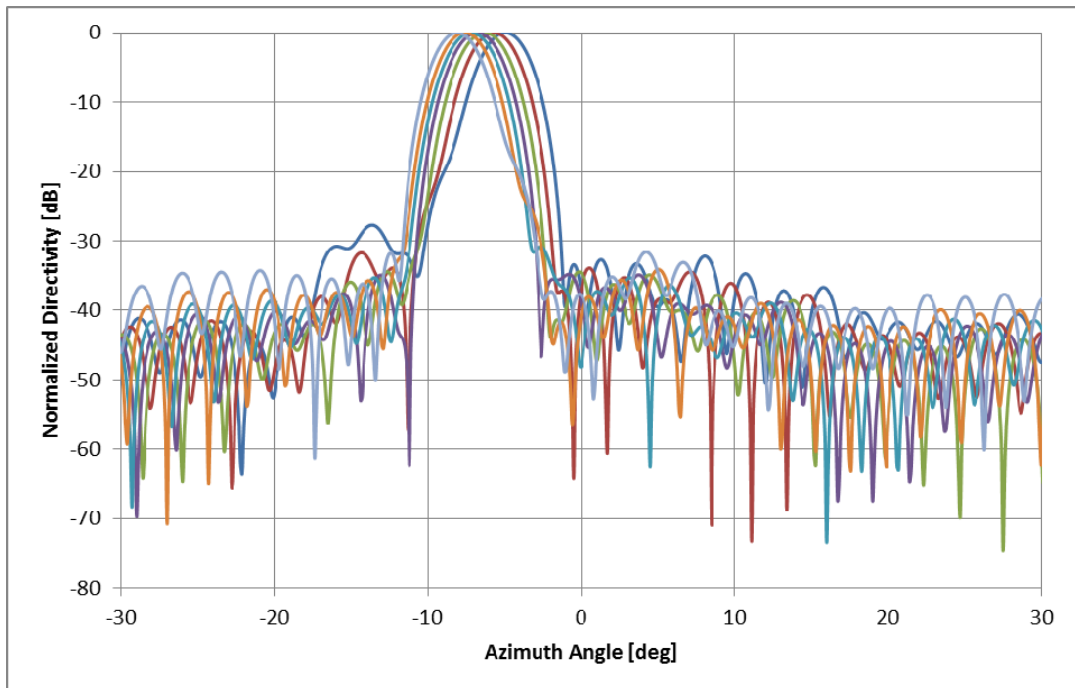


Figure 5.12 Azimuth radiation patterns of the horizontally polarized part of the designed array at 7 different frequencies, obtained with simulation

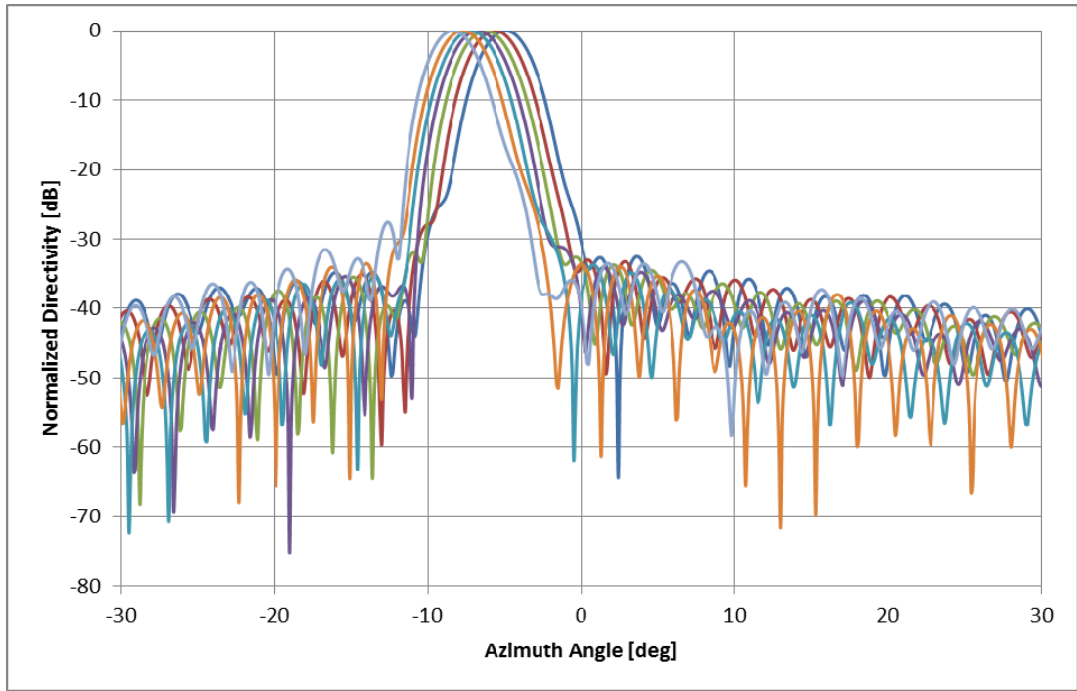


Figure 5.13 Azimuth radiation patterns of the vertically polarized part of the designed array at 7 different frequencies, obtained with simulation

CHAPTER 6

CONCLUSION

An X-band dual polarized SWGA is successfully designed using the broad wall shunt slots and novel non-inclined edge wall slots. 600 MHz operational bandwidth is obtained in terms of radiation pattern, input match and radiation efficiency. The sidelobe level is -35dB at the center frequency and -30dB in the whole frequency band of interest. The efficiency of the antenna is better than 90% in the whole frequency band and the polarization purity is excellent with a cross polarization level better than -60dB under the main beam. Additionally, using non standard waveguide cross sections, waveguide spacings are decreased so that the array is able to electronically scan a ± 35 degrees sector in the elevation plane. The design topology has the advantage of horizontally polarized waveguides acting as baffle structures which suppress the secondary lobes of the vertically polarized array.

The proposed edge wall slot used in the design of the horizontally polarized part of the antenna comprises of a non-inclined edge wall slot which is wrapped around the corners of the waveguide and two excitation insets inside the waveguide. The insets are integrated to the waveguide walls and this leads to an easy to manufacture antenna with 3 axis CNC milling technique.

To characterize all of the slots in the designed array, unit cell based infinite array approximation is introduced. For edge wall slots, a single slot is modeled inside a rectangular cross section unit cell surrounded by periodic boundary conditions. Required progressive phase shifts dictated by the travelling wave nature of the array are applied to the periodic boundaries. Floquet Port option in HFSS is used to terminate the upper boundary of the cell which gives literally zero reflection.

For the broad wall slots, the unit cell geometry is extended to include two slots. This requires the doubling of the progressive phase shift applied to the boundaries and additionally, requires the calculation of the active S parameter of a single slot when the whole array is excited.

For both of the slot geometries, simulations with the introduced unit cells are performed repeatedly by varying slot parameters controlling slot's excitation characteristics. Using these simulation data, characterization polynomials are obtained which are used in the design of the two orthogonally polarized arrays. Designed waveguide rows are simulated using uni-dimensionally infinite array models. Two waveguide rows for two orthogonal polarizations are finally merged to obtain the geometry for the final dual polarized antenna. This antenna is again simulated using an infinite array model.

The manufacturing process of the 31 element by 22 element antenna had begun at the completion phase of this work. It is planned to measure this antenna manufactured at Aselsan A.Ş. at the planar near field measurement setup to verify the design. There are also plans for designing a squintless version of this antenna using sub-arraying techniques with standing wave type arrays. In this case, careful analyses should be performed to determine the required sub array dimensions by taking into account the bandwidth and scan requirements.

APPENDIX

The aim is to find the polarization characteristics of the field radiated by two orthogonally polarized sources separated by an arbitrary distance. For the sake of simplicity, assume that a horizontally polarized isotropic radiator is located on the coordinate system's origin and a vertically polarized radiator is located on the z-axis at a distance d from the origin. Also, assume that the sources are the same except having orthogonal polarizations. The far fields radiated by these two sources are written as:

$$S1: \vec{E}_1(r, \theta, \phi = 0^\circ) = \hat{p}_1 w_1 \frac{E_0}{4\pi r} e^{-jkr} \quad (A.1)$$

$$S2: \vec{E}_2(r, \theta, \phi = 0^\circ) = \hat{p}_2 w_2 \frac{E_0}{4\pi r} e^{jkd \cos \theta} e^{-jkr} \quad (A.2)$$

Where, w_1 and w_2 are the excitation coefficients of the two sources.

Define the normalized electric field vector which is independent of distance “ r ” as:

$$\vec{f} = \vec{E} \frac{4\pi r}{e^{-jkr}} \quad (A.3)$$

This vector can be interpreted as the far field pattern of an antenna giving the relative far field amplitudes, far field phases, and far field polarizations for various directions and is independent from the distance “ r ”. Various normalized electric field vectors belonging to different antennas but written using the same coordinate system can be summed to obtain the overall radiation pattern of an antenna array.

It is desired to obtain a circularly polarized radiation along the direction $\theta=90^\circ$. Therefore, the excitation coefficients are chosen as follows:

$$w_1 = 1$$

$$w_2 = e^{j\frac{\pi}{2}}$$

The normalized far-zone electric field vector is obtained as follows:

$$\vec{f} = E_0(\hat{p}_1 + \hat{p}_2 e^{j\frac{\pi}{2}} e^{jkd \cos\theta}) \quad (\text{A.4})$$

The total field expression obviously contains two orthogonally polarized waves of equal amplitude but with a phase difference as a function of both the observation angle and the distance between the two sources. The phase difference variations with respect to the observation angle for various spacing are seen in Figure A.1.

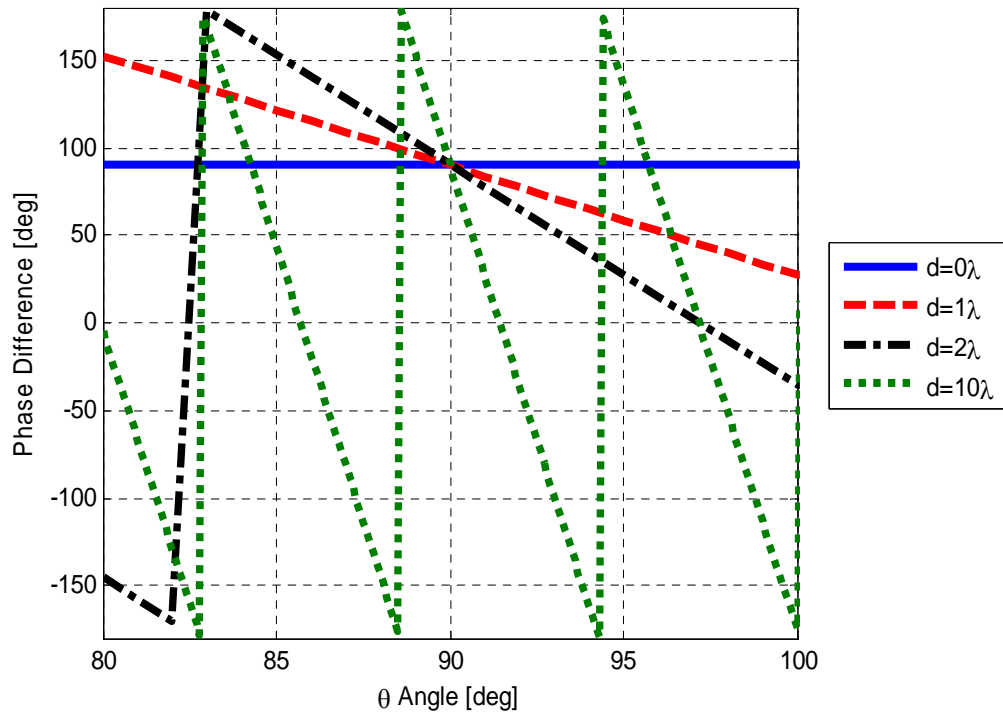


Figure A.1 Far field phase difference variations of the orthogonally polarized components for different source spacing

The change of phase difference with changing observation angle causes the inability to realize a desired polarization for a finite angular sector. As seen from Figure A.2, the desired axial ratio of the polarization ellipse deviates from the desired value of 1 as the observation angle departs from 90 degrees for spacing other than zero. The departure becomes more severe when the spacing is increased. For a practical spacing of λ , antenna becomes useless as a circularly polarized radiator.

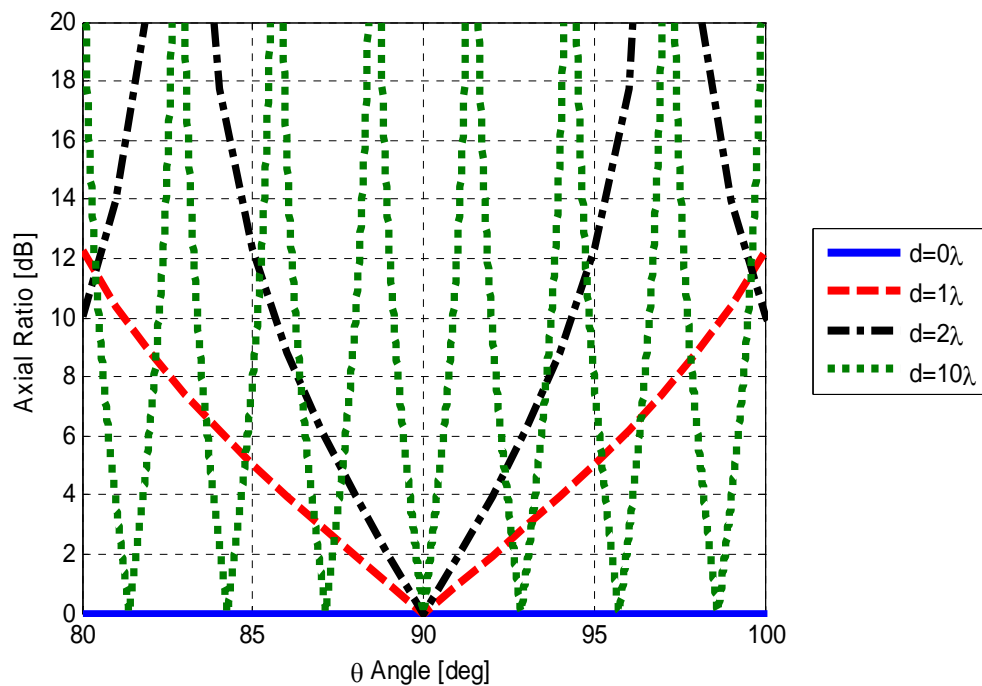


Figure A.2 Axial ratio variations of the polarization ellipse for different source spacing

REFERENCES

- [1] A. Dion, "Nonresonant slotted arrays," *IRE Transactions on Antennas and Propagation*, vol.6, no.4, pp.360-365, October 1958.
- [2] Roland A. Gilbert (chapter author), John L. Volakis (editor), *Antenna Engineering Handbook*, Fourth Edition, McGraw-Hill, 2007.
- [3] P.J Wood, N. Sultan, G. Seguin, "A dual-polarized reconfigurable-beam antenna for the DSAR synthetic aperture radar," *IEEE Antennas and Propagation Society International Symposium*, vol.3, pp.1716-1719, 21-26 Jul 1996
- [4] Wei Wang, Jian Jin, Jia-Guo Lu, Shun-Shi Zhong, "Waveguide slotted antenna array with broadband, dual-polarization and low cross-polarization for X-band SAR applications," *IEEE International Radar Conference*, pp. 653-656, 9-12 May 2005.
- [5] A.G. Derneryd, A. Lagerstedt, "Novel slotted waveguide antenna with polarimetric capabilities," *IEEE International Geoscience and Remote Sensing Symposium*, vol.3, no., pp.2054-2056 vol.3, 10-14 Jul 1995.
- [6] M. Stangl, R. Werninghaus, R. Zahn, "The TERRASAR-X active phased array antenna," *IEEE International Symposium on Phased Array Systems and Technology*, pp. 70-75, 14-17 Oct. 2003.
- [7] L. Josefsson, C.G.M. van't Klooster, "Dual polarised slotted waveguide SAR antenna," *IEEE Antennas and Propagation Society International Symposium*, pp.625-628 vol.1, 18-25 Jul 1992.
- [8] M.G. Guler, "Dual Polarized Slotted Array Antenna," U.S. Patent No: 6,127,985, 3 October 2000.

- [9] Dual mode waveguides for variably polarised slotted waveguide array antennas
- [10] A Polarization-agile Waveguide Slot Antenna
- [11] A.F. Stevenson, "Theory of Slots in Rectangular Waveguides," *Journal of Applied Physics*, pp. 24-38, January 1948.
- [12] R.J. Stegen, "Longitudinal Shunt Slot Characteristics," *Hughes Technical Memorandum*, No. 261, Culver City, CA, November 1951
- [13] A. Oliner, "The impedance properties of narrow radiating slots in the broad face of rectangular waveguide: Part I - Theory," *IRE Transactions on Antennas and Propagation*," vol.5, no.1, pp.4-11, January 1957.
- [14] R.S. Elliott, *Antenna Theory and Design*, Prentice-Hall, pp. 407-414, 1981.
- [15] R.S. Elliott (Chapter Author), Y.T. Lo, S.W. Lee, *Antenna Handbook*, Chapter 12, Van Nostrand Reinhold, 1993.
- [16] R.S. Elliott, "An improved design procedure for small arrays of shunt slots," *IEEE Antennas and Propagation Society International Symposium*, vol.21, pp. 297-300, May 1983.
- [17] C.A. Balanis, *Antenna Theory: Analysis and Design*, 3rd Ed., Wiley-Interscience, 2005.
- [18] L. Kurtz, J. Yee, "Second-order beams of two-dimensional slot arrays," *IRE Transactions on Antennas and Propagation*," vol.5, no.4, pp.356-362, October 1957.
- [19] S. Hashemi-Yeganeh, R.S. Elliott, "Analysis of untilted edge slots excited by tilted wires," *IEEE Transactions on Antennas and Propagation*, vol.38, no.11, pp.1737-1745, Nov 1990.
- [20] D. Dudley Jr., "An iris-excited slot radiator in the narrow wall of rectangular waveguide," *IRE Transactions on Antennas and Propagation*, vol.9, no.4, pp.361-364, July 1961.

- [21] J. Hirokawa, P.-S. Kildal, "Excitation of an untilted narrow-wall slot in a rectangular waveguide by using etched strips on a dielectric plate," *IEEE Transactions on Antennas and Propagation*, vol.45, no.6, pp.1032-1037, Jun 1997
- [22] W.H. Watson, "Resonant slots," *Journal of the Institution of Electrical Engineers - Part IIIA: Radiolocation*," vol.93, no.4, pp.747-777, 1946.
- [23] C.B. Top, "Design of a Slotted Waveguide Array Antenna and Its Feed System," Thesis (M.Sc.), Middle East Technical University, Ankara-Turkey, 2006.
- [24] K. Forooraghi, P.S. Kildal, "Reduction of Second-Order Beams in Slotted Waveguide Arrays Using Baffles," *IEE 7th International Conference on Antennas Propagation*, pp. 725, Apr 1991.
- [25] S. R. Rengarajan, "Mutual coupling between waveguide-fed longitudinal broad wall slots radiating between baffles," *Electromagnetics*, vol. 16, pp. 671, 1996.